University of Nottingham
UK | CHINA | MALAYSIA

School of Pharmacy

α-Amidobenzylboronates and β-Ketobenzylboronates as Inhibitors of Plasma Kallikrein

Thesis submitted to the University of Nottingham for the degree of Doctor of Philosophy

Matthew Allison MSc

4342143

Supervised by:
Prof. Michael Stocks
Prof. Jonas Emsley

31/3/2024

If you hit a wrong note, it’s the next note you play that determines if it’s good or bad.

-Miles Davis

Abstract

Hereditary angioedema (HAE), a rare genetic disorder, is associated with uncontrolled plasma kallikrein (PKa) enzyme activity leading to often severe bradykinin-induced swelling in subcutaneous and submucosal membranes in various locations of the body.

This thesis describes a series of α-amidobenzylboronates (n=7) as highly potent covalent inhibitors of PKa (Figure a). These compounds exhibited time-dependent inhibition of PKa, with the most potent compound, **91**, showing IC_{50} = 66 nM at 1 min, 70 pM at 24 hours. Further compound dissociation studies demonstrated no apparent reversibility comparable to D-Phe-Pro-Arg-chloromethyl ketone (PPACK), a known non-selective covalent PKa inhibitor. Comparison with noncovalent matched pair analogues (n=8) supported the notion of covalent inhibition. Biological evaluation of α-amidobenzylboronates against closely related proteases; FXIIa, FXIa, plasmin, thrombin, and trypsin showed at least 1000-fold specificity towards PKa in the case of each evaluated compound, demonstrating the first selective covalent inhibitors of PKa.

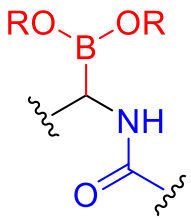

Figure a. Generalised α-amidoboronate structure.

β-ketobenzylboronates were also synthesised (n=2) and showed moderate activity in PKa however no evidence of covalent inhibition was demonstrated from analysis of enzyme binding kinetics and subjection to jump dilution. Lack of covalent binding notwithstanding, compound **125b** showed moderate noncovalent activity in PKa (IC_{50} = 39 nM). Furthermore, β-ketonitrile compounds (n=2) were explored, with one example, compound **129b**, showing apparent covalent inhibition of PKa (IC_{50} = 223 nM at 1 min, 33 nM at 60 min) (Figure b). .

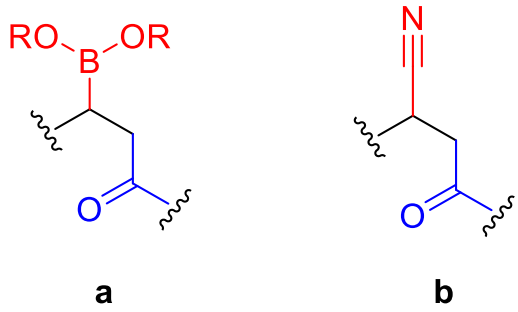

Figure b. Generalised structures of **a)** β-ketoboronates and **b)** β-ketonitriles

Acknowledgements

Firstly, I would like to thank Prof. Michael Stocks for his attentive supervision and substantial contributions throughout the duration of this project. Thanks are also given to Dr. Rebecca Davie for her continued help and support during the project, Prof. Jonas Emsley for interesting insights and discussion, Adrian Mogg, Edward Duckworth and Freya Pinkney for carrying out biochemical evaluation, crucial to this project.

I would also like to thank Sally Hampton and Kalvista Pharmaceuticals Ltd. for providing funding for this project as well as for their support and for welcoming me to their organisation. Furthermore, I would like to thank the EPSRC for funding this project.

I would also like to thank my colleagues and friends; George, Jaffer, Bianca, Jack Scott, Ryan, Jomo, Luke, Mahesh, Rhys, Rebecca, Zarea, Rhianna, amongst others, for maintaining the sanity of everyday life.

Contents

List of Tables

List of Figures

Abbreviations

Ar – Aryl

Bu – butyl

CAS – contact activation system

calcd – calculated

conc. - concentrated

δ – chemical shift

d - doublet

DIPEA - diisopropylethylamine

DMF – *N,N*-dimethylformamide

DMSO – dimethylsulfoxide

EDC - 1-Ethyl-3-(3-dimethylaminopropyl)carbodiimide

ESI – electrospray ionisation

Et - ethyl

EtOAc – ethyl acetate

eq. - equivalents

HATU - hexafluorophosphate azabenzotriazole tetramethyl uronium

HOBt - hydroxybenzotriazole

HPLC – high performance liquid chromatography

HRMS – high resolution mass spectrometry

IC_{50} – half maximal inhibitory concentration

J – NMR coupling constant

KKS – kallikrein-kinin system

LCMS – liquid chromatography mass spectrometry

LiHMDS -lithuium hexamethyldisilazane

M – molecular ion

m - multiplet

Me - methyl

MeCN – acetonitrile

mg - milligrams

MMFF – Merck molecular force field

mmol – millimoles

MOM - methoxymethyl

MTBE – methyl *tert*-butyl ether

m/z – mass-to-charge ratio

nM - nanomolar

NMR – nuclear magnetic resonance

PBS – phosphate-buffered saline

Pin - pinacol

pKa – acid dissociation constant

PKa – plasma kallikrein

ppm – parts per million

Pr - propyl

p-TsOH – *para*-toluenesulfonic acid

q -quartet

RP – reverse phase

rt – room temperature

s - singlet

SAR – structure-activity relationship

t – triplet

TFA – trifluoroacetic acid

THF – tetrahydrofuran

TLC – thin layer chromatography

TMS - trimethylsilyl

TOF – time of flight

UV - ultraviolet

Chapter 1

Chapter 1: Introduction

1.1 Hereditary Angioedema (HAE)

Hereditary angioedema (HAE) is a rare autosomal dominant genetic disease which affects roughly 1 in 50 000 people, afflicting all ethnicities with no sex predominance. Angioedema refers to intense, usually disfiguring localised swelling of a body area, often associated with allergy and diet. HAE symptoms however, are manifested as unpredictable and sometimes life-threatening onsets of severe swelling and inflammation of subcutaneous and submucosal tissues, affecting the arms, legs, face, gastrointestinal tract and the trachea, risking asphyxiation and obstruction of major organs.[1,2]

First described as 'angioneurotic edema' in 1876, the biochemical irregularity responsible for HAE wasn't discovered until 1963 by Donaldson and Evans.[3] C1 esterase inhibitor (C1-INH) is a protease inhibitor belonging to the serpin superfamily, acting as a major regulator of the complement, contact, coagulation and kinin systems. Plasma kallikrein (PKa), factor XIa (FXIa) and factor XIIa (FXIIa) are amongst the enzymes most reliant on C1-INH regulation.[4]

Occurring in three subtypes, HAE types I and II, respectively relate to the deficiency and dysfunction of the *SERPING1* gene, responsible for encoding C1-INH. Type I results from various mutations with deletions or insertions of single or multiple nucleotides within *SERPING1*. Type II is caused by point mutations in areas coding for the hinge region of C1-INH, rendering the protease defunct.[5] Type III HAE was identified long after types I and II and is therefore less understood.

Patients with type III HAE exhibit normal C1-INH levels and function, both during angioedema and under asymptomatic conditions. This variant is believed to result from congenital deficiency of enzymes such as angiotensin converting enzyme (ACE), carboxypeptidase N and α-macroglobulin.[6] C1-INH HAE is the focus of this project.

1.2 The kallikrein-kinin system (KKS)

Ubiquitous in nature, serine proteases represent the most structurally diverse group of proteolytic enzymes.[7] Of these enzymes, the chymotrypsin-like subfamily is the most represented, with over 240 proteases recognised in the MEROPS database.[8] Chymotrypsin-like serine proteases have evolved to perform vital physiological functions including; digestion, haemostasis, apoptosis, signal transduction, reproduction and the immune response.[9] As a result of their broad physiological contributions, chymotrypsin-like serine proteases present themselves as attractive targets for multiple diseases in medicinal chemistry. Specifically, the kallikrein-kinin system (KKS) is the biological system of interest within the scope of this project (Figure 1.1).

Possessing crucial roles in cardiovascular and cerebrovascular functions, the KKS is an endogenous cascade involving chymotrypsin-like proteases, the initiation of which results in the activation of the intrinsic coagulation pathway and proteolytic cleavage of kininogens, resulting in the release of bradykinin (BK).[10,11] Bradykinin

production is known to be a principal role of the KKS *via* digestion of high molecular weight kininogen (HK) by PKa[12].

Inflammation exists as a cellular defence mechanism against biological stressors such as pathogens, damaged cells or irritants to initiate tissue repair and eliminate damaged or necrotic cells, arising from injury.[13] Various diseases may result from atypical activation of these pathways due to the fine balance that exists to promote haemostasis and a regulated inflammatory response.

BK is a nonapeptide capable of binding B_1 and B_2 receptors, which broadly belong to the G-protein coupled receptor (GPCR) superfamily. B_1 receptors are seldom detected in most tissues, however become strongly upregulated during events of inflammation, whereas B_2 receptors are ubiquitously expressed in most tissues. The type 2 bradykinin receptor (B_2R) is an essential GPCR involved in regulating homeostasis of the cardiovascular system as a vasodepressor.[14] B_2R antagonism mainly initiates the Gq signalling pathway during which Gq proteins couple to B_2R upon receptor activation and then disassociate into the Gαq subunit and Gβγ heterodimers.[15] Gαq activates phospholipase C (PLC) resulting in release of Ca^{2+} from endoplasmic reticula and subsequent activation of nitric oxide synthase, upregulation of NO in blood vessels. Ca^{2+} also has the effect of increasing phosphorylation of phospholipase A2 (PLA_2), triggering the production of prostaglandins. Both NO and prostaglandins are potent vasodilators which cause lowering of blood pressure, increased endothelial permeability, leading to capillary leakage of protein rich fluids into interstitial areas, causing inflammation.[16]

The contact activation system (CAS) and KKS are overlapping systems, both initiated by activation of zymogen factor XII (FXII) to FXIIa (Figure 1.1). FXII exists in plasma in the zymogen form, however they become strongly upregulated *via* exposure to negatively charged surfaces, inducing a conformational change to generate the activated protease (FXIIa)[17].

FXIIa is capable of converting PPK to PKa and FXI to FXIa, initiating the KKS and CAS respectively. Liberation of PKa enables conversion of HK to BK, initiating an inflammation response. Endogenously, C1 inhibitor protein (C1-INH) inhibits PKa, downregulating the KKS.[18–20]

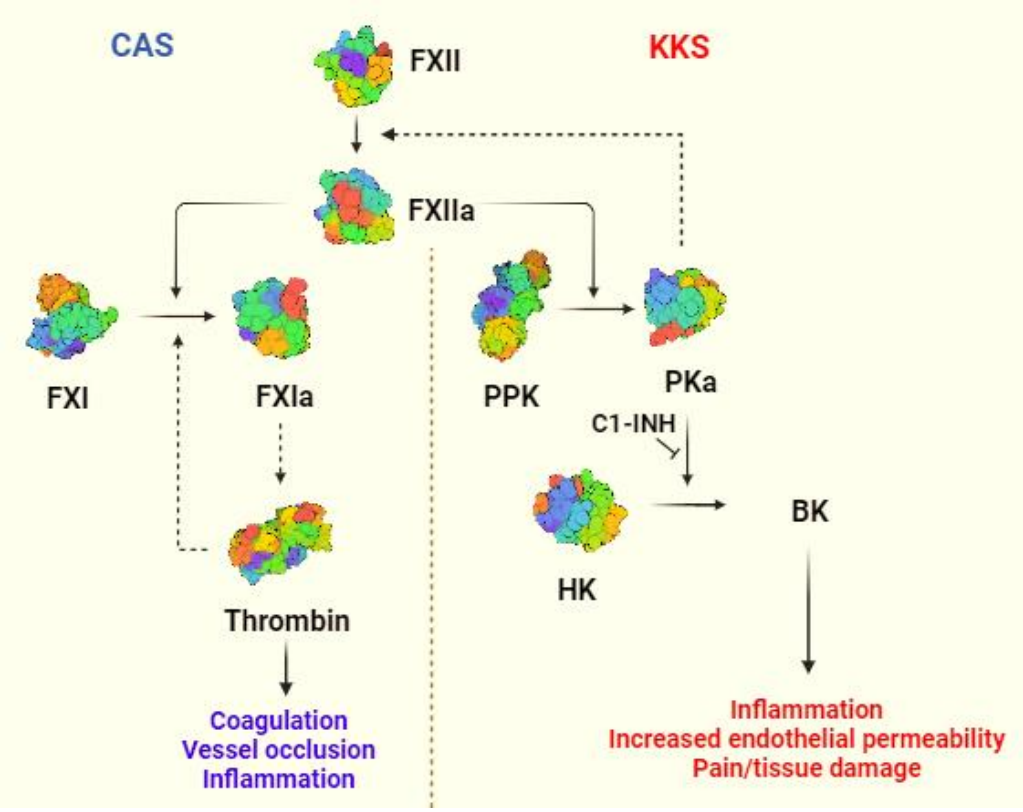

Figure 1.1. Schematic showing key interactions taking place in [left] – contact activation system (CAS) and [right] – kallikrein/kinin system (KKS). (PPK - Plasma prekallikrein, PKa – plasma kallikrein, HK-High molecular weight kininogen, C1-INH – C1 inhibitor protein, BK- bradykinin)

Both the KKS and CAS have an autocatalytic feedback mechanism. In the case of the KKS, PKa is able to upregulate FXII activation, amplifying the KKS. Similarly, within the CAS, thrombin is produced by activation of FXI to FXIa, FXIa activates FIX to FIXa which converts prothrombin to thrombin, initiating a coagulation response. Thrombin is also able to upregulate conversion of FXI to FXIa, activating this pathway.[21] PKa also converts prorenin to renin, establishing an overlap between the KKS and renin-angiotensin system (RAS).[22]

1.3 Current and Developing Treatments for HAE

Multiple therapies have been developed for the treatment of C1-INH deficient HAE. Broadly, these treatments may be categorized as on-demand treatments for acute angioedema and treatments for short or long-term prophylaxis.

1.3.1 On-demand therapies

Acute or on-demand therapies for angioedema refer to treatments taken at the point of onset of an angioedema attack, with the therapy goal being to reduce or sequester the symptoms of an angioedema event. Currently, there are four therapies approved for on-demand usage, discussed herein.

1.3.1.1 Human C1-INH concentrate (C1-INH$_{ci}$, Cinryze®)

Intravenous (IV) plasma derived, nano filtered and purified human C1-INH concentrate (C1-INH_{ci}) increases C1-INH levels in patients that are C1-INH deficient. An independent study determined that administration of a 1000 IU dose can be administered every 3-4 days for prophylaxis to prevent angioedema attacks in HAE patients, or up to two 1000 IU doses may be given at first sign of angioedema for on-demand therapy.[23] Additionally, C1-INH_{ci} is used for pre-procedural prophylaxis, administered 24 hours before surgical or invasive diagnostic procedures to lower risk of angioedema.[24]

Whilst showing clinical relief in 95% of cases and unequivocal relief of the defining symptom in 87% of patients 4 hours after administration, C1-INH_{ci} also shows reduction in frequency and severity of attacks in HAE patients. C1-INH_{ci} is only available as an IV treatment, therefore must be administered by a clinician, limiting access to the treatment.

1.3.1.2 Recombinant Human C1 Inhibitor (rHC1-INH)

Similarly to C1-INH_{ci}, recombinant human C1-INH (rHC1-INH) is approved for use for treatment of angioedema. rHC1-INH showed reduction of mean number of attacks in 32 patients per week from 7.2 to 4.4 when administered on-demand once weekly, and to 2.7 attacks with twice-weekly administration.[25] As with C1-INH_{ci}, drawbacks include limited shelf-life and inability for patients to self-administer.

1.3.1.3 Icatibant acetate

Subcutaneous (SC) Icatibant acetate **1** is an available acute therapy for treatment of HAE. Icatibant **1** is a peptidomimetic drug consisting of ten amino acids, acting as a highly specific, competitive antagonist of bradykinin B_2 receptors (Figure 1.2).

Suppression of excess bradykinin production enables blockage of edema formation. Icatibant has a similar structure to bradykinin but contains five non-proteinogenic amino acids and is resistant to cleavage by bradykinin-targeting enzymes.[26]

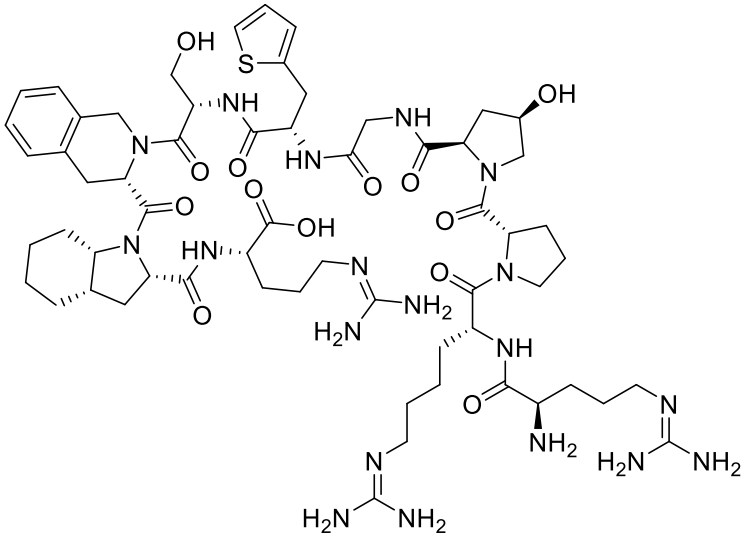

1

Figure 1.2. Structure of icatibant.

In a randomised, double-blind study, the effect of SC icatibant was investigated on patients presenting symptoms of subcutaneous or abdominal angioedema attacks. Icatibant was administered at a dose of 30 mg with the therapeutic goal

of achieving sequestration of primary symptoms of angioedema. The median time to relieve symptoms of patients taking icatibant was 2.5 hours, compared with 4.6 hours for the placebo group.[27]

Provided as 30 mg pre-filled syringes, a key benefit of icatibant as an HAE therapy is the option for patients to self-administer the drug upon onset of angioedema. Adverse effects may arise from use of Icatibant due to its cardio protective properties, enabling the possibility of impaired cardiac function and reduced coronary blood flow. This property has been observed in animal models that developed myocardial infarction after icatibant treatment. This precludes patients with existing cardiac conditions from using icatibant.[28]

Adverse reactions around the site of icatibant injection have also been reported amongst patients. This may be due to the tendency of icatibant to display B_2 agonistic properties when present in higher concentrations. Most commonly, mild to moderate erythema and/or swelling is reported at the injection site due to the high local concentration of icatibant. These symptoms were generally resolved up to 4 hours after injection.[29]

A key disadvantage of icatibant is the fact that it targets the B_2 receptor, therefore it only has the therapeutic ability to block bradykinin downstream signalling, as opposed to acting as a prophylactic treatment against angioedema onset.[30]

1.3.1.4 Ecallantide

Ecallantide is a 60 amino acid peptide approved for the treatment of HAE. Acting as a C1-INH mimetic, ecallantide reversibly inhibits plasma kallikrein (PKa), preventing the conversion of kininogen to bradykinin, reducing symptoms of angioedema.[31,32]

In a double-blind, placebo controlled clinical trial, a patient-reported treatment outcome score was used to assess efficacy of ecallantide against a placebo, this measure describes the severity of patient symptoms before and after administration of the treatment, ranging from -100 to +100. Four hours after administration, the ecallantide group reported a median score of 50.0, suggesting a positive response to the treatment, whereas the placebo group recorded a score of 0.0 suggesting no improvement.[33]

Key advantages of ecallantide include lack of risk of viral contamination in comparison to plasma derived therapies, high selectivity, fast onset of action and ability for subcutaneous administration. Safety concerns however exist regarding hypersensitivity reactions. Adverse effects are reported to include headache and fever.[34]

1.3.1.5 Haegarda®

Haegarda® was introduced in 2017 as the first C1-INH concentrate preparation available for subcutaneous (SC) administration, reducing treatment burden compared with IV route of administration.[35]

1.3.2 Short-term prophylaxis (STP)

Short term prophylaxis, or pre-procedure prophylaxis, describes treatment administered before medical or surgical procedures, as well as vital life events such as exams or weddings to prevent angioedema onset.[36]

The primary treatment of choice for STP is Intravenous (IV) plasma derived, nanofiltered and purified human C1-INH concentrate (C1-INH$_{ci}$, Cinryze®), rhC1INH has also been proven efficacious as an STP treatment[37,38] (mentioned in Section 1.3.1).

1.3.2.1 Danazol

In cases where plasma based treatments are unavailable or inconvenient to administer, danazol **2** may be for up to 5 days before and 2-3 days after a given procedure (Figure 1.3).[30]

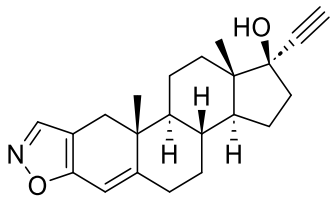

2

Figure 1.3. Structure of danazol.

Danazol is a mild androgen and anabolic steroid, primarily used in the treatment of endometriosis, fibrocystic breast disease and hereditary angioedema.[39] The mechanism of action for danazol is complex as it modulates numerous biological receptors including sex hormone receptors, enzymes involved in steroidogenesis and steroid hormone carrier proteins.[40] The use of oral danazol in HAE treatment emerged due to observed enhancement of hepatic C1-INH production and plasma aminopeptidase P (APP) activity. APP is a major metallopeptidase involved in kinin inactivation which exhibits low activity in angioedema patients. In a clinical study of 147 HAE patients, treatment with danazol resulted in a significant increase in APP activity, without affecting other metalloprotease activities. In all patients increased APP activity was shown to reduce severity of HAE symptoms.[41]

The use of attenuated androgens *e.g.* danazol in HAE treatment is inherently limited by the numerous adverse effects associated with these drugs. Particularly undesirable in female patients, masculinising side effects such as acne, excessive hair growth and voice deepening are observed in many danazol users.[42]

1.3.3 Long-term prophylaxis

Long-term or routine prophylaxis (LTP) describes treatment aimed at decreasing the frequency, severity and duration of angioedema attacks for patients whose condition may not be adequately supressed by on-demand treatments alone.[43]

Previously mentioned plasma based C1-INH injectables are approved for the treatment of LTP, however suffer from difficulty of administration. Danazol has

also been approved for LTP treatment, however suffers from numerous common adverse effects.[44]

1.3.3.1 Tranexamic acid

Trenexamic acid **3** is a synthetic analogue of lysine which competitively inhibits activation of plasminogen, used as a therapy for HAE, amongst many other clinical applications (Figure 1.4).

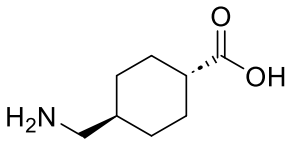

3

Figure 1.4. Structure of tranexamic acid

Functioning as an anti-fibrinolytic agent, **3** blocks lysine binding sites on plasminogen molecules, inhibiting interaction between plasminogen and plasmin or fibrin, resulting in stabilisation of fibrin networks formed by secondary haemostasis, reducing the need for C1-INH recruitment.[45]

Whist clinical efficacy is shown in studies of tranexamic for reducing frequency and/or severity of angioedema attacks[46], the real world benefit to patients taking tranexamic acid for LTP remains low. Clinical data have not demonstrated a dose

that is effective in large numbers of patients, signifying that responses to tranexamic acid treatment may differ on an individual basis.[47]

As a non-specific agent used in the treatment of numerous conditions,[48] tranexamic acid is considered inferior to many other options including ecallantide or plasma based treatments, however advantageous compared with no treatment. Tranexamic acid is used substantially in paediatric settings due to its low risk and minimal adverse effects.[49]

1.3.3.2 Landelumab

Landelumab is a human monoclonal antibody administered by subcutaneous injection, which targets plasma kallikrein (PKa), limiting bradykinin production *via* sustained inhibition of PKa. Landelumab showed potent inhibitory activity in *in vitro* studies (PKa IC_{50} = 1.3 nM, K_i = 0.12 nM) and showed equivalent affinity for both free PKa and HMWK-bound PKa, whilst exhibiting markedly diminished affinity for zymogen prekallikrein.[50] Furthermore, Landelumab showed roughly a 200 fold faster association rate towards PKa in comparison to endogenous C1-INH, enabling therapeutic efficacy at low concentrations.[51]

In clinical studies, it was shown that administration of two doses of subcutaneous Landelumab, of 300-400 mg, 14 days apart was safe and effective in preventing angioedema attacks, showing 88-100% fewer attacks with respect to the placebo group. The dose-response relationship of Landelumab was shown to be linear with a prolonged half-life of around 14 days, allowing for infrequent injection.[52]

Adverse effects from Landelumab include injection site reactions, worsening headache, and night sweats, occurring in roughly one in four patients from a clinical study. No patients were discontinued from the trial due to adverse effects, suggesting Landelumab is generally well-tolerated.[52]

Overall, Landelumab is a first-in-class monoclonal antibody inhibitor of PKa, showing powerful inhibition properties and effectiveness in supressing angioedema events with minimal adverse reactions for a treatment in this class. Self-administration is possible in infrequent intervals, however more data is required regarding long-term safety in HAE patients.[50]

1.3.3.3 Berotralstat

Berotralstat **4** is the most recent HAE therapy to emerge, gaining FDA approval in 2020, as a first-in-class, orally available small-molecule inhibitor of PKa (Figure 1.5).

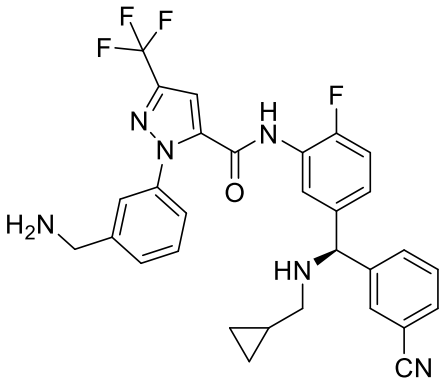

4

Figure 1.5. Structure of berotralstat

Berotralstat acts as a competitive, reversible inhibitor of PKa, targeting the S1, S1' and S2 binding sites, developed from a previous generation inhibitor (Avoralstat), improving oral bioavailability through replacement of a benzamidine P1 group with benzylamine.[53]

Berotralstat was designed as a once-daily oral prophylactic treatment for HAE, circumventing the need for SC or IV injection. Early *in vitro* studies indicated that **4** exhibits high potency against Pka (IC_{50} = 1.0 nM, K_i = 0.4 nM). Furthermore, berotralstat showed high levels of selectivity towards Pka in comparison with other plasma serine proteases such as trypsin, plasmin, thrombin and FXIIa.[54]

Clinical trials determined that Berotralstat is efficacious for long term prophylaxis, showing reductions in attack rate and severity at both 110 and 150 mg doses, with adverse events being generally mild and self-limited cases of maculopapular rash and gastrointestinal symptoms. A key benefit of Berotralstat over other therapies is the ability to administer orally, reducing the treatment burden when compared with alternative injectable therapies.[55,56]

1.3.4 HAE Treatments in Development

1.3.4.1 Sebetralstat

Sebetralstat **5** is a potent and selective orally available small-molecule inhibitor of Pka, targeting the S1 and S4 binding sites, for on-demand prophylactic treatment of HAE (Figure 1.6)

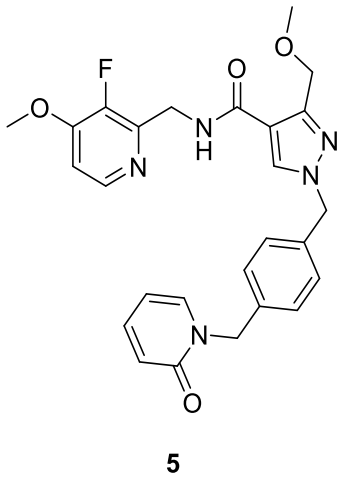

5

Figure 1.6. Structure of sebetralstat

Conventionally, the development of orally bioavailable inhibitors of PKa proves challenging due to the frequent use of basic, positively charged P1 groups such as benzylamine or aminopyridine to elicit a strong interaction with Asp_{189} in the S1 pocket. In the development of sebetralstat, a series of 'neutral', non-basic P1 groups was explored as a means of improving oral bioavailability. In a fragment screen, 3-fluoro-4-methoxypyridine was shown to have high S1 binding. The high affinity of this P1 group is thought to be due to displacement of a water molecule from a local hydrophobic environment around Tyr_{228} by the methoxy substituent.

The pyridone portion of **5** extends into the S4 pocket of PKa and is known to undergo π-stacking with Tyr_{174}.[57]

In vitro, Sebetralstat showed high affinity for PKa (IC_{50} = 6.0 nM) with high selectivity towards PKa in a screen against related proteases such as tissue kallikrein (KLK1), FXIa and FXIIa.

In a clinical trial, it was shown that sebetralstat rapidly achieves near complete PKa inhibition and in the vast majority of cases was safe and well tolerated, with all adverse events being mild in a group of 98 participants.[58] A separate study determined that a 600 mg dose of sebetralstat maintained greater than 95% PKa inhibition for 8 hours and prevented HMWK cleavage for 12 hours, blocking contact system activation for up to 6 hours.[59] Time taken to treat a conventional attack within 12 hours of participants receiving a 600 mg dose of sebetralstat was significantly reduced compared to the placebo group (15.1% vs. 30.2% respectively). Additionally, sebetralstat reduced time taken to reduce symptoms compared to the placebo (1.6 hours vs. 9 hours, respectively).[59]

1.3.4.2 Garadacimab

Garadacimab (CSL) is a humanised IgG4 monoclonal antibody that targets FXII, inhibiting KKS activation and bradykinin release.[60] A phase III clinical trial was completed in 2017 for both SC and IV delivery methods of garadacimab, concluding that monthly SC injections of garadacimab significantly reduced rate of angioedema attack in participants, when compared with the placebo group. Patients receiving garadacimab experienced median 0.27 attacks per month compared with 2.01 for those on placebo over a 6 month period.[61]

1.3.4.3 ATN-249

ATN-249 **6** (Attune Pharmaceuticals) is a plasma kallikrein inhibitor for oral administration to treat C1-INH deficient angioedema, with 2000-fold selectivity in favour of PKa in comparison to related plasma proteases such as thrombin, FXa and FVIIa (Figure 1.7).

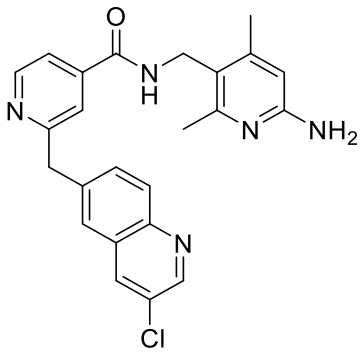

6

Figure 1.7. Structure of ATN-249.

In a controlled study, it was observed that ATN-249 exhibited greater than 10-fold higher PKa inhibition and contact activation in comparison to Cinryze®[62]. ATN-249 completed a phase I randomised, double-blind clinical trial in 2017 to 48 healthy male participants. Dose dependent inhibition of Pka and reduction in cleavage of HMWK was observed 2 hours after administration, with no severe adverse effects being noted.[59] At present, ATN-249 remains an investigational therapy, having completed a phase I study.

1.3.5 Other Relevant PKa Inhibitors

Structures of a series of novel, highly potent PKa inhibitors, bearing highly novel P4 groups were released by Merck Sharp & Dohme Corp in 2022 (Figure 1.8).[63]

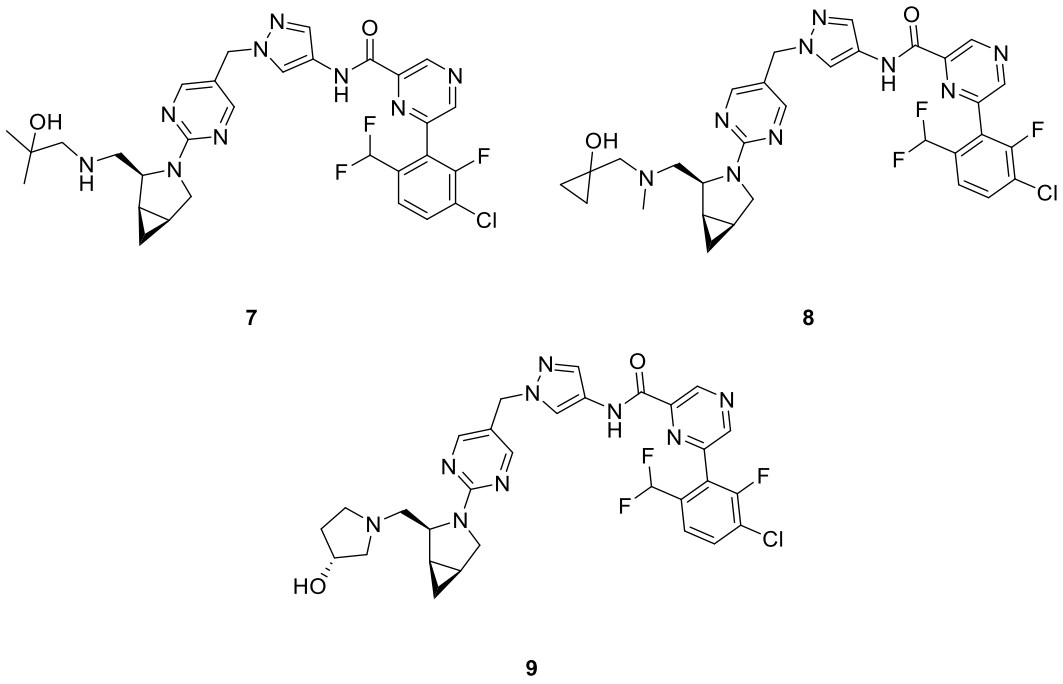

Figure 1.8. Structures of Merck novel PKa inhibitors.

Compounds **7-9** showed potent biological activity against PKa with respective IC_{50} values of 0.3, 0.2, and 0.4 nM.[63]

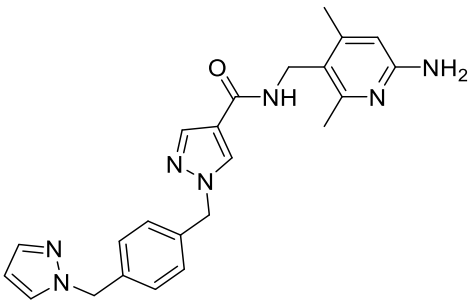

10

Figure 1.9. Structure of novel PKa inhibitor **10**.

10 was found to be a specific, potent, competitive reversible inhibitor of PKa (IC_{50} = 1 nM), showing around 10,000-fold binding preference for PKa over trypsin, FXIIa, FXIa, FXa, thrombin and plasmin (Figure 1.9).[64,65]

1.3.6 Summary

Hereditary angioedema treatment encompasses the prevention and severity reduction of angioedema in both on-demand (acute) and prophylactic measures for patient harm-reduction and improved quality of life. Many earlier therapies have focused on the delivery of the deficient C1-INH protein as a means of on-demand HAE treatment.[66] Whilst effective, C1-INH-based injectables contraindicate patient preference for oral administration.[67] B_2R antagonists such as icatibant block downstream signalling of bradykinin, however these are on-demand therapies, used to manage but not prevent angioedema attacks. The emergence of small-molecule PKa inhibitors such as berotralstat and sebetralstat affords the patient an oral, daily prophylactic measure to reduce probability and

severity of an angioedema attack, representing significant advancement in the landscape for HAE treatment.[68]

1.4 Plasma Kallikrein Mechanism and Inhibition

Plasma kallikrein (PKa) is an attractive drug target for the treatment of HAE as effective inhibition of PKa has been shown to supress the KKS, thus reducing symptoms characteristic of an angioedema onset.[69]

The term 'kallikrein' was initially used to describe the proteolytic activity from the pancreas responsible for the cleavage of kininogen. Kallikreins can be broadly divided into two categories; plasma kallikrein (PKa) which cleaves kininogen to BK, and tissue kallikreins (KLK) which cleave kininogen to Lys-BK (kallidin), later converted to BK by aminopeptidases.[70] Structurally, PKa bears close similarity to FXIa possessing 66% sequence identity, whereas sequence identity between PKa and the KLK family ranges from 30 to 36%.[71] This structural homology between PKa and coagulation factors such as FXIa, FXa, FIXa, FVIIa and thrombin causes many inhibitors designed for PKa to also show off-target effects in these related enzymes, largely stemming from a shared preference for arginine binding in the S1 binding site.[72]

1.4.1 Mechanism of Plasma Kallikrein

Mechanistically, chymotrypsin-like serine proteases, such as PKa, utilise a conserved nucleophilic serine residue to hydrolyse scissile amide bonds, cleaving substrates between the S1 and S1' subsites. Activation of the catalytic serine is achieved through a canonical system of amino acid residues within the active site, known as the Asp_{102}-His_{57}-Ser_{195} catalytic triad.[73] Such residues comprise a region of the protease domain known as the oxyanion hole, serving to stabilise transition states within the enzyme-substrate complex and to aid in nucleophilic attack by Ser_{195} (Figure 1.10).

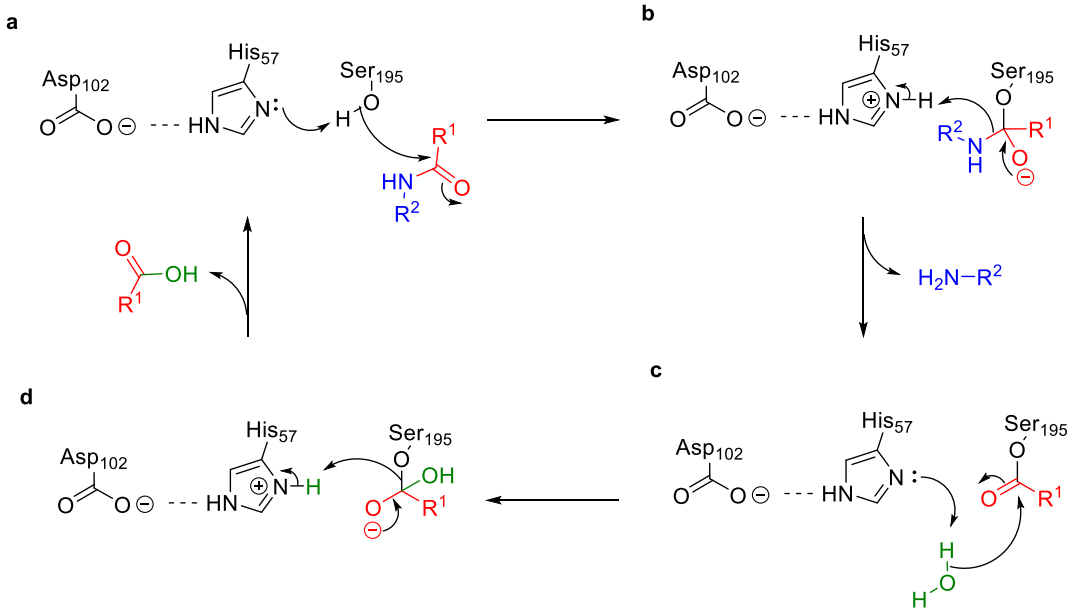

Figure 1.10. Representative mechanism of amide bond cleavage by Asp_{102}-His_{57}-Ser_{195} catalytic triad.

The Asp_{102} component of the catalytic triad exists to productively orient the imidazole ring of His_{57} with respect to Ser_{195}, as well as promoting increased basicity of the imidazole sp^2 nitrogen *via* hydrogen bonding of the Asp_{102} carboxylate to His_{57}, enabling deprotonation of Ser_{195} and subsequent nucleophilic attack of an amide carbonyl (Figure 1.10, a). Consequently, a tetrahedral intermediate is generated, the degradation of which is driven by removal of a proton from the imidazolium cation, releasing a free amine and in turn generating an *O*-acyl serine species (Figure 1.10, b). The basic nitrogen from the imidazole group of His_{57} then generates a hydroxide ion through deprotonation of a water molecule which attacks the carbonyl of the *O*-acyl Ser_{195} species (Figure 1.10, c). The resulting tetrahedral complex is cleaved from Ser_{195}, again driven by deprotonation of the charged imidazolium residue from His_{57}, enabling the release of a carboxylic acid and regeneration of the catalytic triad (Figure 1.10, d).[74–76]

1.4.2 Plasma Kallikrein Inhibitor Design

Figure 1.11 shows surface representations of the PKa proteolytic domain, including key residues and selectivity pockets. The naming of the selectivity pockets has been done according to the nomenclature of Schechter and Berger, where the region between S1 and S1' denotes the site of proteolytic cleavage, S1, S2 *etc.* denote subsites and P1, P2 *etc.* denotes the chemical group of a substrate or inhibitor which targets the corresponding subsite.[57,72,77]

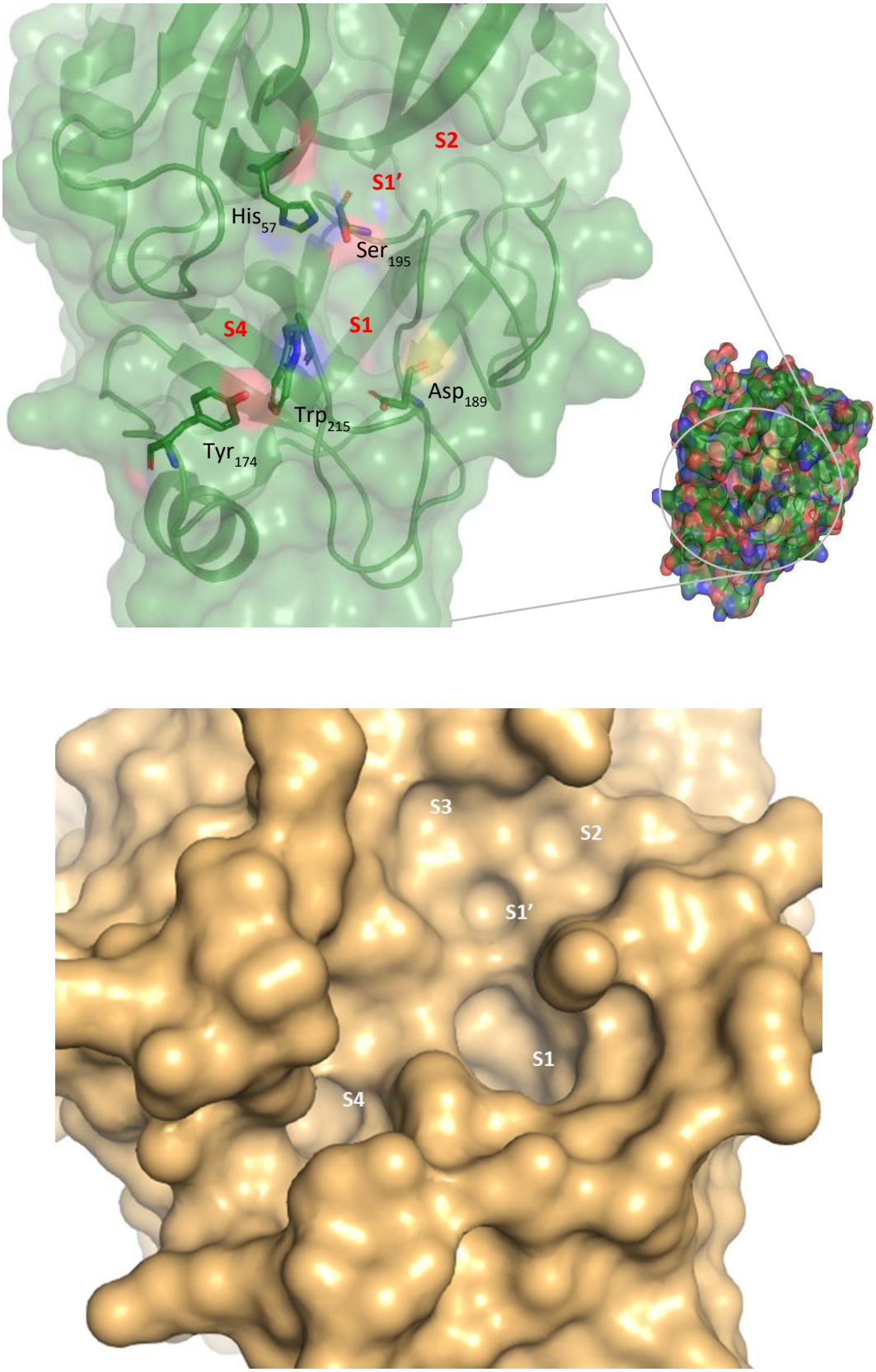

Figure 1.11. Surface models of PKa protease domain with labelling of key residues and selectivity sites (PDB6O1S)[64]

PKa inhibitors such as berotralstat **4** and sebetralstat **5**,[54,57] target the S1 and S4 pockets of PKa, linking the P1 and P4 fragments with a central bridging scaffold (Figure 1.12).

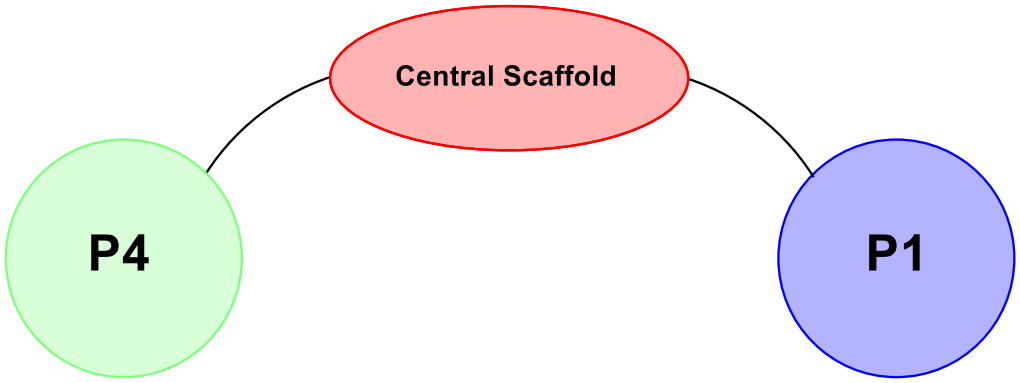

Figure 1.12. Representation of S1 and S4-targeting inhibitor design strategy

The appeal of this design strategy stems from the nature of the S1 and S4 pockets. Both of these pockets are comparatively deep in comparison to the S2 and S1' regions and contain residues that may be targeted using conventional medicinal chemistry strategy such as Asp_{189}, Tyr_{174} and Trp_{217}. Moreover, P4 binding groups are known to induce the S4 pocket *via* a conformational change in in the active site known as the 'Trp-flip', which possibly contributes towards rigidification of the PKa binding domain, reducing plasticity within the active site, potentially resulting in more favourable enzyme-inhibitor interaction.[78]

1.4.3 Basic S1-Binding Groups in PKa

The first structural elucidation of the PKa protease domain was achieved through crystallographic analysis of the PKa-benzamidine complex. Asp_{189} plays a critical role in recognising arginine residues from endogenous substrates within the S1 binding site and binds benzamidine **1** in an analogous mode (Figure 1.13).[70]

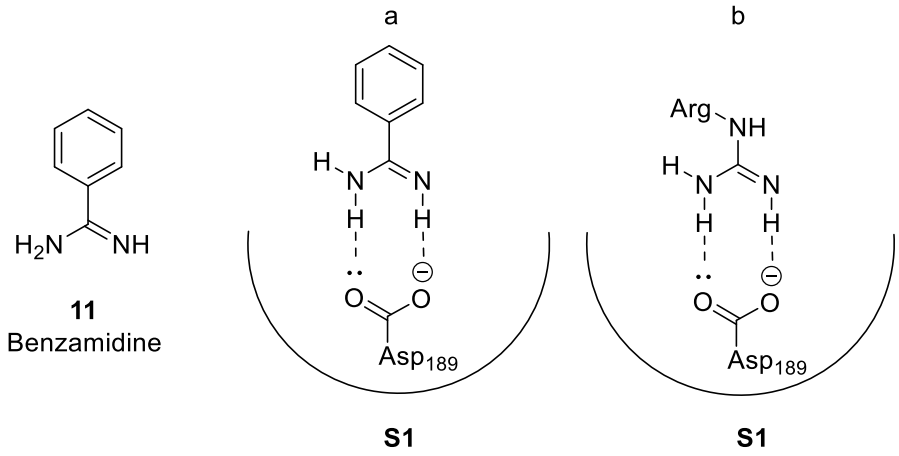

Figure 1.13. Representation of binding of a) benzamidine **11** and b) arginine residues to Asp_{189} in S1 binding site

As a result of this S1 binding character, many plasma kallikrein inhibitors have used basic P1 groups such as aminopyridine, benzylamine, benzamidine and guanidine to target the S1 site. An example of the use of basic S1 groups in PKa inhibitors can be seen in the development of avoralstat **12** and berotralstat **4**.

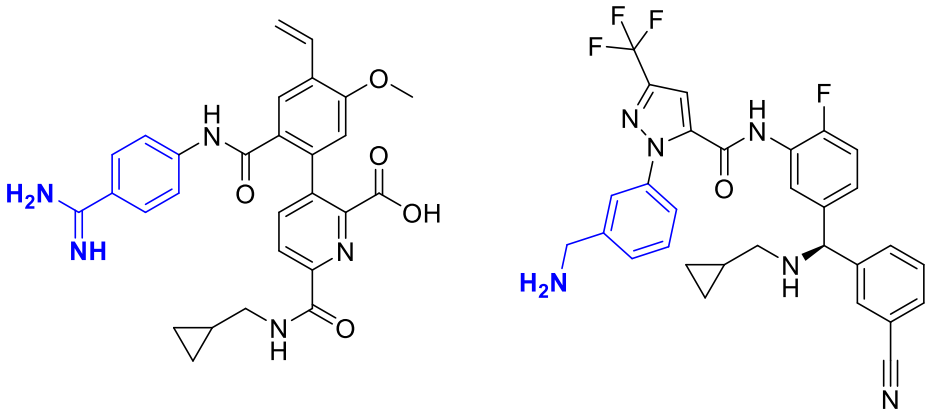

12

PKa K_i = 2.6 nM

4

PKa K_i = 4.4 nM

Figure 1.14. Structures of avoralstat and berotralstat, (P1 groups shown in blue).

In the cases of **12** and **4** the basic benzamidine or benzylamine groups, highlighted in blue, act as S1-binding groups in PKa (Figure 1.14), whilst the remaining portion of the molecule extends into the S1' region. Both compounds show comparable potency in PKa, **12** was discarded due to its poor oral bioavailability, a key challenge seen with the use of highly polar groups, due to their poor passive permeability and oral absorption. **4** showed enhanced oral bioavailability with respect to **12** due to the decreased basicity of benzylamine in comparison with benzamidine, resulting in improved solubility in **4** at pH 7.0, improving bioavailability.[54]

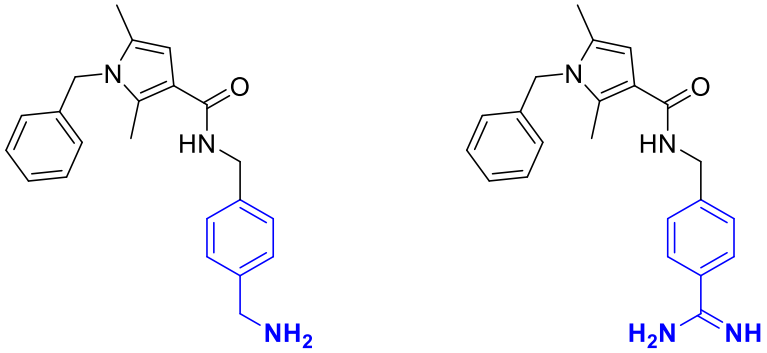

13

PKa IC_{50} = 3700 nM

Calculated pKa = 9.1

14

PKa IC_{50} = 5.5 nM

Calculated pKa = 11.6

Figure 1.15. Structures of benzylamine and benzamidine P1 compounds from development of sebetralstat, (P1 groups shown in blue).

Examples of basic P1 SAR can be seen in the development of sebetralstat **5**. During lead identification, it was seen that benzamidine exhibits roughly 1000-fold enhanced activity in PKa when comparing compounds **13** and **14**. All pKa calculations were carried out using ACD/Laboratories Percepta software (Figure 1.15).[57,79]

Further SAR studies compared the activity of a benzylamine P1 group **15** with weakly-basic aminoisoquinoline **16**, a bioisostere of benzamidine (Figure 1.16).

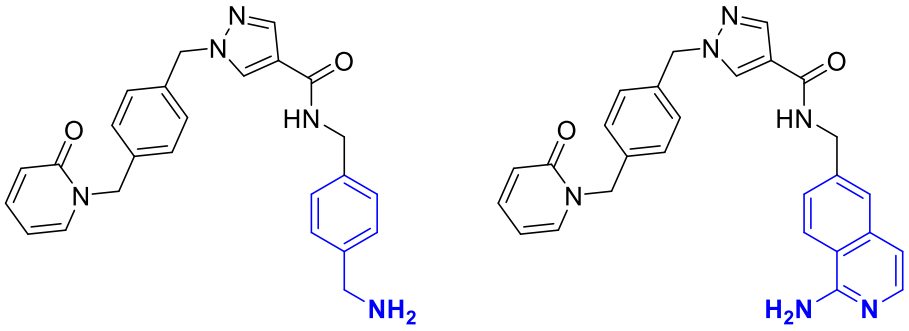

15

PKa IC_{50} = 4.4 nM

Calculated pKa = 9.1

16

PKa IC_{50} = 0.59 nM

Calculated pKa = 7.5

Figure 1.16. Structures of benzylamine and aminoisoquinoline P1 compounds from development of sebetralstat, (P1 groups shown in blue).

Both **15** and **16** contain basic P1 groups, shown in blue, and pyridone P4 groups joined by a pyrazole central scaffold. **16** shows approximately a 10-fold increase in PKa affinity with respect to **15**, due to the enhanced ability of aminoisoquinoline to bind Asp_{189} in an analogous mode to benzamidine as well as rigidification of the P1 group in comparison to benzylamine. Aminoisoquinoline shows decreased basicity with respect to benzamidine due to the incorporation of the amine into the aryl system. **16** showed poor membrane permeability, whilst subsequent aminoisoquinoline analogues of showed high internal clearance in human liver microsomes. Despite this, it was demonstrated that potent PKa inhibitors could be developed using mildly basic P1 groups.[57]

1.4.4 Non-basic S1-Binding Groups in PKa

In order to circumvent the issue of poor oral absorption associated with basic or highly polar groups in PKa inhibitors, there has been significant exploration into the identification of non-basic or 'neutral' P1 groups, shown in green.

3-Chlorophenyl is a known, albeit weak S1-binding fragment in PKa which appears in compounds **17** and **18** (Figure 1.17).[80]

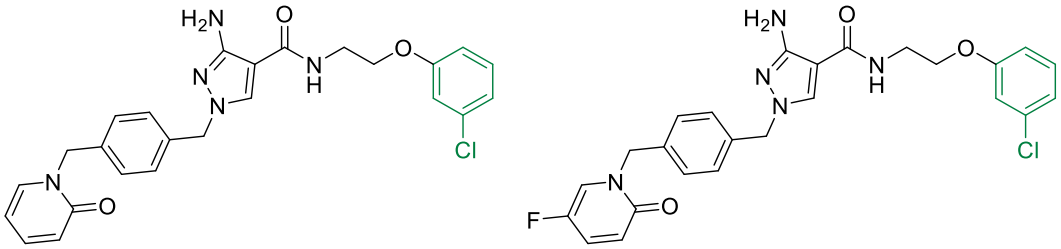

17

PKa IC_{50} = 2.9 nM

18

PKa IC_{50} = 6.2 nM

Figure 1.17. Structures of PKa inhibitors with 3-chlorophenyl P1 group (shown in green).

An aryl aminoethanol linkage connects the 3-chlorophenyl group of **17** and **18** to an aminooyrazole central scaffold leading to a pyridone P4 group. **17** and **18** demonstrated similar biological activities in PKa with a 10 000-fold preference for PKa against KLK1 and FXIa.

19 features a *p*-tolyl P1 group, which whilst highly lipophilic, demonstrates appreciable PKa activity (IC_{50} = 88 nM). The presence of the methyl group in this

case is thought to displace a water molecule bound to Asp_{189} in the S1 pocket, making the binding of the *p*-tolyl fragment entropically favoured (Figure 1.18).[81]

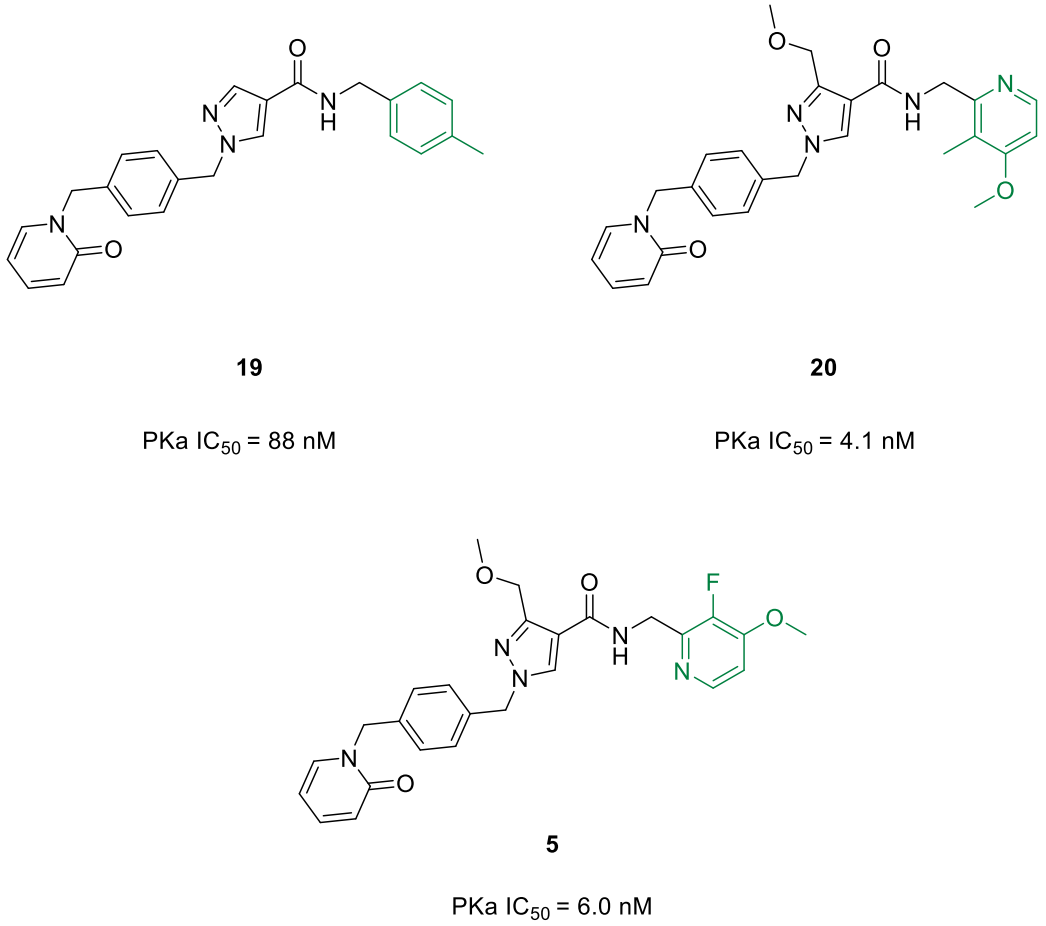

Figure 1.18. Structures of PKa inhibitors with non-basic monocyclic P1 groups, (shown in green).

20 includes a novel heterocyclic P1 group which elicits high levels of activity in PKa (IC_{50} = 4.1 nM). Sebetralstat **5**, also incorporates a novel monocyclic heterocycle as a P1 group which was selected for clinical trial advancement due to its low clearance and high oral bioavailability in rat studies . Additionally, **5** demonstrated high selectivity towards PKa when screened against related proteases, showing at least a 1600-fold preference for PKa.[57]

1.4.5 S4-binding Groups in PKa

P4 groups have the ability to induce the S4 pocket in PKa *via* a phenomenon known as the 'Trp$_{215}$ flip', arising from the induced-fit movement of Trp$_{215}$ upon binding of an active fragment. This forms an induced hydrophobic pocket enabling a ligand to make π-stacking interactions with Tyr$_{174}$ and Trp$_{215}$, in addition to hydrogen bonding with Gly$_{99}$.[70] Binding to the S4 region in addition to the S1 pocket therefore provides a valuable foothold, enabling the development of highly potent inhibitors.

With π-stacking being the most common mode of binding for inhibitors targeting the S4 pocket, aryl groups often feature in P4 fragments, shown in red.

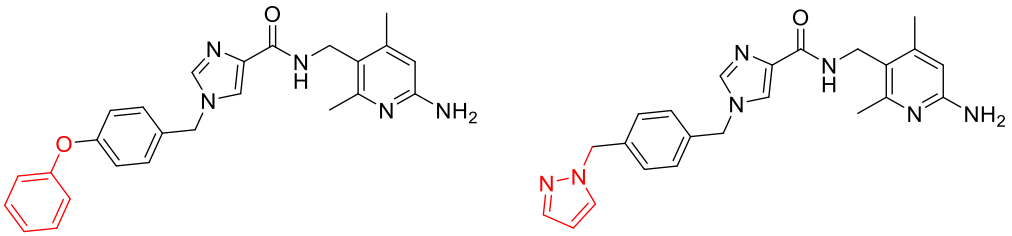

21

PKa IC_{50} = 9 nM

22

PKa IC_{50} = 0.2 nM

Figure 1.19. PKa inhibitors including *O*-Phenyl and pyrazole P4 groups, (shown in red).

Replacement of the P4 aryl ether in **21** for a benzylpyrazole group in **22** results in significantly increased PKa activity due to its smaller size and increased π-density with respect to *O*-phenyl (Figure 1.19).[82]

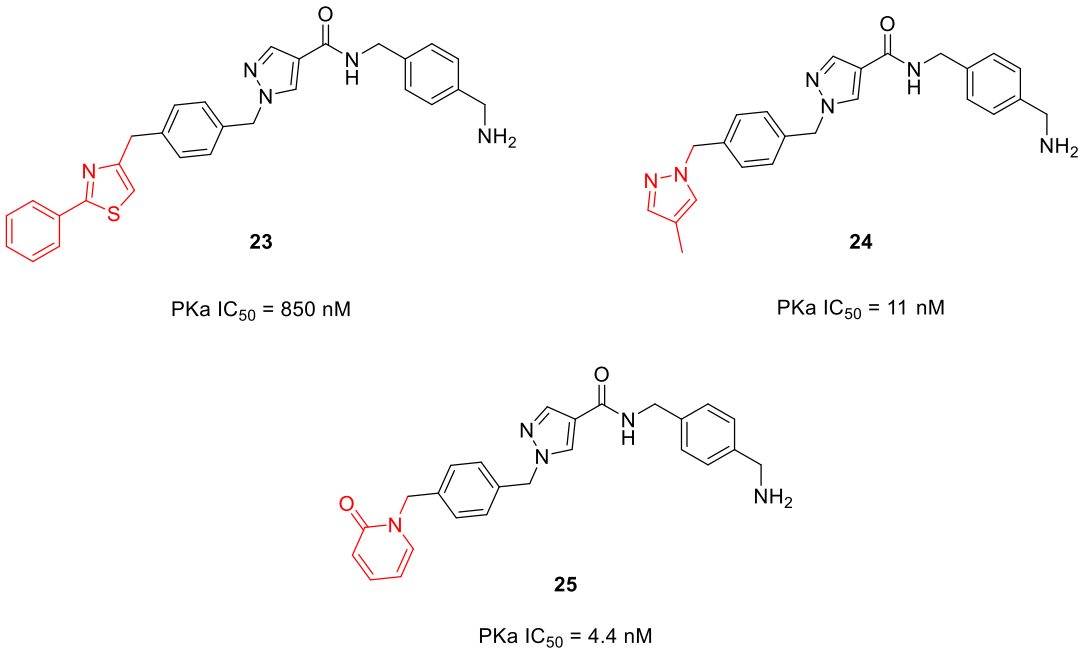

Figure 1.20. P4 groups used in the development of Sebetralstat, (shown in red).

Multiple P4 groups were explored in the development of Sebetralstat **5** (Figure 1.20). **23** used a phenylthiazole group to target the S4 pocket, this analogue showed moderate activity in PKa (IC_{50} = 850 nM). Changing the phenylthiazole fragment for methylpyrazole in **24** showed a drastic improvement in IC_{50} potency of around 80-fold. Pyridone was found to be the most biologically active P4 group in **25**, further advancing IC_{50} potency to 4.4 nM. Crystal structure analysis of the binding of **5** in PKa shows π-stacking of the pyridone P4 group with Tyr_{174} (Figure 1.21).

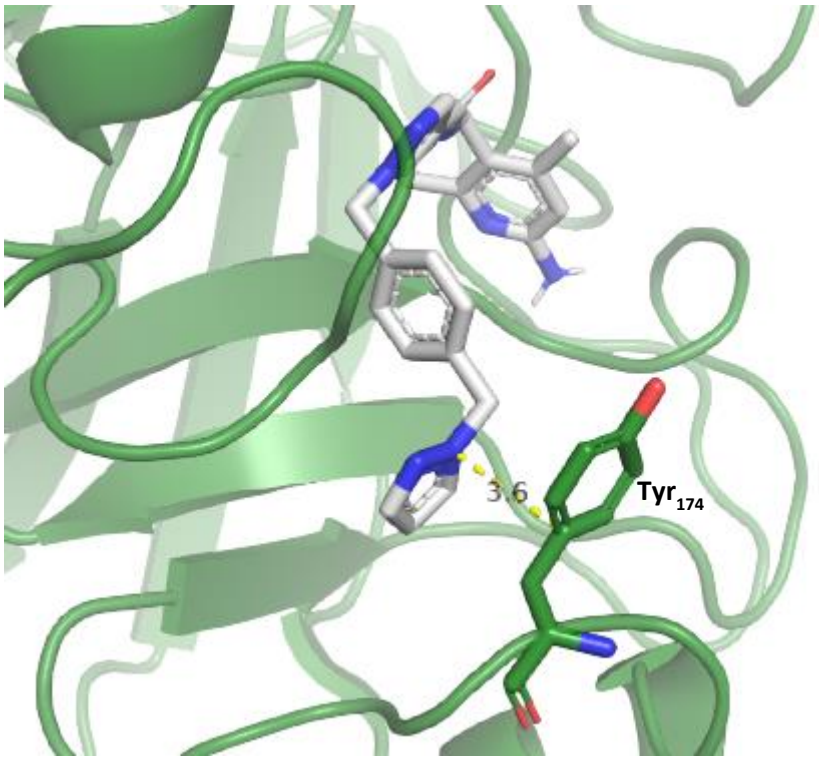

Figure 1.21. Depiction of π-stacking between P4 pyrazole of **10** with Tyr_{174} in PKa active site showing measured distance of 3.6 Å (PDB6O1S)

1.5 Targeted Covalent Inhibitors (TCIs)

Traditional small molecule drug design generally focusses on the production of noncovalent, reversibly binding ligands as equilibrium modulators of biological receptors. Such reversible binding states are fast, limiting the maximum duration of a therapeutic response.[83] Maximising the duration of binding between a ligand and its target receptor can therefore promote a prolonged physiological response. Targeted covalent inhibitors (TCIs) bind covalently to specific target residues within a biological receptor in two steps; first an equilibrium step, forming a noncovalent enzyme inhibitor complex (EIC), and secondly covalent bond formation with the target residue, with the final state often being irreversible (Figure 1.22). The therapeutic benefit of TCIs over conventional inhibitors is the prolonged duration of action and high potency, owing to covalent modification of the target receptor.[84]

a) Noncovalent (reversible) inhibition

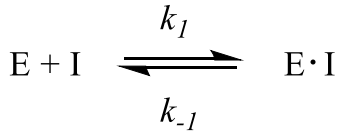

b) Covalent (irreversible) inhibition

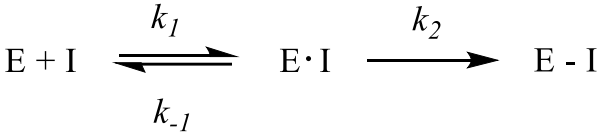

c) Covalent (reversible) inhibition

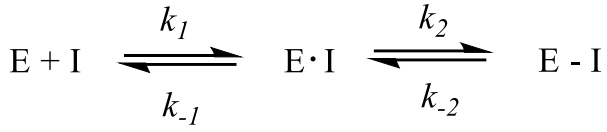

***Figure 1.22*.** Equations representing a) noncovalent inhibition, b) irreversible covalent inhibition and c) reversible covalent inhibition.

The kinetic rate constant k_1 is often used to describe association of an inhibitor to an enzyme to form an enzyme-inhibitor complex (E·I), whilst K_{-1} describes the corresponding inhibitor dissociation. In the case of irreversible covalent inhibitors, a second, nonequilibrium step exists to describe the formation of a covalent enzyme-inhibitor complex (E-I), often described by the rate constant k_2 or k_{inact}, denoting inactivation of the enzyme. Reversible covalent inhibition is another possible mode of binding where the second step is an equilibrium step and unbinding of the bound covalent species is denoted by the rate constant k_{-2}.

Covalent inhibitors first emerged in medicine in the 1890s with the discovery of aspirin, later realised to be responsible for the selective acylation of Ser_{530} in

prostaglandin endoperoxide (PGH) synthase-1.[85] At present, covalent inhibitors comprise roughly 30% of all marketed drugs.[83] Key advantages in the development of covalent inhibitors as pharmaceuticals include; improved efficiency and lower dosing due to prolonged physiological action, increased compliance due to less frequent dosing, reduced possibility of patients developing drug resistance and possibility of targeting shallow binding sites that are difficult to occupy with conventional inhibitors.[86]

Alongside these clear advantages, there exist numerous disadvantages in the development of TCIs, for example, toxicity and hypersensitivity are frequent concerns due to potential off-target covalent interactions. Additionally, TCIs may not be suitable for targeting biological receptors that are rapidly turned over or degraded.[83,87] Another challenge in the design of TCIs is warhead selection to elicit the appropriate level of reactivity in the desired target, whilst minimising off-target effects.

1.5.1 Examples of Covalent Inhibition in Serine Proteases

A warhead is a reactive group strategically installed onto a reversible ligand, targeting a biological receptor, with the intention of facilitating specific covalent modification of a target residue.[88] Generally, covalent warheads feature electrophilic groups, aiming to bind nucleophilic residues within the desired target, however the use of highly reactive electrophiles is discouraged due to toxicity concerns. Consequently, a selective covalent inhibitor must exhibit appreciable noncovalent affinity (k_1) to ensure appropriate residence time is achieved within the desired target, whilst the reaction rate of the bound inhibitor (k_{inact}) must be substantial enough to ensure likelihood of covalent bond formation within the lifetime of the noncovalent complex. Since highly reactive electrophiles must be avoided, this reaction rate must be achieved by optimal positioning of the electrophilic warhead, relative to the target nucleophilic residue.[89]

1.5.1.1 Acylating Agents

The transfer of an acyl group from an inhibitor to the serine oxyanion within a serine protease is a common method of covalent modification (Scheme 1.1). This method relies on tuning the acyl group to be cleaved within the target protein without reacting with other species in the endogenous environment.

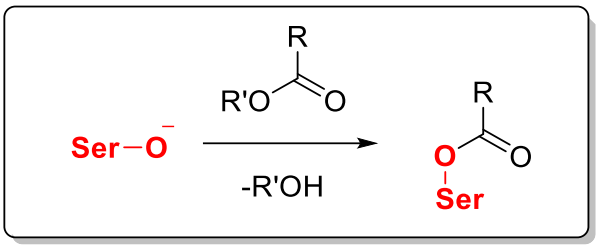

Scheme 1.1. Representative example of serine acyl transfer mechanism

A key benefit of this approach is the potential for hydrolysis of the Ser-acyl complex under biological conditions, regenerating the apo-enzyme. This may limit the toxicity profile of such compounds due to slow reversibility, whilst eliciting potency and duration of action concomitant with that of a covalent inhibitor.[90]

Literature examples of serine-acylating compounds include inhibitors of fatty acid amide hydrolase (FAAH) **26** and coagulation Factor XIIa **27** (Figure 1.23).[91,92]

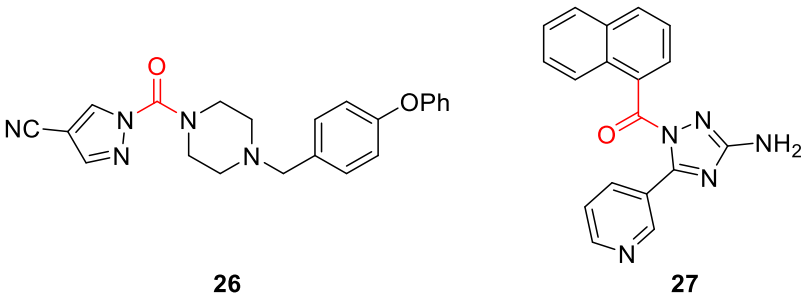

26 **27**

Figure 1.23. Structures of acylating agents of FAAH and FXIIa.

26 selectively inhibits FAAH (K_i = 0.1 nM after 3 hours preincubation), with intended application in modulating endocannabinoid signalling for analgesic purposes. It was also demonstrated that tuning the nature of the acyl group

altered reactivity (amide > carbamate > urea) and including an electron withdrawing pyrazole C4 substituent (CN > H > Me) increased the reactivity of **26** towards FAAH. Curiously, the *N*-acyl pyrazole urea scaffold showed higher inhibition that the intrinsically more reactive amide analogues, suggesting a unique enzyme reaction taking place.[92]

27 was discovered to be a potent acylating agent of FXIIa through exploration of numerous *N*-triazole acyl substituents, concluding that 1-naphthyl showed the highest potency (29 nM after 1 hour preincubation). It was shown by mass spectrometry analysis that the resulting naphthoyl- serine complex could be hydrolysed by desalination of the assay buffer, regenerating FXIIa.[93]

1.5.1.2 1,2-Addition

The incorporation of electrophilic ketones and nitriles into active pharmacophores is a strategy for covalent modification of serine proteases. Examples include α-ketoamide and reactive nitrile moieties (Scheme 1.2).

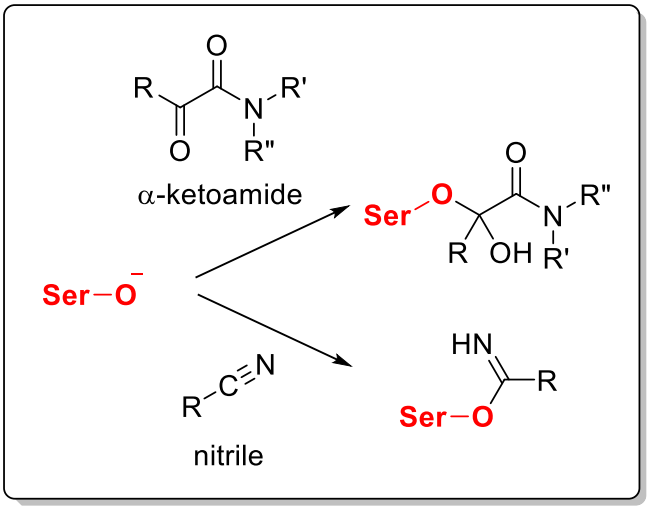

Scheme 1.2. Representative example of α-ketoamide moiety as a serine covalent trap

The strong electrophilic nature of the α-ketoamide carbonyl is induced by the presence of the adjacent amide, withdrawing electron density from the sp^2 carbon of the reactive carbonyl. The serine-bound complex features a hemiacetal group, which may interconvert with the α-ketoamide, making this a reversible process.[94]

Telaprevir **28** is an example of a covalent serine protease inhibitor which utilises the α-ketoamide warhead. Intended for the treatment of hepatitis C, **28** inhibits the HCV NS3-4A protease (K_i = 0.007 μM), involved in viral genome replication (Figure 1.24).[95,96]

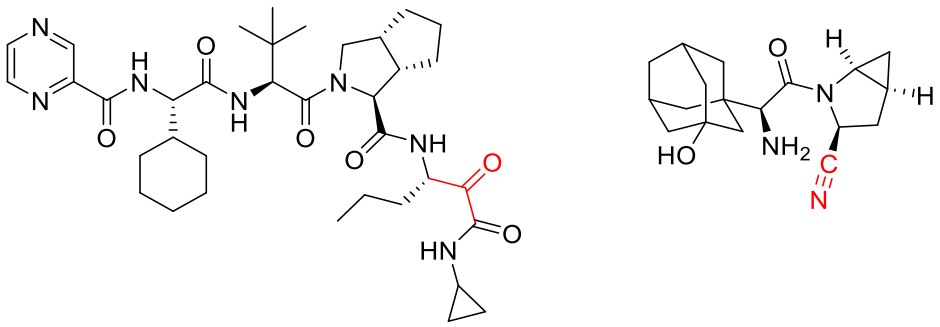

28 **29**

Figure 1.24. Structures of telaprevir and saxagliptin.

The nitrile group is also known as a warhead for serine proteases (Scheme 1.2). The electrophilic nature of the nitrile *sp* carbon may permit the addition of a nucleophile to reversibly generate an imine, which may be stabilised by other local residues.

Saxagliptin **29** is a medication approved for the treatment of type 2 diabetes targeting the dipeptidyl peptidase IV (DPP-IV) (K_i = 0.6 nM after 30 minutes incubation). Inhibition of DPP-IV reduces the release of glucagon-like peptide I (GLP-I), reducing blood glucose levels (Figure 1.24).[97]

1.5.1.3 Sulfur (VI)-fluoride Exchange

Sulfonyl fluorides have emerged as highly reactive warheads for the sulfonylation of various nucleophilic residues such as serine, lysine, threonine and histidine in target proteins (Scheme 1.3).[88]

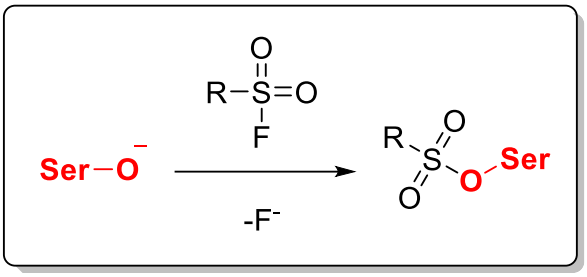

Scheme 1.3. Representation of sulfonyl fluorides as serine protease warheads

With respect to serine proteases, sulfonyl fluorides have been reported as irreversible inhibitors of chymotrypsin. **30** was discovered through screening of various amino-acid derived scaffolds incorporating the sulfonyl fluoride warhead (Figure 1.25)

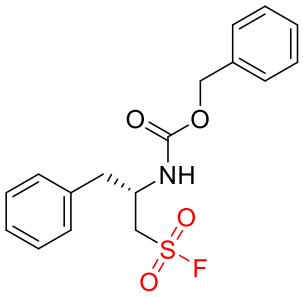

30

Figure 1.25. Structure of sulfonyl fluoride covalent inhibitor of chymotrypsin.

It was determined that the phenylalanyl derived scaffold showed the highest activity in chymotrypsin (K_i = 22 μM, K_{inact} = 0.33 min^{-1}). The described β-aminoethanesulfonyl fluorides of this type all exhibited irreversible covalent inhibition. It was postulated that varying the *N*-substituent for a peptide group may improve the K_i value.[98]

1.5.1.4 Alkylating Agents

Peptidyl halomethyl ketones emerged amongst the first covalent modulators of serine proteases and the first site-directed irreversible inhibitors of any protein.[99] Interestingly, halomethyl ketones were originally thought to be histidine specific binders, however crystallographic evidence later showed halomethyl ketones to be transition-state irreversible inhibitors[100] (Scheme 1.4).

Rather than displacing the halomethyl ketone halogen atom, Ser_{195} forms a tetrahedral adduct by binding to the carbonyl on account of its 'harder' electrophilicity. The hemiacetal adduct then forms an epoxide *via* intramolecular displacement of the halogen. The nearby His_{57} residue opens the epoxide, forming an irreversible covalent adduct between enzyme and inhibitor.

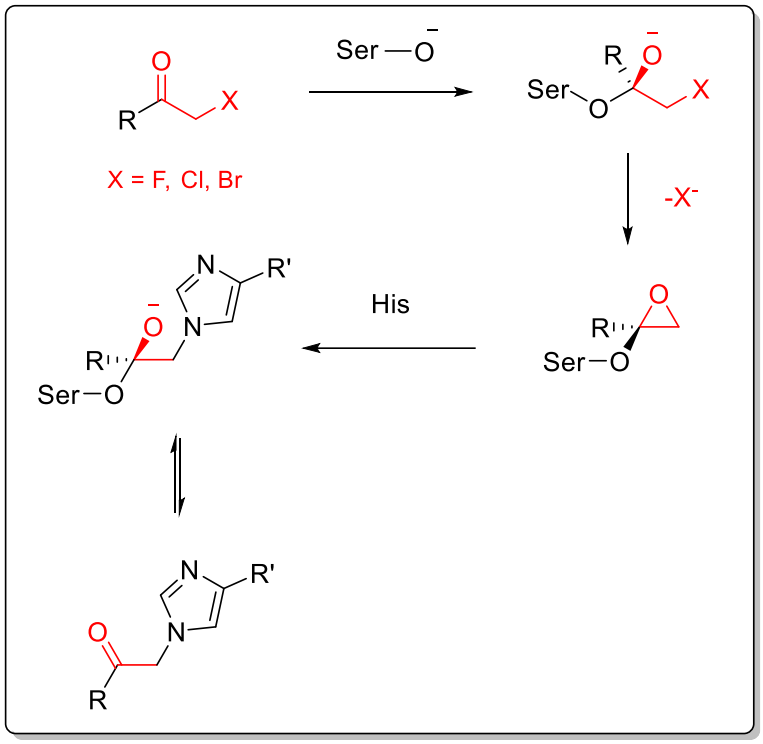

Scheme 1.4. Proposed mechanism of covalent inhibition of serine proteases by halomethyl ketones[101]

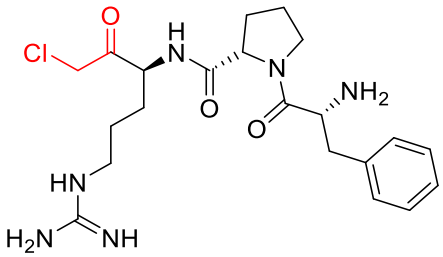

31

Figure 1.26. Structure of PPACK

D-Phe-Pro-Arg-CH_2Cl (PPACK) **31** was initially developed as a covalent inhibitor of thrombin and its mode of binding was confirmed by crystallographic analysis.[102] It was later determined that PPACK acted as a potent broad spectrum inhibitor of

multiple trypsin-like serine proteases such as plasmin, plasma kallikrein, urokinase, FXa and trypsin (Figure 1.26), (Table 1.1).[101,103]

Table 1.1. Second-order rate constants of reaction of **31** with various serine proteases reported by Powers *et al*.[104]

Inhibitor	k_2/K_i ($M^{-1}s^{-1}$)					
	plasmin	PKa	thrombin	urokinase	FXa	trypsin
31	1000	800	9600000	1000	2300	3500000

The majority of second-order rate constants for the reaction of **31** with proteases in Table 1.1 lie in the 10^3 $M^{-1}s^{-1}$ range, however increased activity is observed for thrombin and trypsin in the 10^6 $M^{-1}s^{-1}$ range.

1.5.1.5 Boronic Acids and Boronates

Boron is a highly useful element in organic chemistry, owing to its vacant *p*-orbital enabling acceptance of an electron pair from a Lewis base, forming a Lewis adduct. This Lewis acidic character may also be exploited in a biological setting.[105] Many bioactive molecules incorporate boronic acid or organoboronate moieties in order to target key nucleophilic residues within biological receptors. A distinctive property of boron-containing covalent warheads in comparison with other electrophiles used in medicinal chemistry, is the ability to display multiple coordination modes with biological targets. For example, boron may bind to a target residue to form either a neutral trigonal planar, or anionic tetrahedral complex (Scheme 1.5). With a multitude of accessible interaction modes, boron shows utility as a flexible anchoring element that can adapt to structural changes upon binding.

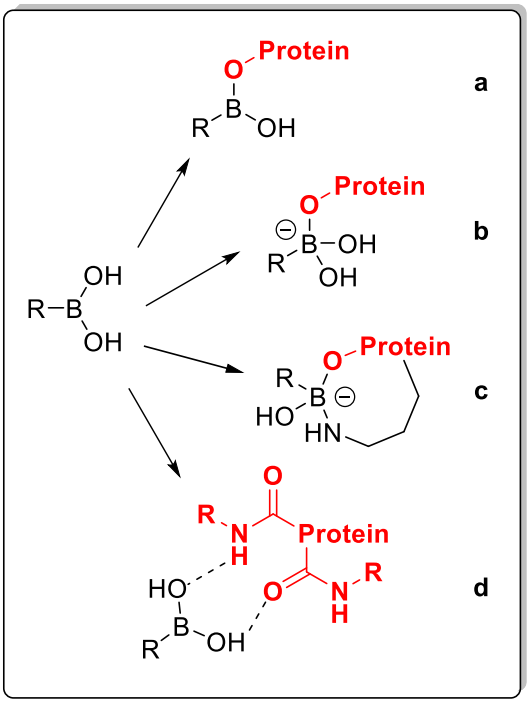

Scheme 1.5. Representation of different binding modes of boronic acids during biological target engagement. **a –** trigonal covalent, **b –** tetragonal covalent (O, O, O), **c –** tetragonal covalent (O, O, N), **d** – trigonal noncovalent[105,106]

Initially, boron was incorporated into peptide substrates *via* replacement of the scissile amide bond with a boronic acid moiety, generating a peptidyl boronic acid. These compounds have been used as peptidomimetic substrates, aiming to covalently target catalytic residues within proteases. For example, Bortezomib **32** is a peptidyl boronic acid inhibitor of the 26S proteasome, a multicatalytic enzyme that degrades abnormal or misfolded proteins targeted for destruction, for use in the treatment of multiple myeloma in combination with other chemotherapy agents.[107]

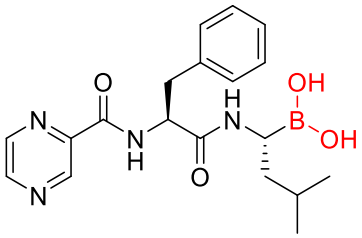

32

Figure 1.27. Structure of bortezomib.

The boronic acid motif of bortezomib targets a catalytic threonine residue of the 26S proteosome, while a backbone amide residue stabilises the oxyanion hole by hydrogen-bridging to one of the acidic boronate hydroxyl groups. The tetrahedral boronate adduct is further stabilized by a second acidic boronate hydroxyl moiety, which hydrogen-bridges the *N*-terminal threonine amine atom, functioning as a catalytic proton acceptor (Figure 1.27).[108]

One of the specific actions of bortezomib is to inhibit key cell survival pathways to destroy malignant myeloma cells. Even in low nanomolar concentrations, it has been found that bortezomib is effective in the sequestration of transcription of genes involved in such cell survival pathways. Proteasome inhibition by bortezomib has also been shown to upregulate pro-apoptotic genes and downregulate anti-apoptotic genes.[109,110]

Taniborbactam **33** was discovered as a pharmaceutical means of circumventing an antibiotic resistance mechanism in Gram-negative bacteria, to be administered in combination with β-lactam antibiotics.

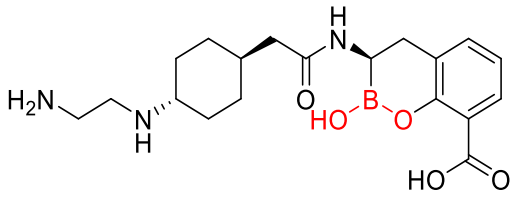

33

Figure 1.28. Structure of taniborbactam.

The continued use of β-lactam antibiotics has caused the emergence of β-lactam resistance in certain pathogens, taking the form of β-lactamase enzymes, responsible for the cleavage and subsequent inactivation of the β-lactam motif in antibiotic agents such as penicillins, cephalosporins and monobactams.[111] Through inhibition of these β-lactamases, this evolved resistance mechanism may be circumvented, enabling effective action of the antibiotic agent. Taniborbactam, **33** (Figure 1.28), is an example of a β-lactamase inhibitor which utilises a boronate motif in order to covalently bind serine β-lactamases, forming a tetrahedral adduct. Taniborbactam also acts as a noncovalent inhibitor of zinc metallo-β-lactamases *via* coordination of zinc ions to the electronegative oxygen atoms of the boronate motif. These combined mechanisms of action enable for pan-spectrum anti- β-lactamase activity.[112]

The *N*-(2-aminoethyl)-cyclohexylamine side chain of **33** plays an important role in in broad spectrum inhibition of β-lactamases in addition to facilitating outer membrane permeability and periplasmic accumulation in Gram-negative bacteria. Crystallographic studies have revealed that the bicyclic boronate motif functions *via* mimicking the tetrahedral transition states of both the serine-based and zinc-

based hydrolytic processes. **33** showed high potency across a large range of bacterial cells and demonstrated selectivity towards bacterial enzymes and non-toxicity towards mammalian cells. As a result, taniborbactam, is the first pan-spectrum β-lactamase inhibitor to enter clinical development.[111,113]

Other uses of boronates in clinical applications include the development of topical anti-fungal agent tavaborole **34** developed for the treatment of onychomycosis, a common fungal infection of the nails, especially prevalent in diabetic and elderly patients (Figure 1.29).[114,115]

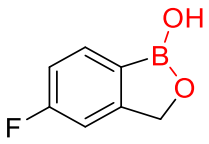

34

Figure 1.29. Structure of tavaborole.

Mechanistically, **34** acts *via* targeting dermatophytes, fungi that dwell on hair skin and nails. Specifically, **34** exerts anti-fungal activity through inhibition of the enzyme yeast cytoplasmic leucyl-aminoacyl transfer RNA (tRNA) synthetase, a key enzyme participating in fungal protein synthesis, inhibiting fungal reproduction.[114]

Structure-activity analysis reveals that a stable adduct is formed between the boron of tavaborole and the terminal adenosine of the target enzyme, forming a tetrahedral complex. Moreover, it was demonstrated that replacement the boron of **34** with a carbon atom removed all biological activity.[116,117]

Compound **35** was discovered as a potent, non-selective inhibitor of PKa (IC_{50} = 45 nM), FXIIa (IC_{50} = 190 nM), trypsin (IC_{50} = 52 nM), plasmin (IC_{50} = 394 nM) and FXIa (IC_{50} = 13 nM). crystallographic data of the complex of **35** with FXIIa revealed that the boronic acid group forms a tetrahedral adduct with Ser_{195} (Figure 1.30).[118]

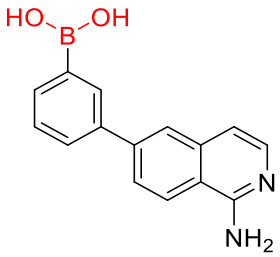

35

Figure 1.30. Structure of novel boronic acid inhibitor of PKa.

Incorporating an aryl boronic acid onto an aminoisoquinoline S1 scaffold, **35** achieves covalent inhibition of PKa. **35** appears to be the only boron-containing literature covalent inhibitor of PKa.

1.5.2 Reactivities of Serine-binding Covalent Warheads

Generally, covalent inhibitors of trypsin-like serine proteases aim to target the catalytic Ser_{195} residue. Attempting to characterise the reactivity of different fragments against a free serine molecule offers a useful tool in warhead through gaining understanding of the order of electrophilicity of different functional groups. Utilising NMR reaction monitoring, a kinetic assay was used in order to

evaluate the difference in reactivity of various known warheads with respect to a protected serine molecule **36** in phosphate buffered saline (PBS) solution (Figure 1.31).[119]

This study found 6-aminopenicillic acid **37** to be the weakest electrophile of the group that was screened with no observable covalent binding to serine, whilst this reaction is known to take place *in vivo*, specific conditions are required for serine-β-lactam binding with respect to pH and other molecular components, not mimicked by the assay.[120]

Other weaker electrophiles included Michael acceptors acrylamide **38** and vinyl-phenyl-ketone **41**, displaying steady covalent bond formation with the serine nucleophile, whilst showing drastically higher reactivity towards the softer equivalent cysteine nucleophile. Vinyl sulfonamide **40** also showed appreciable reactivity towards **36**, however its reaction with the equivalent cysteine nucleophile was at least two orders of magnitude greater than for serine. Lactam **39** shows steady covalent binding towards **36** due to its conformational restriction allowing the carbonyl to allow as an electrophile, however this reaction is fully reversible, reducing the overall rate of covalent binding. The nitrile warhead of **42** is highly electrophilic due to adjacent electron-withdrawing pyrimidyl heteroatoms, however, elicits a reversible reaction with **36,** slowing the rate of binding. Alkynylphenylketone **43** acts a Michael acceptor, showing better kinetic binding to the protected serine with respect to **41** as the alkyne group is a harder electrophile than the equivalent alkene. β-Lactam **44** shows greatly improved kinetic binding than its structural isomer **39** as **44** is a tertiary amide it is more

likely to trap the covalent adduct, resulting in lower reversibility. Sulfonyl fluoride **45** is a potent electrophile, owing to the electronegative properties of fluorine rendering it a strong leaving group, enabling sulfonylation of target residues, hence showed high reactivity with respect to **36**. Unlike other Michael acceptors in this study, **46** showed markedly enhanced reactivity towards the nucleophilic serine this may be due to protonation of the dimethylamino- nitrogen at physiological pH, increasing electrophilicity of the double bond or enabling more facile deprotonation of the serine hydroxyl. This effect from the dimethylamino-nitrogen showed similar binding kinetics between serine and cysteine with respect to **36**. Benzoxaborole **47** showed the highest reactivity of any covalent fragment in this screen, as a strong Lewis acid, boron has oxophilic properties enabling binding of the serine oxyanion to generate a stable boronate anion complex.

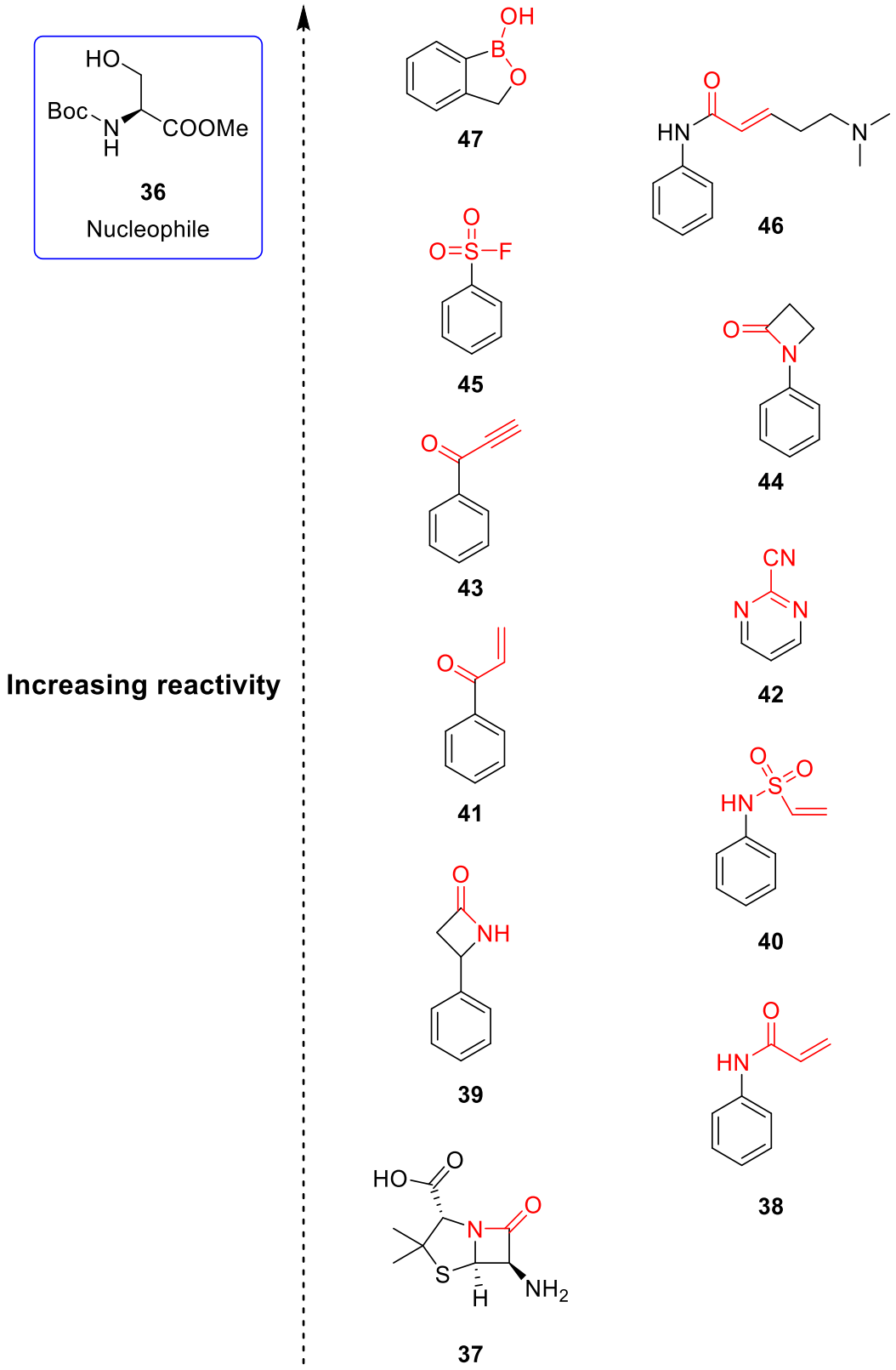

Figure 1.31. Assessment of reactivities of various covalent, serine-binding fragments with electrophilic moieties shown in red.[119]

1.6 Summary

HAE is a disease with unmet clinical need with respect to available treatments. Whilst small molecule prophylactic treatments are emerging onto the market, higher potency prophylactics may have the benefit of lower effective dose and/or less frequent need for administration. In this work, covalent inhibitors of PKa are examined as possible progenitors to more effective prophylactic treatments for HAE.

Numerous reactive chemical entities or 'warheads' are at the disposal of the medicinal chemist for the targeting of nucleophilic residues within biological targets. The selection of a warhead in the design of a covalent biological receptor modulator relies on factors including ease of incorporation of the warhead into a given scaffold, spatial arrangement of the warhead with respect to the target residue, and ultimately, observed biological potency.

Of the serine protease-specific warheads discussed in this chapter, those containing boronic acid or boronate motifs are of particular interest due to the proven efficacy of such warheads in serine proteases and their high reactivity towards serine. Accordingly, the design and synthesis of boronate-containing inhibitors of PKa is a key theme of this work.

1.7 Project Hypothesis and Aims

1.7.1 Hypothesis

Covalent warheads have been incorporated into myriad scaffolds in order to maximise both potency and physiological duration of action in the development of pharmaceuticals.[87] To date, there are no literature examples of selective covalent inhibitors of PKa, possibly due to the strong homology of PKa with related proteases such as thrombin, FXa and FXIa. Introduction of covalent warheads to scaffolds which target PKa may have the potential to produce highly potent PKa inhibitors with a view to establish more effective and lower dosage treatments for HAE.

Key aims of the project included development of potent boronate-derived covalent inhibitors of PKa, building selectivity into these structures *via* targeting the S4 pocket of PKa, and assessment of the activity and viability of these compounds, using a suite of *in vitro* and *in vivo* assays. Specifically, these objectives are outlined below:

- Identification, optimisation and comparison of boronate covalent inhibitors of PKa through determination of *in vitro* IC_{50} values.
- Evaluation of covalent biding of active compounds *via* time-dependent IC_{50} kinetics, jump dilution assays, and noncovalent matched pair activity comparison.
- Obtaining X-ray crystal structure of key compounds to assess binding modality.

- Screening of active compounds in PKa-related proteases such as FXIIa, FXIa, thrombin, plasmin and trypsin to gain insights into PKa specificity of active compounds.
- Placement of selected compounds into an *in vivo* model to assess potential pharmacological viability of identified covalent inhibitors in living systems.
- Exploring variation of warheads to compare and contrast against efficacy of boronate warhead in PKa.

Initial explorations focussed on examination of the crystal structure of **10** bound with PKa (PDB 6O1S)[64] (Figure 1.32). Upon inspection of the binding position of **10** it is apparent that the benzylic carbon extending from the P1 fragment (highlighted in red) sits directly adjacent to Ser_{195}. Accordingly, it was postulated that the installation of a boronate warhead at this position could result in covalent engagement of the catalytic serine residue.

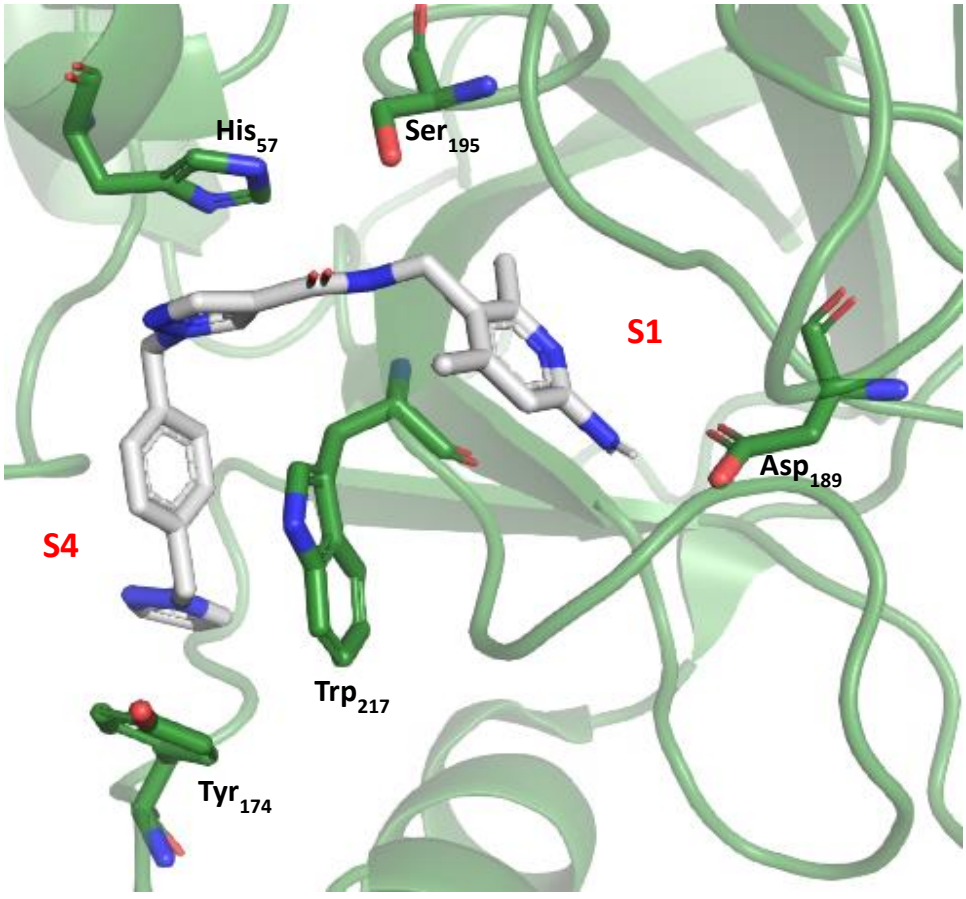

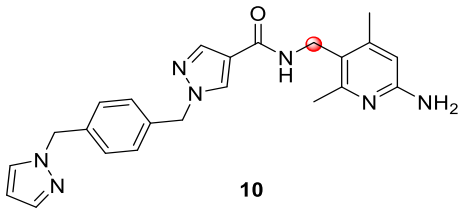

10

Figure 1.32. Binding pose of **10** in PKa active site (PDB 6O1S).[64]

A working model was established from truncation of **10** and replacement of the basic aminopyridine P1 group with 3-chlorophenyl, whilst keeping the central pyrazole linking moiety, (compound **48**) for initial synthetic ease and due to the possible incompatibility of nucleophilic functional groups with boron-containing molecules (Figure 1.33).

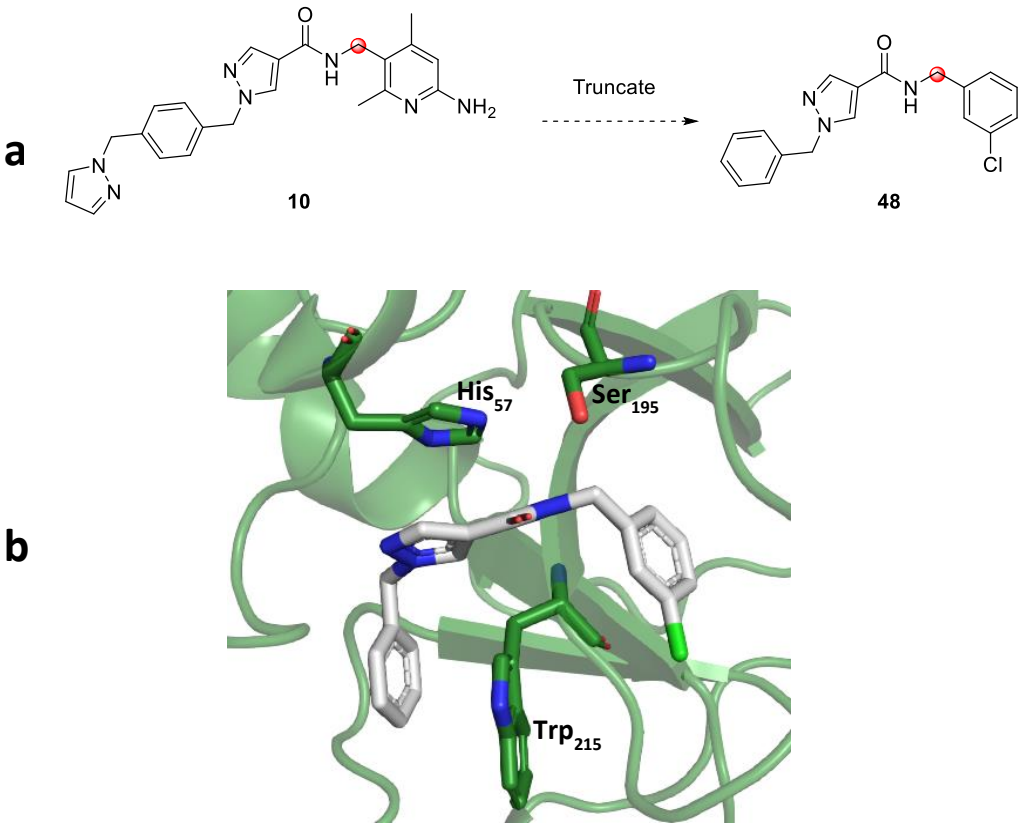

Figure 1.33. a) Truncation of **10** to non-basic P1 compound **48** b) Docking of **48** into PDB 6O1S crystal structure using OpenEye 'hybrid' docking.[121]

Molecular docking of **48** into a PKa model from PDB 6O1S showed that the close positioning of the α-benzylic carbon relative to the position of Ser_{195} was retained.

Consequently, **48** was used as an initial scaffold to explore synthetic and pharmacological viability of installing a boron warhead at the highlighted α-benzylic carbon.

1.7.2 Discovery of α-Amidobenzylboronates as Highly Potent and Selective Covalent Inhibitors of Plasma Kallikrein

Utilising the chemistry of boron (*vide infra*), it is possible to perform homologation reactions on arylboronic esters to access highly functionalised α-substituted benzyl species. Homologation of monocyclic aryl P1 fragments containing a boronic ester functionality enabled the synthesis of an α-amino- substituted benzylboronate. Amide coupling of this fragment to a central scaffold bearing a carboxylic acid and a P4 fragment produced a series of α-amidobenzylboronates, the biological activities of which were assessed against PKa amongst other related proteases (Scheme 1.6).

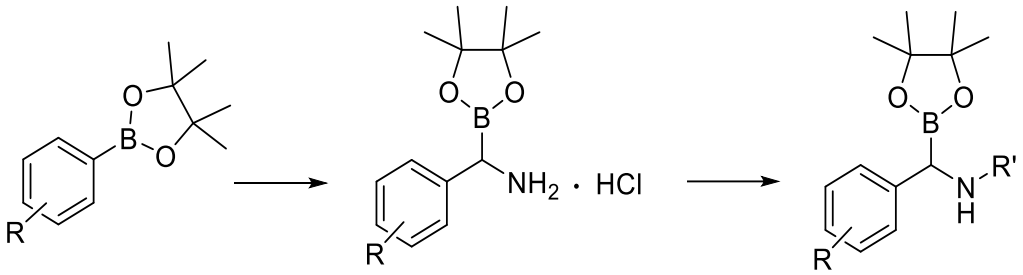

Scheme 1.6. Planned route to access α-amidobenzylboronates.

Compound potency against PKa and related proteases was evaluated through the use of a fluorescence assay. Validation of covalent binding of compounds synthesised in this work was evaluated through the use of jump-dilution assays, as well as through comparison of potency and binding kinetics with noncovalent matched pairs.

The development of synthetic methods for the synthesis and SAR of α-amidobenzylboronates and their matched pairs, as well as pharmacological evaluation of these compounds will be described in **Chapter 2**.

1.7.3 Synthesis and Biological Evaluation of β-Ketoboronates as Inhibitors of Plasma Kallikrein

A key challenge in the synthesis and handling of α-amidobenzylboronates is the tendency of these compounds to decompose *via* protodeborylation under acidic conditions and heat. A strategy to attempt to circumvent this problem was employed through catalytic borylation of an α,β-unsaturated carbonyl precursor to produce the nitrogen 'deletion' analogues of the compounds described in Section 1.7.2 (Scheme 1.7).

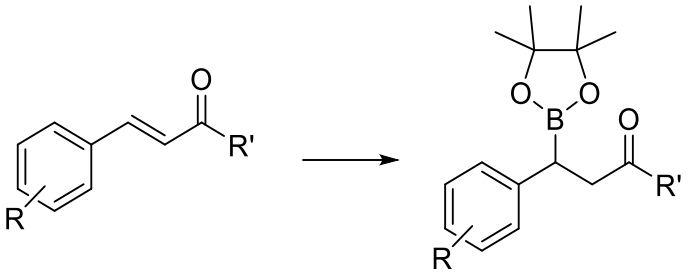

Scheme 1.7. Planned route to access β-ketoboronates.

These compounds were subjected to the same pharmacological evaluation as those described in Section 1.7.2. The synthesis and pharmacology of these compounds will be described in **Chapter 3**.

1.7.4 Conclusions and Future Directions

Chapter 4 will summarise the progress made in this work towards the development of covalent inhibitors of PKa. Additionally, an outline of the key advances will be used to inform future work that may be undertaken which was not successfully carried out due to time constraints.

Chapter 2

Chapter 2: Discovery of α-Amidobenzylboronates as Highly Potent and Selective Covalent Inhibitors of Plasma Kallikrein

2.1 Introduction

Boronic esters are broadly useful functional groups for the formation of carbon-carbon and carbon-heteroatom bonds.[122] The insertion of a -CHCl group from $LiCHCl_2$ into the C-B bond of boronic ester has been extensively studied towards the synthesis of highly functionalised boronates as well as secondary alcohols and sequences of adjacent stereocentres, with the potential for stereoselectivity.[123,124] This reaction was first described by Donald Matteson in 1980 and was later used in the directed synthesis of chiral amino acids from boronic esters. This reaction is termed the Matteson homologation (Scheme 2.1).[125,126]

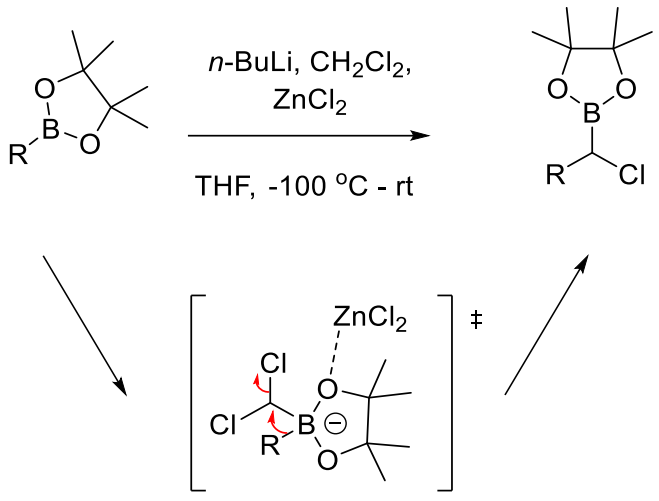

Scheme 2.1. Matteson synthesis of α-chloroboronates from boronic acid pinacol esters.

Proceeding through the generation of lithiated dichloromethane, the Matteson homologation features a rearrangement of a tetrahedral borate adduct

intermediate in which a carbon-boron bond migrates to displace a chlorine atom to generate a charge-neutral species. $ZnCl_2$ is often used as an additive as it is able to coordinate boronic ester oxygen atoms, stabilising the borate intermediate, however numerous examples exist of the reaction being performed with no Lewis acid additive present.[127]

The Matteson homologation reaction serves as a route to α-haloboronic esters which may be subjected to further functionalisation. Matteson reported that these α-haloboronic esters may be subjected to hard nucleophiles such as organolithiums and Grignard reagents to access a multitude of functionalities at the α-position (Scheme 2.2).[125]

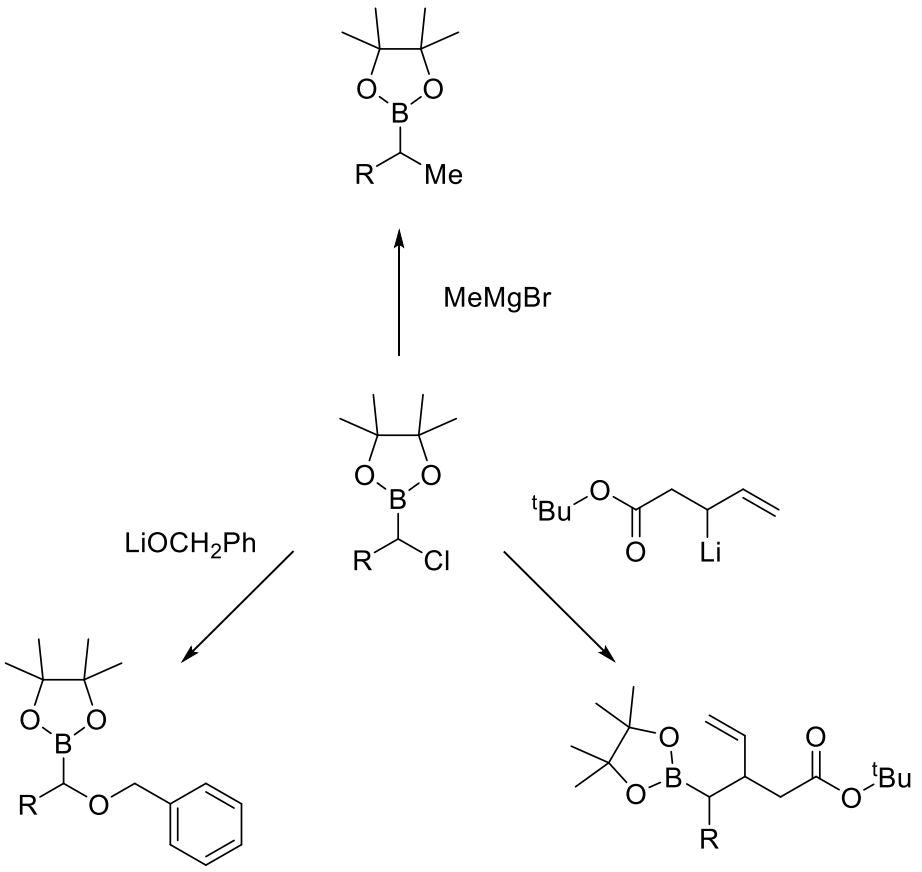

Scheme 2.2. Examples of displacement reactions carried out on α-chloroboronate pinacol esters by Matteson *et al.*[128]

Through the use of a homologation-displacement sequence, boronic esters may be converted to secondary alkyl boronic esters, benzyloxy-boronic esters and functionalised allyl derivatives amongst other species in a two-step, one-pot process.

This synthetic methodology was applied in the synthesis of taniborbactam **33** and related compounds (Scheme 2.3).[111–113]

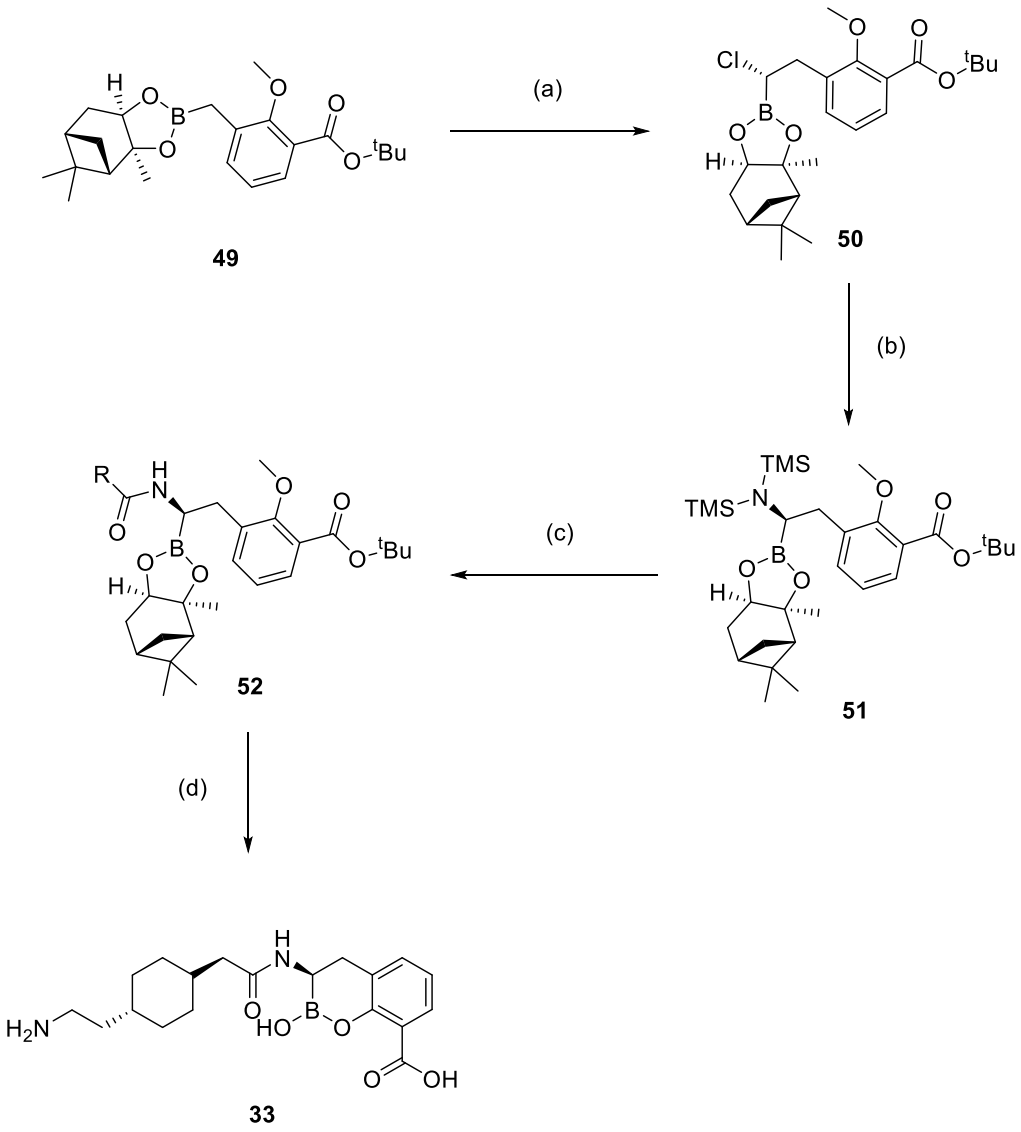

Scheme 2.3. Synthesis of taniborbactam. Reagents and conditions: (a) *n*-BuLi, CH_2Cl_2, THF, -100 °C (b) LiHMDS, THF, -20 °C (c) RCO_2H, HATU, NMM, DMF, rt (d) BCl_3, 0 °C, THF

Starting from intermediate **49**, a Matteson homologation was performed to afford the α-chloro- species **50**. In this case the pinanediol moiety acts as a chiral auxiliary, enabling enantioselective generation of the α-chloro- species. LiHMDS is used to displace the α-chloro- atom to produce silylated amine intermediate **51** which is subsequently coupled to a carboxylic acid to give intermediate **52**. The aryl methoxy substituent of **52** is deprotected with BCl_3, simultaneously enabling generation of a cyclic benzoxaborine system and deprotection of the pinanediol ester to yield **33**.

The synthesis of bortezomib **32** features similar chemistry, in which the generation of an α-aminoboronate species is utilised for subsequent amidation. A key point of difference in this case is in the preparation of an α-aminoboronate salt **56** as an isolable reagent (Scheme 2.4).[129–131]

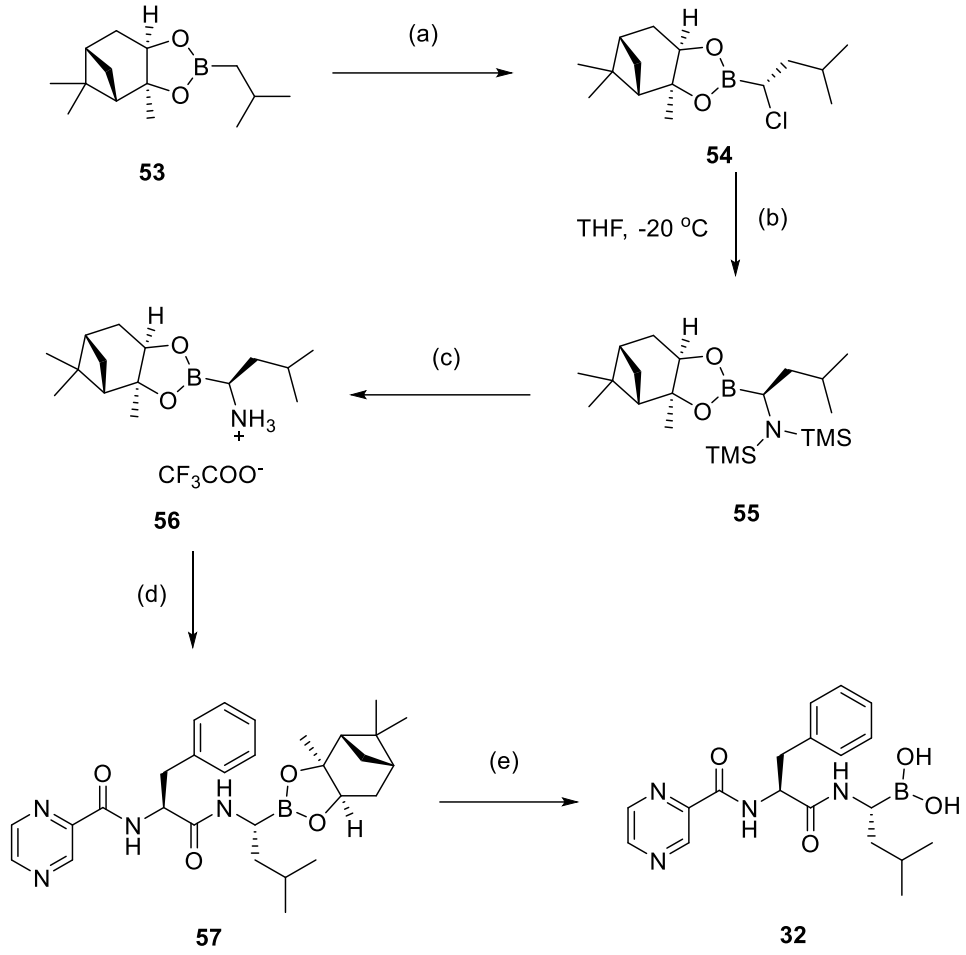

Scheme 2.4. Synthesis of bortezomib. Reagents and conditions: (a) 1. LDA, CH_2Cl_2 2. $ZnCl_2$, THF, -100 to -65 °C (b) LiHMDS, THF, -20 °C (c) TFA, $^{i}Pr_2O$, -60 °C (d) RCOOH, TBTU, CH_2Cl_2, 0 °C to rt (e) ^{i}*Bu*B(OH)$_2$, 1M HCl, MeOH/hexane, rt.

Starting from isobutyl pinanediol boronic ester **53**, a Matteson homologation is performed to stereoselectively generate α-chloro- intermediate **54**, which is subjected to LiHMDS to yield silylated amine **55,** which under subjection to TFA at low temperature undergoes silyl deprotection to yield an α-aminoboronate TFA salt **56**. Coupling of **56** to a peptide carboxylic acid fragment gave boronate **57** which was deprotected *via* transesterification under mild acidic conditions to give bortezomib **32**.[132]

A further example of the synthesis of aminoboronate HCl salts for amidation uses azide in the initial displacement of the α-chloro- intermediate followed by reduction to the amine. Lejon *et al* reported the use of this chemistry in the synthesis of boron-containing anti-tubercular peptidomimetic drugs (Scheme 2.5).[133,134]

Treatment of bromomethyl boronate **58** with sodium azide in the presence of tetramethyl ammonium bromide gives rise to azidomethyl boronate **59**, upon which a Matteson homologation was performed to give **60**. The α-chloroboronate was treated with benzylmagnesium chloride to afford **61** which was reduced to the ammonium HCl salt **62** upon subjection to lithium aluminium hydride and HCl. **62** was coupled to *N*-Boc-L-Lysine, then deprotected under acidic conditions, before acid hydrolysis of the boronate to afford boronic acid **64**.

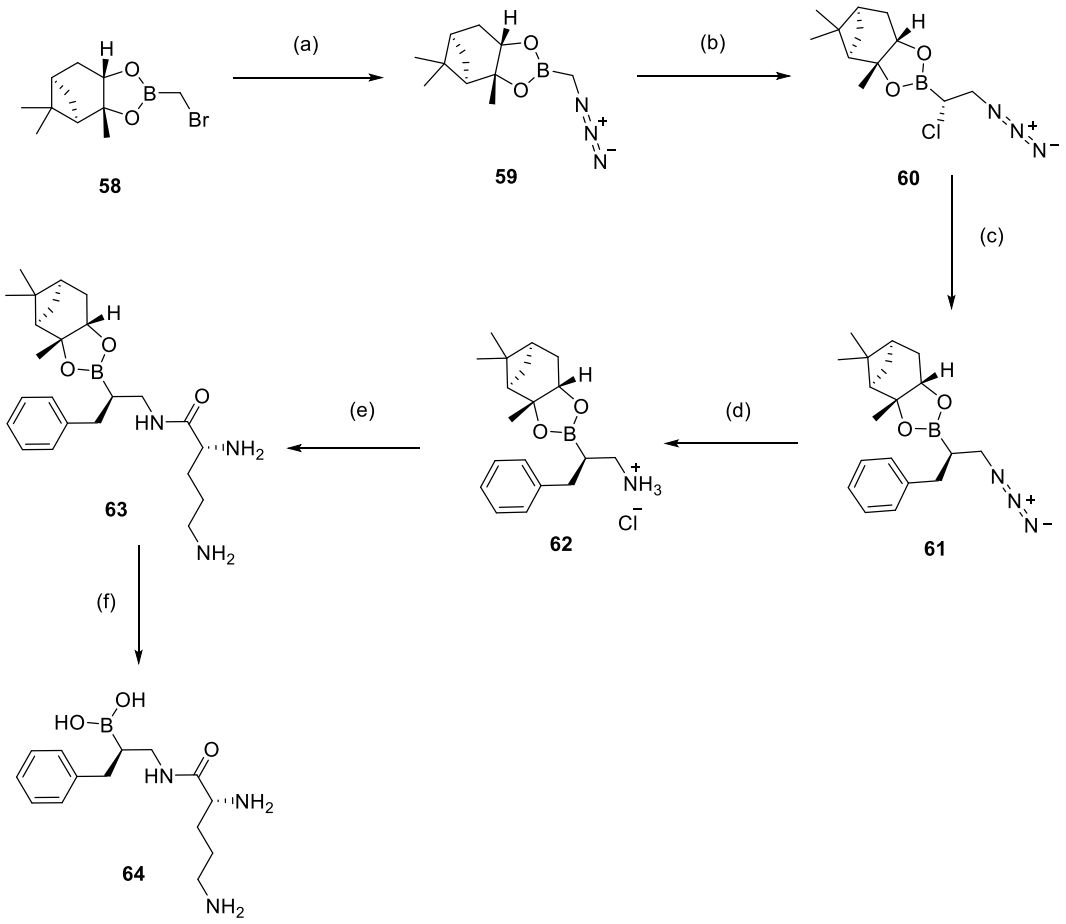

Scheme 2.5. Synthesis of peptidomimetic anti-tubercular agent **64**. Reagents and conditions: (a) NaN_3, $(Bu_4N)Br$, CH_2Cl_2/H_2O, rt (b) 1. *n*-BuLi, CH_2Cl_2 2. $ZnCl_2$, THF, -100 to -78 °C (c) BnMgCl, $ZnCl_2$, THF, -78 °C (d) 1. $LiAlH_4$, THF, 0 °C 2. HCl, MeOH, rt (e) 1. *N*-Boc-L-Lys, HOBt, EDC, NMM, CH_2Cl_2 2. HCl, MeOH (f) 3M HCl, H_2O, 90 °C.

2.1.1 Summary

Synthetic methodologies exploiting the Matteson homologation have been well explored in the development of boron-containing pharmacophores. Specifically, the ability to install an amine functionality α- to a boron centre has enabled amide coupling of boron-containing fragments, enabling access to drugs such as bortezomib and taniborbactam. Whilst boronic acids and boronates have been used as inhibitors of PKa, this chemistry has not yet been exploited in their design.

2.2 Results and Discussion

2.2.1. Synthetic Chemistry

It was posited that the use of an amino acid-based structure would provide a useful synthetic handle for the attachment of a covalent warhead to **48**. 3-Chlorophenyl glycine methyl ester was coupled to *N*-benzylpyrazole-4-carboxylic acid to offer a scaffold for the attachment of a warhead (Scheme 2.6).

65 was esterified *via* methanol reflux in the presence of thionyl chloride to provide ester-protected intermediate **66**, which underwent amidation with carboxylic acid **67**, yielding amido-ester **68**, which was subsequently hydrolysed to the corresponding carboxylic acid **69**.

In an effort to install a boronic acid moiety to scaffold **69**, methylaminoboronate **72** was prepared *via* displacement of bromomethyl boronic acid pinacol ester with LiHMDS, followed by silyl deprotection in HCl to give ammonium salt **72**. Coupling of **69** and **72** was achieved in the presence of EDC and HOBt. The mixture was purified by reverse phase flash chromatography in acetonitrile/water causing hydrolysis of the pinacol ester to provide compound **73** in moderate yield.

Upon inspection of the initial molecular docking simulation (Figure 1.33), it seemed the side chain bearing the boronic acid motif in **73** was too large to occupy the space beneath Ser_{195}, hence a methodology was sought to shorten this motif, encouraging covalent engagement with the catalytic serine (Figure 2.1).

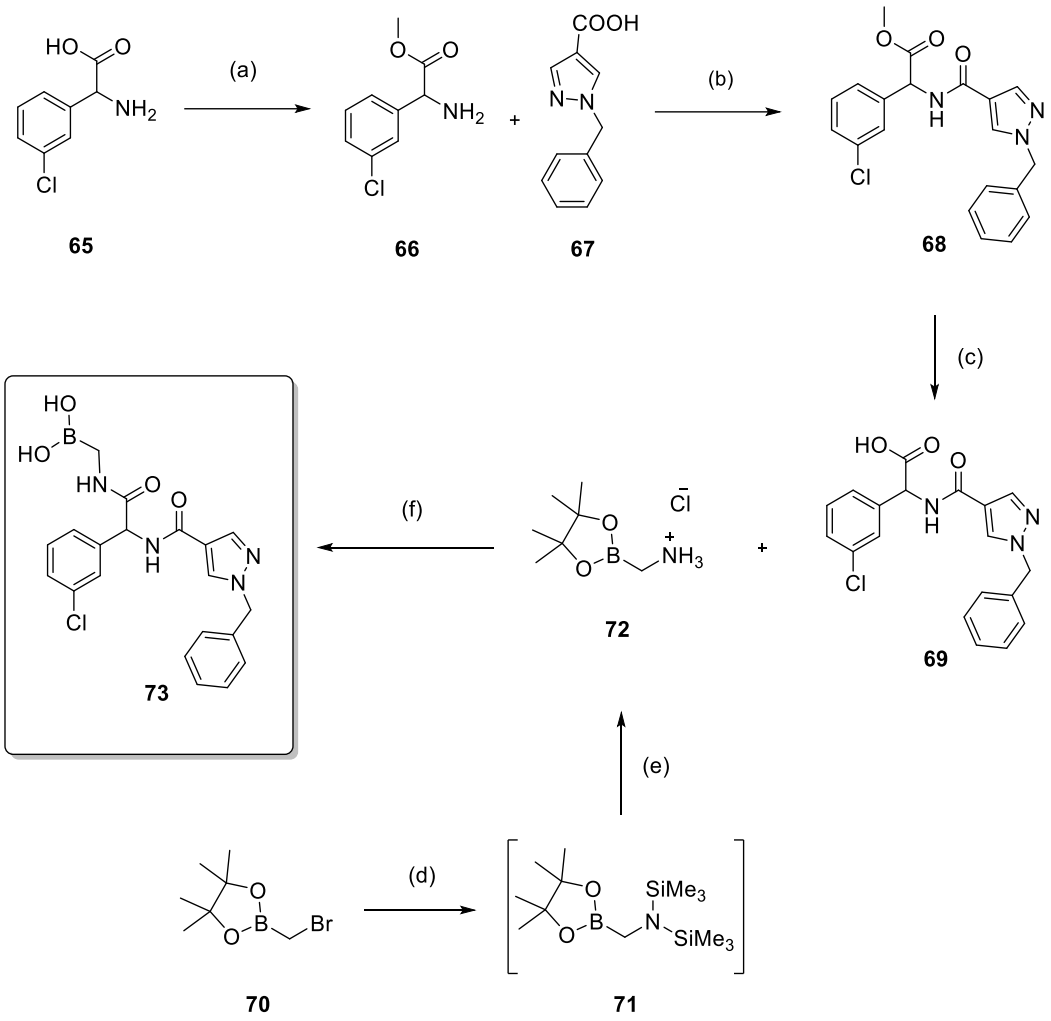

Scheme 2.6. Installation of amidoboronic acid functionality to 3-chlorophenyl glycine-based scaffold. Reagents and conditions: (a) $SOCl_2$, MeOH, 70 °C, 16 h, 88% (b) EDC, HOBt, DIPEA, DMF, rt, 3 h, 64% (c) NaOH, EtOH/H_2O, 50 °C, 3 h, 95% (d) LiHMDS (1M in THF), THF, -78 °C, 1 h (e) 1. 4N HCl in dioxane, Et_2O, -78 °C, 1 h, 58% (2 steps) (f) EDC, HOBt, DIPEA, DMF, rt, 3h 2. RP-purification, 36%.

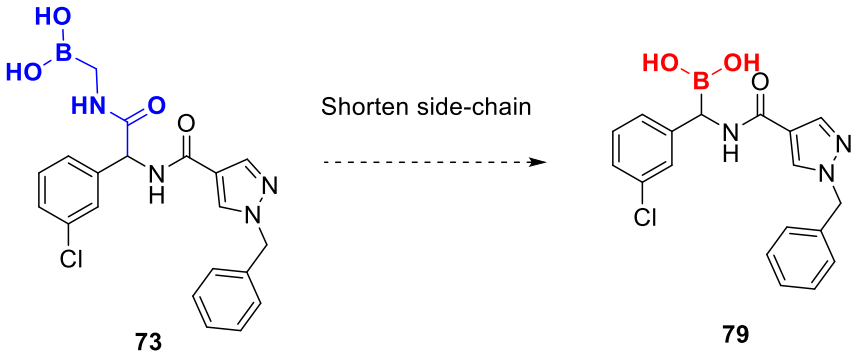

Figure 2.1. Planned modification of warhead-bearing side chain***.***

Matteson chemistry was employed to enable the synthesis of aminoboronates **77a-c** (Scheme 2.7). 3-Chlorophenyl boronic acid pinacol ester **74a** was subjected to *n*-butyllithium in the presence of dichloromethane. Displacement of **75a** with LiHMDS gave intermediate **76a** which was deprotected in the presence of HCl in order to precipitate salt **77a** from ethereal solution.

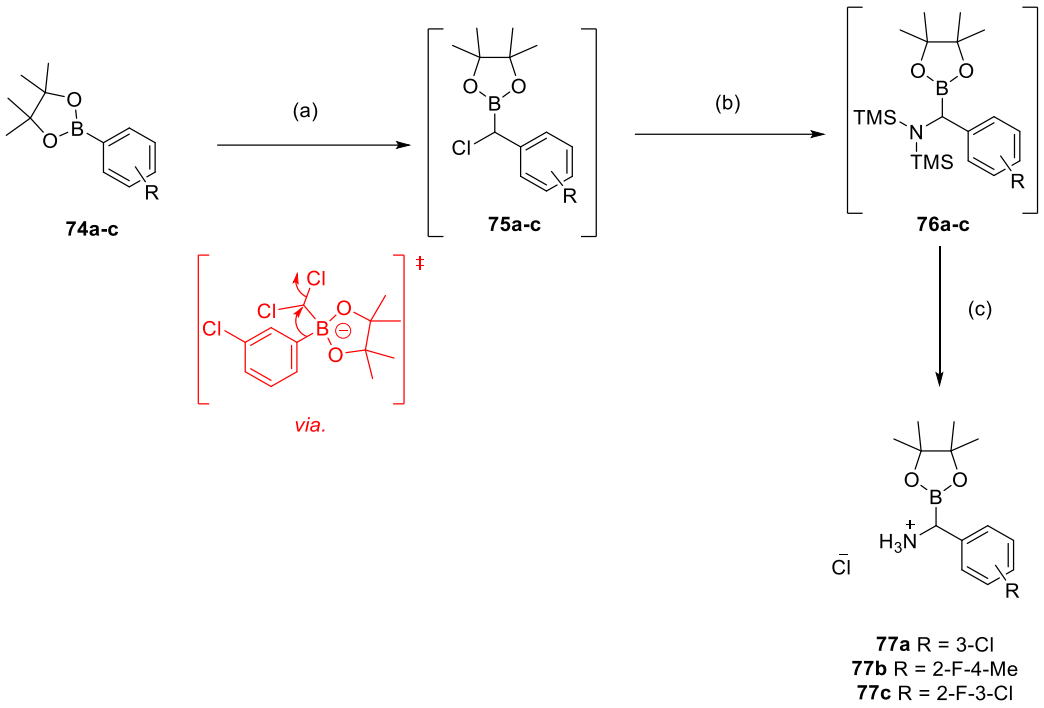

Scheme 2.7. Preparation of α-aminoboronate salts **77a-c**. Reagents and conditions: (a) *n*-BuLi, CH_2Cl_2, THF, -78 °C – rt, 16 h(b) LiHMDS 1M in THF, THF, -78 °C – rt, 16 h (c) 4N HCl in dioxane, Et_2O, -60 °C, 3h, 7-40% (3 steps).

Despite successful synthesis and isolation of aminoboronate salts **77a-c** on multiple occasions, this chemistry presented significant challenges, due to the hygroscopic nature as well as acid, moisture, and heat sensitivity of these compounds. It was observed numerous times by TLC that protodeborylation to the benzylamine species was occurring upon exposure of **76a-c** to the acidic conditions required to precipitate aminoboronates **77a-c**. It has been reported in the literature that free-amine α-aminoboronates are inherently unstable, hence the need to isolate by precipitation.[135–138] It was also found that the stability of the aminoboronate salts was limited, and due to their hygroscopic nature would

have a typical shelf-life of around a week before full decomposition by protodeborylation.

Numerous efforts were made to circumvent these issues, including *in situ* deprotection of **76a-c** and subsequent amide coupling, in line with the method used for the synthesis of taniborbactam (Scheme 2.3).[111,139–141] Direct reaction of the silylated aminoboronate with a corresponding acyl chloride in the presence of a mild protic additive such as methanol has been accomplished in the literature,[140] this methodology was attempted, however no conversion to the desired amides was observed in these cases due to protodeborylation of the starting material, observed by TLC.

Varying the acid and solvent was also examined, attempting to find optimal conditions for the precipitation of α-aminoboronate salts, the results of which are displayed in Table 2.1.

Limited success was seen from varying such parameters. Whilst used in the literature for carrying out this reaction, TFA is seemingly too strong an acid to be used in conjunction with these particularly acid-sensitive substrates, forcing decomposition *via* protodeborylation. Diethyl ether seemed to have preferable properties to cyclohexane and MTBE in its ability to dissolve both substrate and acid without forming an emulsion, which was observed for reactions in cyclohexane and MTBE.

Table 2.1. Attempted optimisation of conditions for precipitation of α-aminoboronate salts

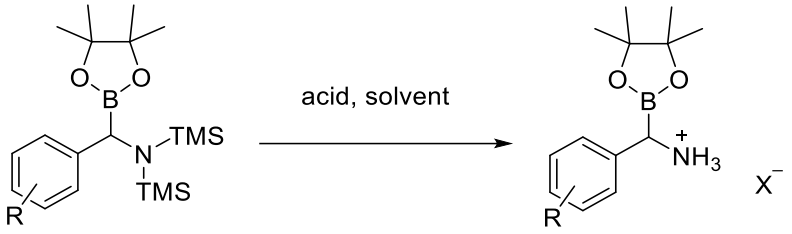

R	Solvent	Acid	% Yield*
3-Cl	Et_2O	4N HCl in dioxane	40
2-F-4-Me	Et_2O	4N HCl in dioxane	22
2-F-3-Cl	Et_2O	4N HCl in dioxane	7
3-Cl	Cyclohexane	4N HCl in dioxane	0
2-F-4-Me	Cyclohexane	4N HCl in dioxane	0
2-F-3-Cl	Cyclohexane	4N HCl in dioxane	0
3-Cl	MTBE	4N HCl in dioxane	0
2-F-4-Me	MTBE	4N HCl in dioxane	0
2-F-3-Cl	MTBE	4N HCl in dioxane	0
3-Cl	Et_2O	TFA	0
2-F-4-Me	Et_2O	TFA	0
2-F-3-Cl	Et_2O	TFA	0
3-Cl	Cyclohexane	TFA	0
2-F-4-Me	Cyclohexane	TFA	0
2-F-3-Cl	Cyclohexane	TFA	0
3-Cl	MTBE	TFA	0
2-F-4-Me	MTBE	TFA	0
2-F-3-Cl	MTBE	TFA	0

*Isolated yield

Amidation of **77a** with **67** was undertaken in the presence of HATU and DIPEA to provide α-amidoboronate **78**. Deprotection of the pinacol ester of **78** took place

via transesterification with hexylboronic acid under mild acidic conditions (Scheme 2.8).

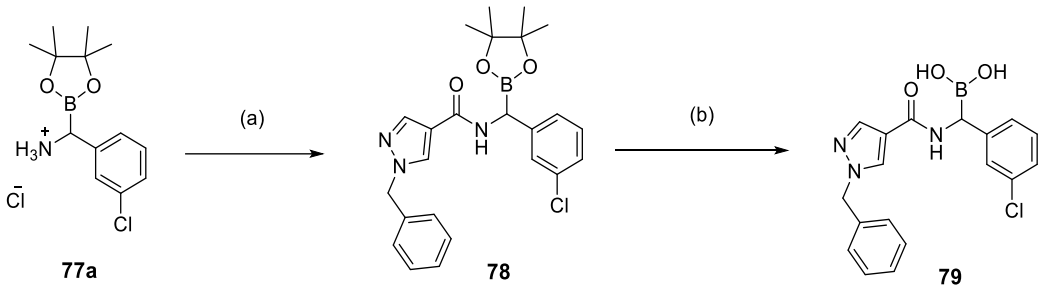

Scheme 2.8. Amidation of **77a** with **67** and subsequent pinacol deprotection. Reagents and conditions: (a) **67**, HATU, DIPEA, MeCN, 0 °C to rt, 2 h, 58% (b) 3N HCl/H_2O, $C_6H_{11}B(OH)_2$, 1:1 MeOH/cyclohexane, rt, 16 h, 23%.

Boronic acid **79** was observed to be unstable under acidic conditions, protodeborylating when subjected to LCMS in the presence of formic acid. Interestingly, partial decomposition of **78** was observed by LCMS, first to boronic acid **79,** then to the deborylation product, however, a mass ion was also observed consistent with an intramolecular borocycle species **80**, potentially elucidating a decomposition pathway (Scheme 2.9). This same activity was observed for all subsequent α-amidoboronate analogues by LCMS.

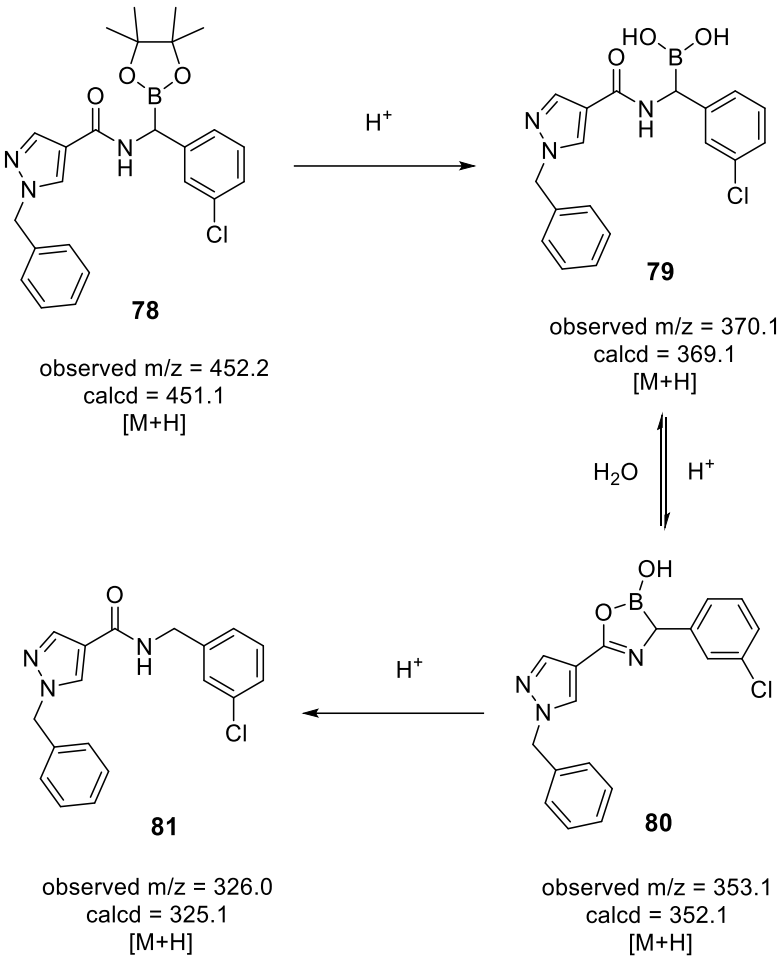

Scheme 2.9. Proposed decomposition pathway of **78** from observed molecular ions by LCMS.

From these LCMS observations, a putative deborylation mechanism for **79** was devised based on the mechanism studied by Kuivila[142] in which the C-B bond is cleaved in **79a**, enabled by the borate anion gaining charge neutrality upon protonation of the P1 benzylic carbon to give **79b** (Scheme 2.10).

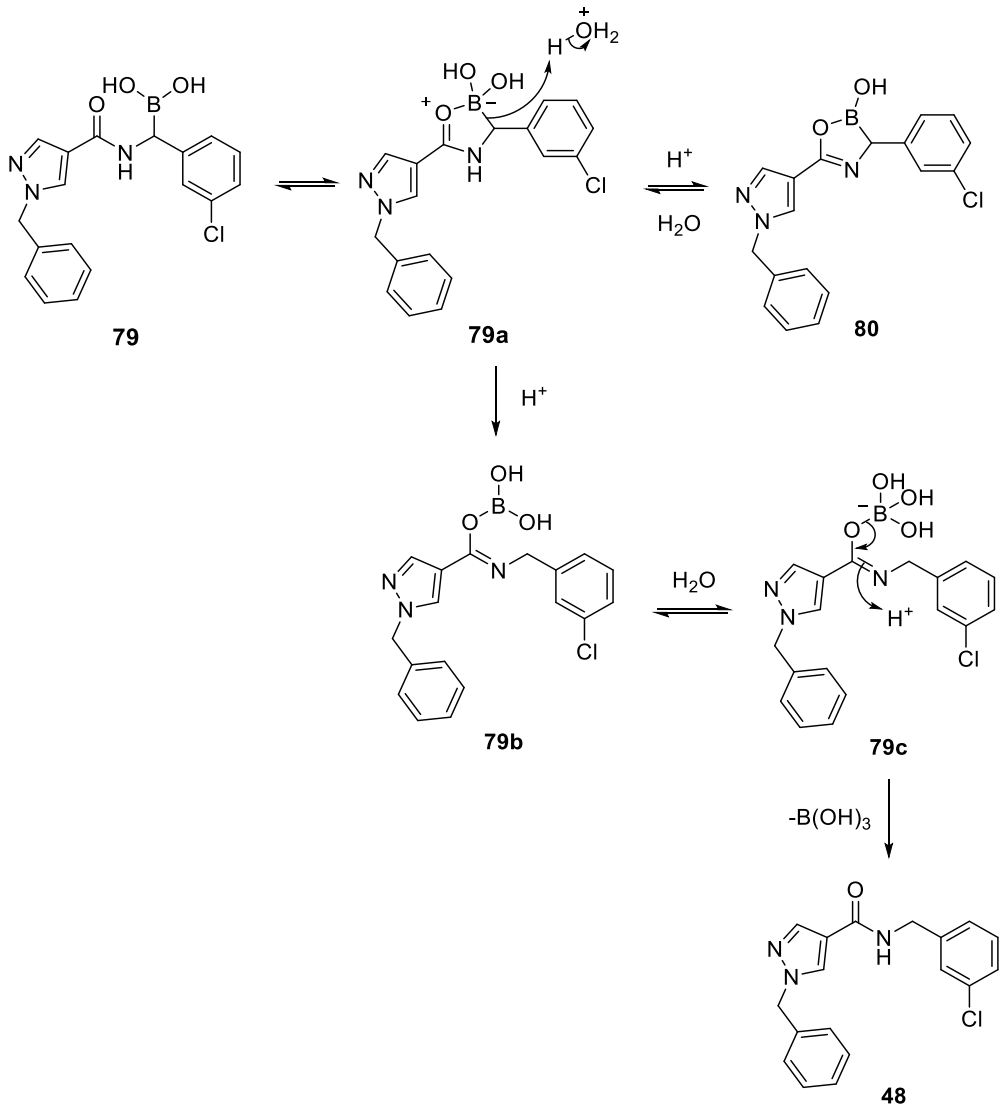

Scheme 2.10. Proposed mechanism of deborylation of **79** under acidic conditions

Synthesis of further amidoboronate analogues aimed to explore the S4 pocket of PKa, in order to elicit enhanced affinity. Gaining insight from compounds such as Sebetralstat **5** and **10**, **78** was elongated to include methylpyrazole and methylpyridone P4 groups. This was achieved through the synthesis of carboxylic acid analogues of **67** which included the aforementioned P4 groups (Scheme 2.11).

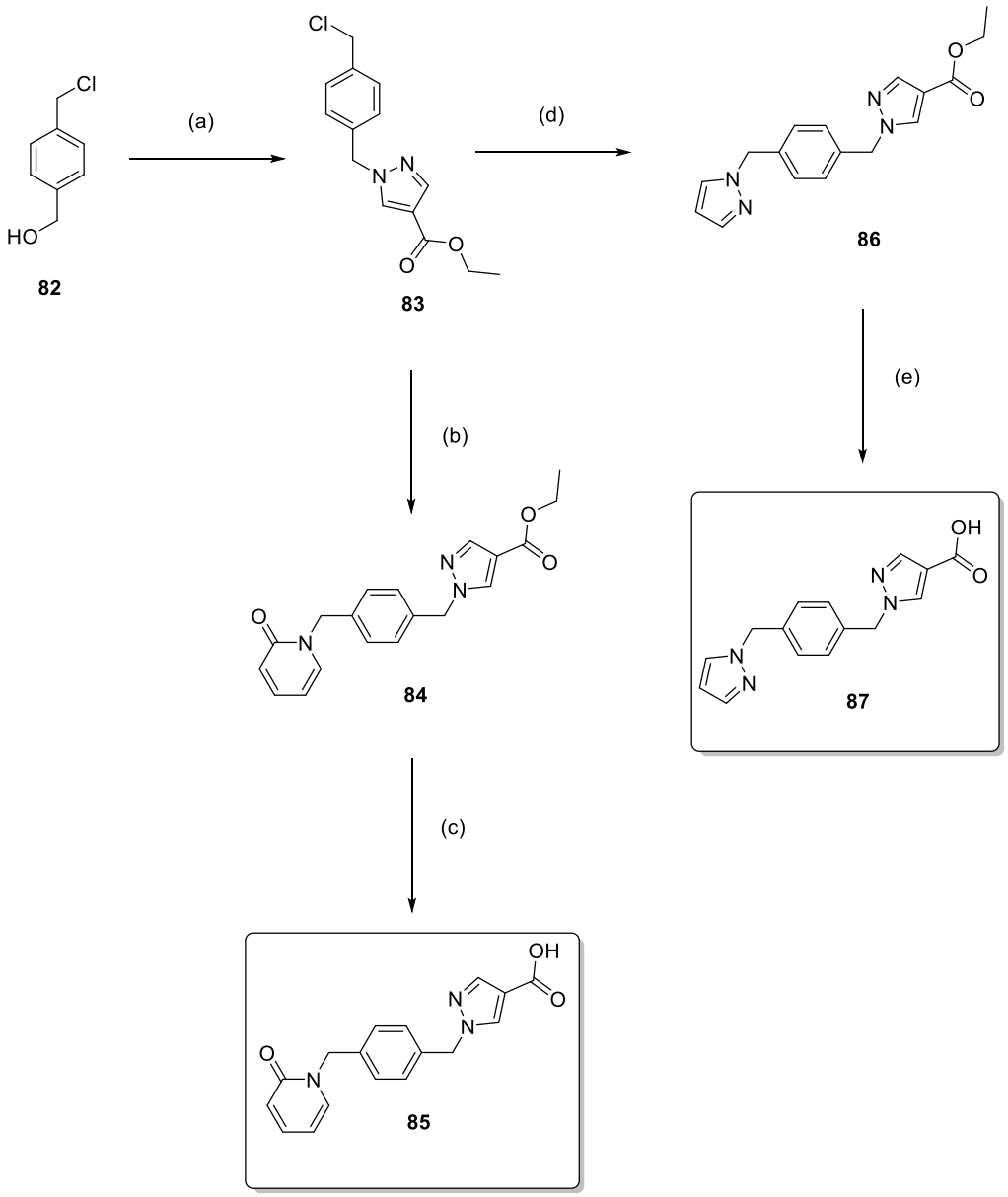

Scheme 2.11. Synthesis of carboxylic acid analogues with pyrazole and pyridone P4 groups. Reagents and conditions: (a) ethyl 4-pyrazole carboxylate, DIAD, PPh_3, THF, rt, 16 h, 76% (b) pyridone, K_2CO_3, DMF, 50 °C, 16 h, 51% (c) LiOH, THF/H_2O (5:1), 50 °C, 16 h, 53% (d) pyrazole, NaH, DMF, rt to 50 °C, 2 h, 54% (e) LiOH ,THF/H_2O (5:1), rt, 16 h, 83%.

Mitsonobu reaction of **82** with ethyl 4-pyrazole carboxylate gave a common intermediate **83**, which was reacted with either pyrazole or pyridone to give esters **84** and **86**, enabling generation of the corresponding carboxylic acids by hydrolysis with LiOH.

Further amidoboronate analogues were accessed through amidation of **77a-c** with **65**, **85** and **87**. Purification of these compounds was achieved by reverse-phase flash chromatography ($MeCN/H_2O$), without the use of an acidic additive.

Carboxylic acids **88** and **89** were obtained from the compound library of KalVista Pharmaceuticals Ltd. and were used in the synthesis of **93** and **94** (Figure 2.2), (Scheme 2.12).

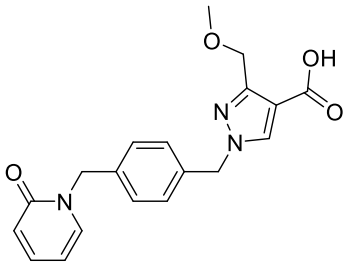

88

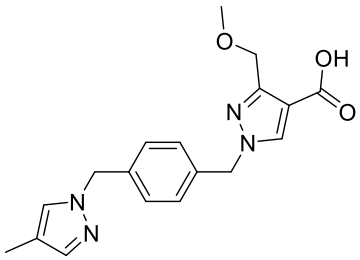

89

Figure 2.2. Structures of carboxylic acids **88** and **89**.

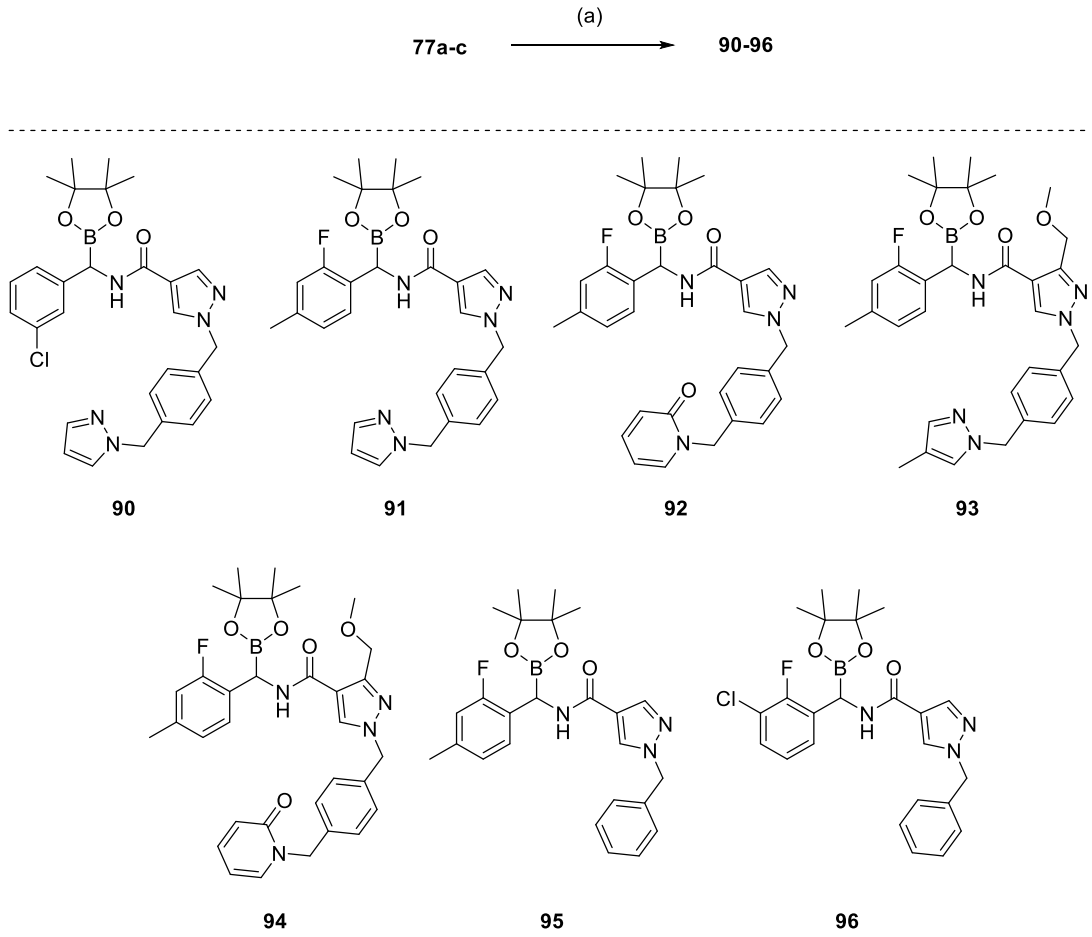

Scheme 2.12. Synthesis of P4-elongated α-amidoboronates. Reagents and conditions: (a) RCOOH, HATU, DIPEA, MeCN, 0 °C to rt, 3-40%.

Generally proceeding in moderate yield, with the exception of **92** and **93** which experienced solubility issues, compounds **90**-**96** were isolated for pharmacological evaluation (Section 2.2.2). As with **78**, hydrolysis of the pinacol ester of the P4-elongated compounds was attempted under the same mild acidic conditions, however the boronic acid derivatives of **90**-**96** experienced the same stability issues as for **78**. Synthesis of the pinanediol-ester analogues of **77a-c** was

attempted, however no suitable conditions for the precipitation of pinanediol α-aminoboronate salts could be established.

Synthesis of dioxaborolane analogues of **90** was also explored *via* direct displacement of α-chloro- Matteson homologation products **75a-c** with carboxylate or alkoxide derivatives, whilst formation of the desired product was observed by LCMS, this was followed by rapid decomposition (Scheme 2.13).

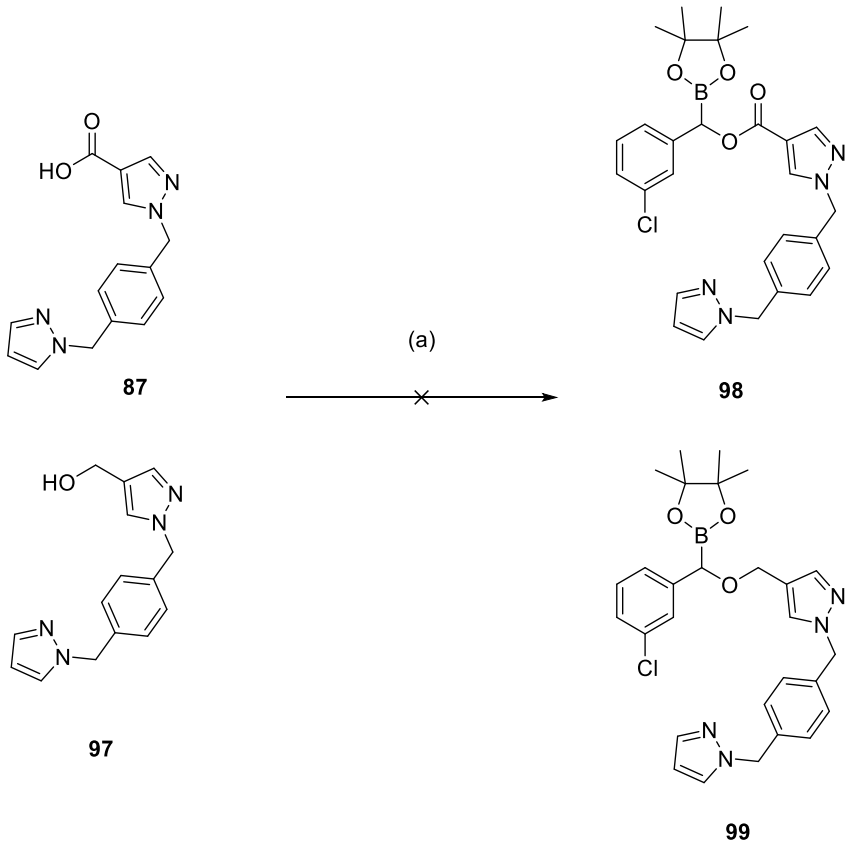

Scheme 2.13. Attempted synthesis of dioxaborolane analogues. Reagents and conditions: (a) **75a**, *n*-BuLi or ^{t}BuOK, THF, -78 ^{o}C

To assess possible covalent binding of α-amidoboronates in PKa, a series of matched pairs was synthesised, omitting the pinacol boronate warhead. These compounds would serve as a means of comparison against boronate analogues for pharmacological evaluation, both in terms of relative potency and binding kinetics (Scheme 2.14).

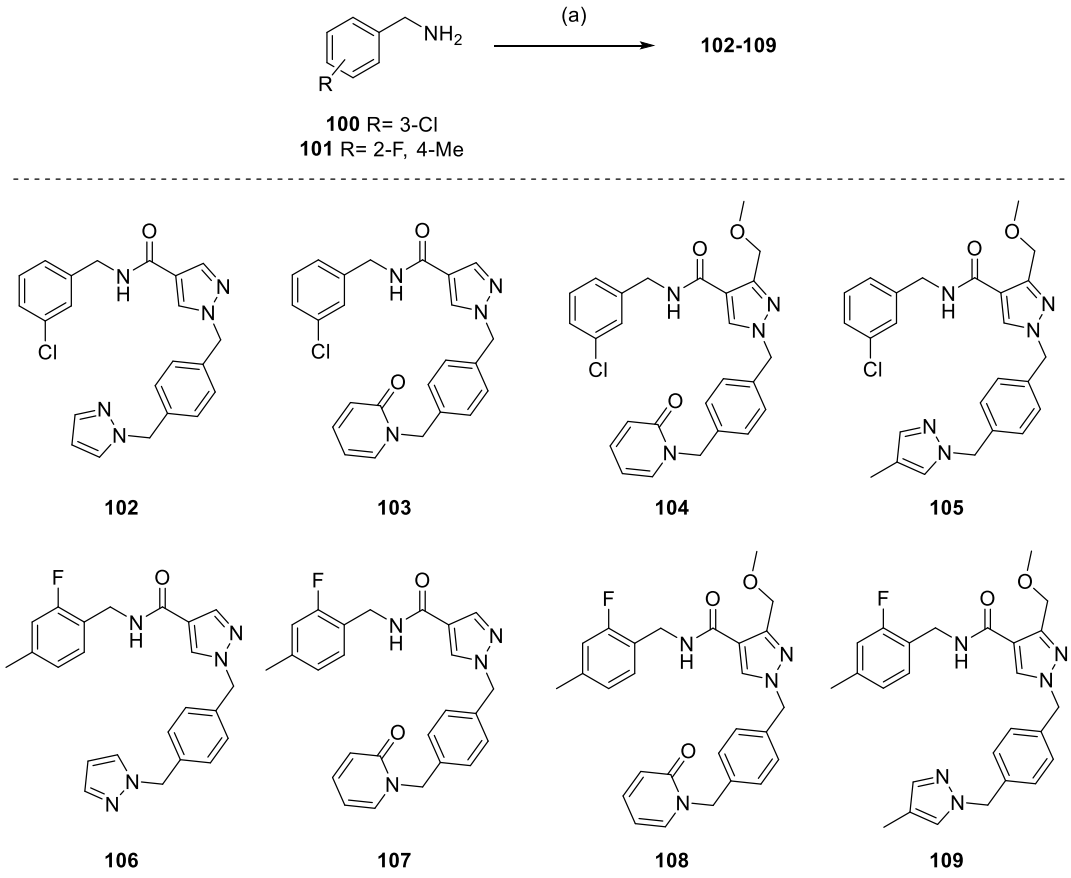

Scheme 2.14. Synthesis of matched pair benzyl amide analogues. Reagents and conditions: (a) RCOOH, HATU, DIPEA, MeCN, rt, 1 h, 34-89%.

2.2.2 Pharmacology

2.2.2.1 Evaluation of Inhibitor Potency and Selectivity

Evaluation of PKa binding was carried at Kalvista Pharmaceuticals Ltd. by Edward Duckworth, Freya Pinkney and Adrian Mogg out using a Pro-Phe-Arg-AFC fluorescent substrate assay to determine IC_{50}, where inhibitor binding showed inverse proportionality to fluorescence intensity. Assays were carried out against PKa, as well as against FXIIa to check for non-specific binding. Binding assays were carried out with readings taken at various incubation time points to assess covalent binding. For an irreversible covalent inhibitor, measured potency is expected to continue to increase over time due to increasing active site occupancy, where maximal observable potency is defined by half assay enzyme concentration. A reversible noncovalent inhibitor is expected to maintain the same observed potency over all time points.[143–145]

Initial evaluation of **68, 69** and **73** showed limited activity in PKa. **68** showed weak association in both PKa and FXIIa after 60 minutes (23% and 40% inhibition respectively), however no observable inhibition at any other time point, suggesting a degree of slow binding in both enzymes. **69** showed no observable inhibition at any time point and **73** displayed weak binding to PKa at 60 minutes (19% inhibition) with no binding seen in FXIIa (Table 2.2).

The lack of significant differentiation in the activities of **68** and **73** led to the assertion that the amidoboronic acid functionality of **73** was not interacting with Ser_{195}, leading to the synthesis of examples **78** and **79** (Table 2.3).

Table 2.2. Biological activity of **68**, **69** and **73** against PKa and FXIIa

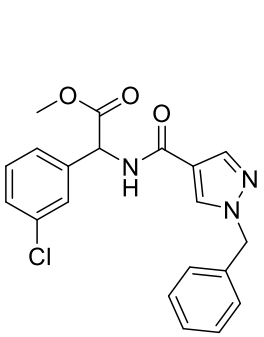

68

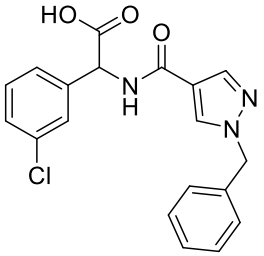

69

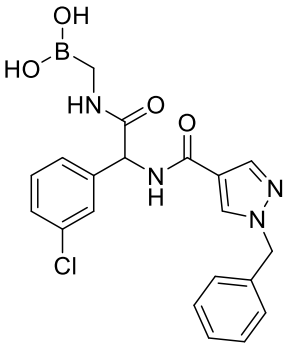

73

Example	Enzyme Binding (%)[a]					
	PKa			FXIIa		
	1 min	10 min	60 min	1 min	10 min	60 min
68	NI*	NI	23%**	NI	NI	40%**
69	NI	NI	NI	NI	NI	NI
73	NI	NI	16%**	NI	NI	NI

*NI = no observed inhibition, **% inhibition at 400 µM testing concentration

[a]Data are expressed as mean of 2 experiments, where each experimental curve was performed in triplicate.

No inhibition was observed for **77a** or **79** in either PKa or FXIIa. In the case of **79,** the lack of observed biological activity is likely due to the previously noted instability. Interestingly, **78** showed no observable activity at the 5 minute time point, however displayed 64.2 µM binding after 60 minutes, indicating slow k_{on} kinetics commonly observed for covalent inhibitors.

Table 2.3. Biological activity of **77a**, **78** and **79** against PKa and FXIIa

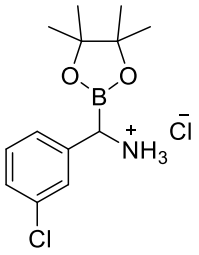

77a

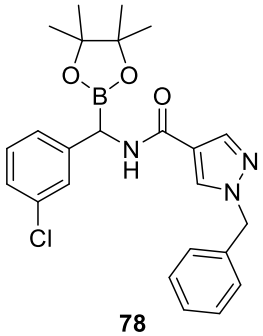

78

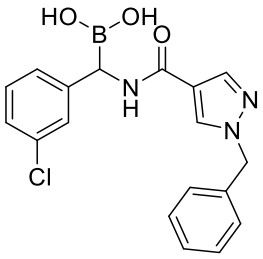

79

Example	IC_{50} (μM)[a]			
	PKa		FXIIa	
	5 min	60 min	5 min	60 min
77a	NI*	NI	NI	NI
78	NI	64.2	NI	NI
79	NI	NI	NI	NI

*NI = no observed inhibition

[a]Data are expressed as mean of 2 experiments, where each experimental curve was performed in triplicate.

In light of this observed binding in PKa, examples **90-96** were subsequently evaluated for their biological activity in PKa and FXIIa (Table 2.4). Inclusion of pyrazole and pyridone fragments, targeting the S4 pocket of PKa showed a significant improvement in potency in comparison to **78**, potentially due to induction of the S4 pocket enabling a more rigid binding conformation and better placement of the boronate warhead in relation to Ser_{195}.

Table 2.4. Biological activity of **90-96** against PKa and FXIIa

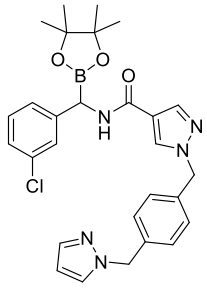

90

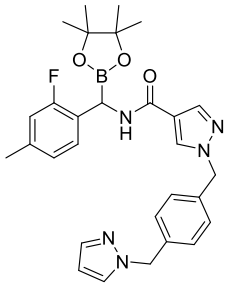

91

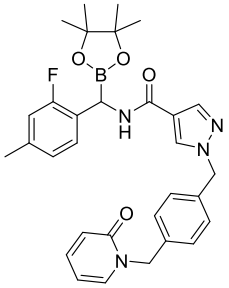

92

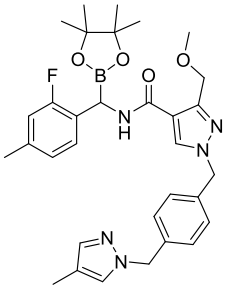

93

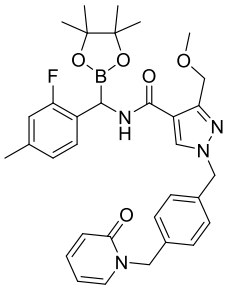

94

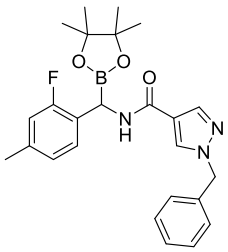

95

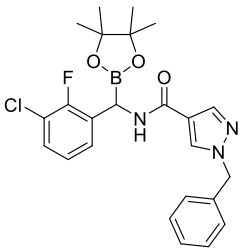

96

Example	IC_{50} (nM)[a]					
	PKa			FXIIa		
	1 min	10 min	60 min	1 min	10 min	60 min
90	255	46	5.2	>400	>400	>400
91	66	6.9	0.3	>400	>400	>400
92	94	17	1.9	>400	>400	>400
93	250	35	3.8	>400	>400	>400
94	78.6	10.9	0.9	>400	>400	>400
95	2307	152	33	>400	>400	>400
96	2635658	345934	59781	>400	>400	>400
31	86	15	2.1	1288	467	39

[a]Data are expressed as mean of 2 experiments, where each experimental curve was performed in triplicate.

All compounds displayed binding kinetics consostent with covalent inhibition as evidenced by comparison with covalent control **31**. For example, **90** shows IC_{50} values of 255 nM at 1 minute, 46.2 nM at 10 minutes and 5.2 nM at 60 minutes. This steady increase in PKa binding over time represents rising active site occupancy, indicating covalent inhibition.

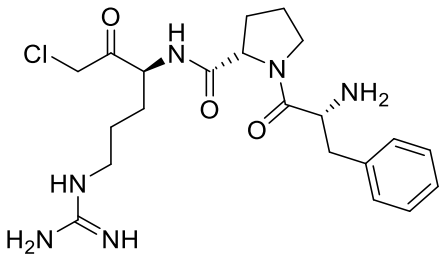

31

Whilst the interaction of Ser_{195} with the boronate warhead is considered the most significant binding interaction with respect to observed potency, the P1 and P4 fragments play a crucial role in both initial binding to form the non-covalent enzyme-inhibitor complex as well as 'anchoring' the scaffold within the active site to allow a productive interaction between the catalytic serine and the boronate warhead.

It was found that the 2-fluoro-4-methylphenyl was superior to 3-chlorophenyl as a non-basic monocyclic P1 group, with **91** showing the strongest biological activity of this compound series (0.3 nM IC_{50} at 60 minutes). 2-Fluoro-3-chlorophenyl was also explored as a P1 group, however, showed inferior activity to 2-fluoro-4-methylphenyl, as observed by comparison of **95** and **96**.

The pyrazole P4 group showed marginally improved potency in comparison to pyridone by comparison of **91** and **92.** Compounds **93** and **94** which included the methoxy-methylpyrazole core unit were also nanomolar inhibitors of PKa at the 60 minute time point with the pyridone P4 group showing better activity with respect to 4-methylpyrazole. Interestingly, no activity was observed in FXIIa for **90**-**96**, indicating a degree of selectivity towards PKa.

The best performing compound, **91**, was subjected to an extended time point assay in which IC_{50} readings were taken at 1 minute, 10 minutes, 2 hours, and 24 hours to assess maximal achievable enzyme inhibition (Table 2.5).

Table 2.5. Extended time point biological evaluation of **91** against PKa

Example	**PKa IC_{50} (nM)[a]**			
	1 min	10 min	2 hr	24 hr
91	66	6.9	0.29	0.07

[a]Data are expressed as mean of 2 experiments, where each experimental curve was performed in triplicate.

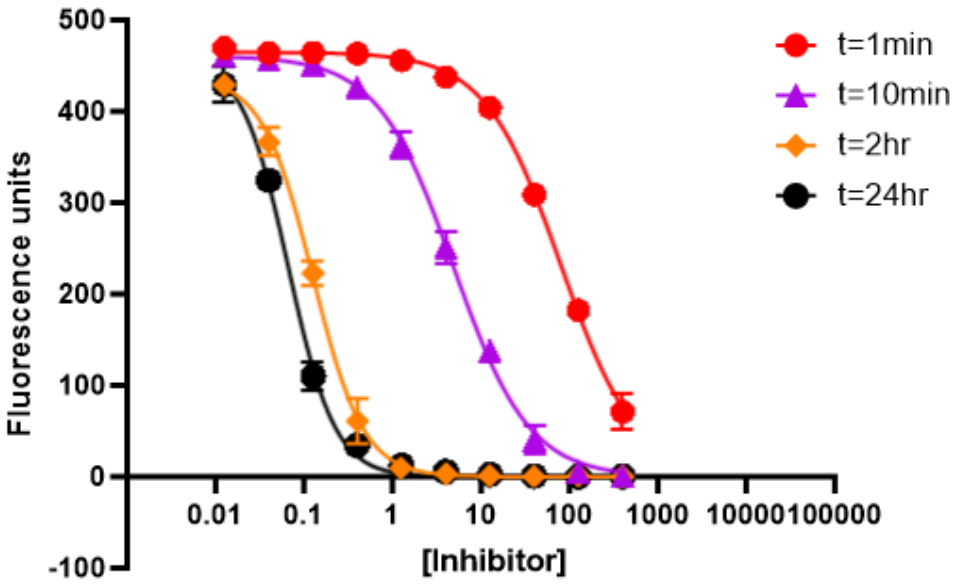

Figure 2.3. Extended time point IC_{50} curves for **91** against PKa

The extended time point data of **91** against PKa shows a continual increase in binding to PKa with no observed drop-off in potency, reaching a top IC_{50} value of 70 pM at 24 hours, strengthening the premise that covalent binding is taking place (Figure 2.3).

Further validation of covalent binding was achieved through biological evaluation of matched pair compounds **102**-**109** (Table 2.6). **102-109** all showed binding kinetics consistent with non-covalent inhibitors with no significant change in IC_{50} observed over the 3 time points.

As with **90**-**96**, the 2-fluoro-4-methylphenyl P1 group outperformed 3-chlorophenyl for IC_{50} potency. For example, **102** showed no observable activity within the assay, however **106** showed an IC_{50} value of around 200 nM.

Interestingly, the pyridone P4 group showed better activity than the corresponding pyrazole for **102-109**, with **107** showing the highest IC_{50} potency of around 35 nM. The pyridone P4 group has previously shown greater S4 affinity than pyrazole,[57] however it is also significantly larger than pyrazole potentially affecting the placement of the boronate warhead for pyridone P4 analogues.

Overall, this data indicates that **90-96** are covalently binding to PKa, as omission of the boronate warhead alters the binding kinetics from showing time dependence for **90-96** to equilibrium binding with no significant change in IC_{50} at each time point for **102-109**.

Table 2.6. Biological activity of **102-109** against PKa

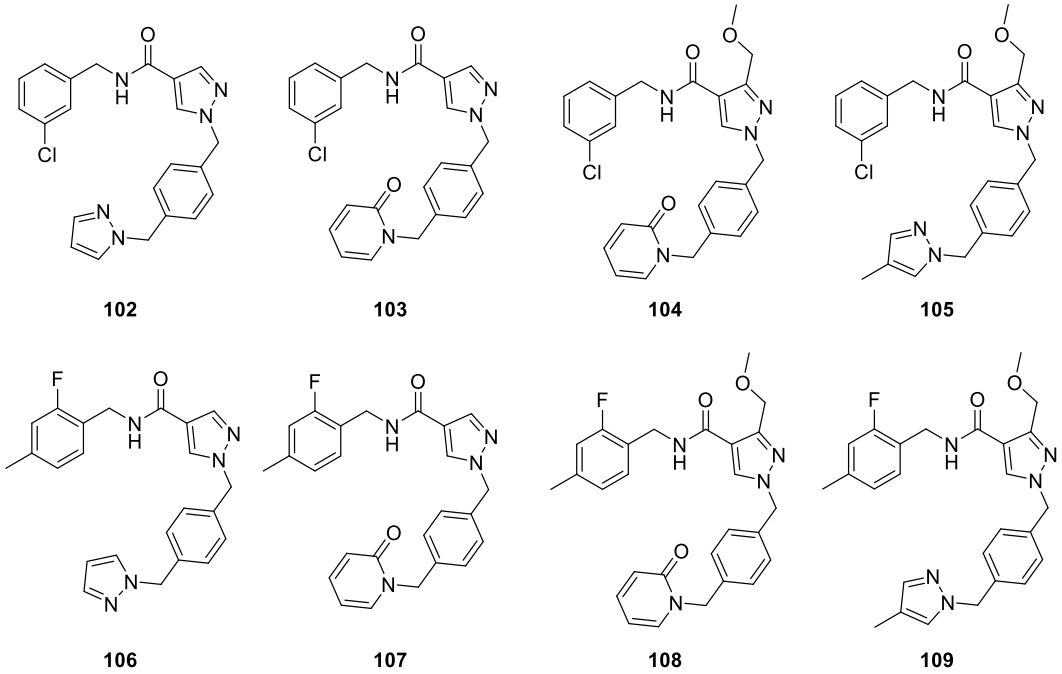

Example	PKa IC_{50} (nM)[a]		
	1 min	10 min	60 min
102	>400	>400	>400
103	270	284	278
104	330	337	334
105	>400	>400	>400
106	199	203	196
107	37.3	37.1	34.5
108	128	123	116
109	>400	>400	>400

[a]Data are expressed as mean of 2 experiments, where each experimental curve was performed in triplicate.

FXIa has the closest structural homology to PKa of any plasma protease with 66% sequence identity.[146] Selectivity data was gained through evaluation of **91**, **92** and **94** against FXIa (Table 2.7).

Table 2.7. Biological activity of **91, 92** and **94** against PKa and FXIa

Example	IC_{50} (nM)[a]					
	PKa			FXIa		
	1 min	10 min	60 min	1 min	10 min	60 min
91	66	6.9	0.3	30122	20814	6596
92	255	46	5.2	>40000	>40000	>40000
94	94	17	1.9	>40000	>40000	26219
31	86	15	2.1	>40000	>40000	16460

[a]Data are expressed as mean of 2 experiments, where each experimental curve was performed in triplicate.

A strong preference for binding to PKa over FXIa was observed with **91** showing a roughly 1000-fold binding preference for PKa. No activity was observed for **92** in FXIa, and very modest activity (26 µM) was seen for **94** in FXIa after 60 minutes. Interestingly, despite minimal activity in FXIa, a degree of covalent binding is observed as IC_{50} potency of **91** and **94** is seen to increase over the 3 time points.

This selective binding behaviour may be reflective of the difference in S4 pocket structure between PKa and FXIa. The Tyr_{174} residue in PKa is replaced for a Glu residue in FXIa, possibly preventing a key π-stacking interaction in the S4 site of FXIa.[147]

Further selectivity data were obtained for **91** against related serine proteases trypsin, plasmin and thrombin (Table 2.8).

Table 2.8. Biological activity of **91** against trypsin, plasmin and thrombin.

Example	IC_{50} (nM)[a]								
	Trypsin			**Plasmin**			**Thrombin**		
	1 min	10 min	60 min	1 min	10 min	60 min	1 min	10 min	60 min
91	>40000	>40000	>40000	22010	19810	14430	>40000	>40000	>40000
31	484	165	27.8	3639	1222	648	3550	981	187

[a]Data are expressed as mean of 2 experiments, where each experimental curve was performed in triplicate.

91 showed no observable binding in trypsin or thrombin, mild apparent covalent activity was seen in plasmin in the 10 μM range, demonstrating high specificity of **91** as a PKa inhibitor, in contrast to nonspecific covalent inhibitor **31**.

2.2.2.2 Jump Dilution Assays

Further validation of covalent inhibition can be obtained through performing a jump dilution assay. This aims to evaluate reversibility of inhibitor binding and to quantify residence time of the enzyme-inhibitor complex. Practically, this involves dilution of the assay medium with buffer after a defined period of preincubation.[145,148,149]

91 was evaluated by 62.5-fold jump dilution, alongside covalent control **31** and non-covalent control **110**, following a 10 minute period of preincubation, with inhibitor dissociation being monitored using the Pro-Phe-Arg-AFC fluorogenic substrate[69] (Figure 2.4).

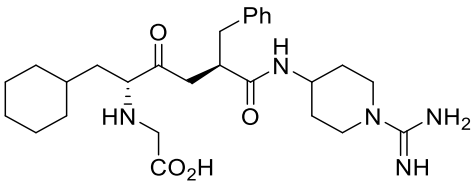

110

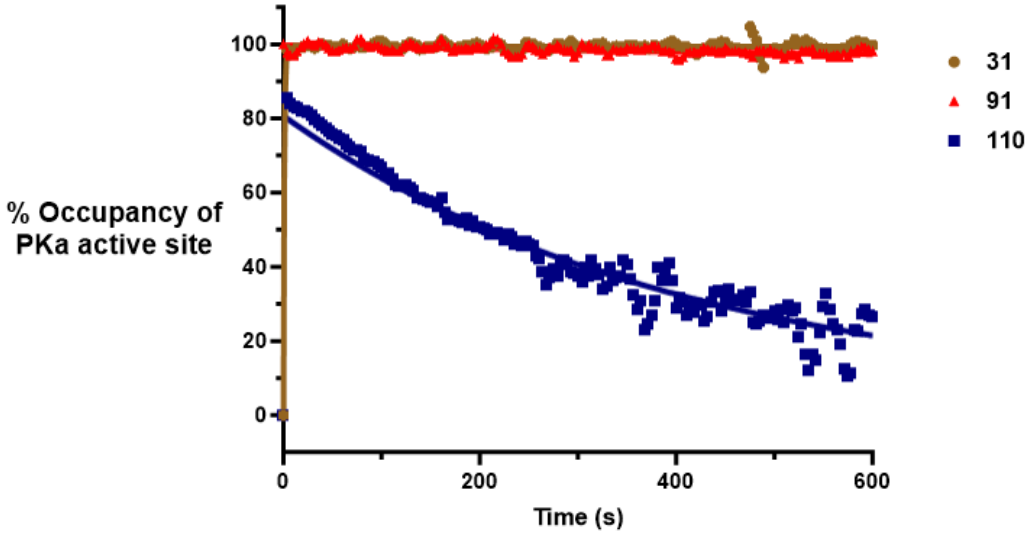

Figure 2.4. Jump dilution assay dissociation curves of **31**, **91** and **110.**

The dissociation curves of **31** and **91** showed similar profiles, with no apparent reversibility over the measured 10 minute period. However, **110**, a known non-covalent inhibitor of PKa (FE99026, IC_{50} = 4.6 nM) demonstrated slow dissociation from PKa.[150]

This experiment demonstrates that **91** matches the non-reversible binding character of known covalent inhibitor **31** when subjected to dilution, suggesting that **91** is a covalent inhibitor of PKa.

Compounds **102** and **106** were also evaluated for reversibility by jump dilution for further validation of **91** being a covalent inhibitor (Figure 2.5)

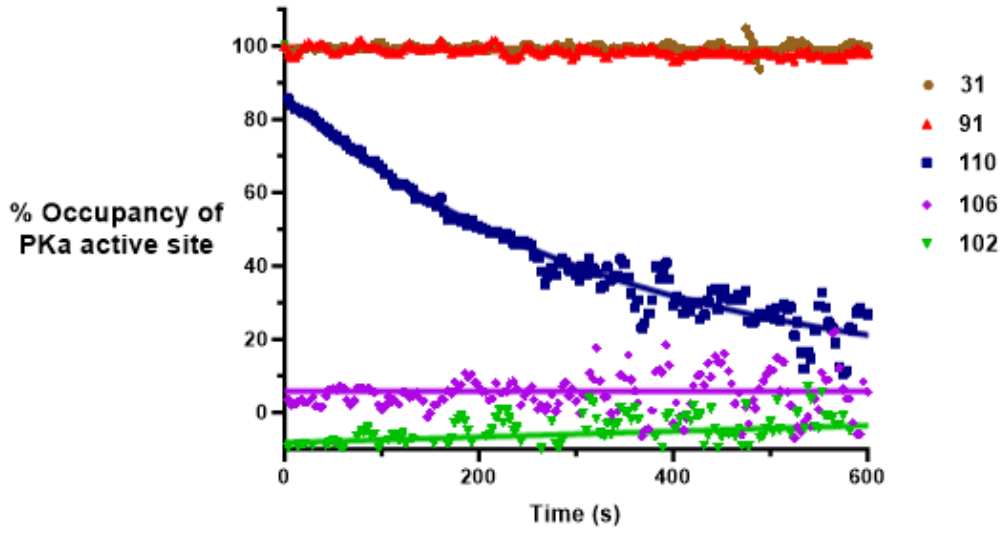

Figure 2.5. Jump dilution assay dissociation curves of **31**, **91**, **110**, **106** and **102.**

Interestingly, **102** and **106** showed fast dissociation from PKa, in contrast to **110** which displayed slow k_{off} kinetics. Overall, this supports that **91** is a covalent inhibitor by comparison with the dissociation profiles of matched pairs **102** and **106.**

2.2.2.3 Whole Plasma Binding Evaluation

Following determination of **91** as a potent covalent inhibitor in isolated enzyme assays, its potency was measured against PKa within human blood plasma to assess its effectiveness in a putative biological setting.[57] **91** was evaluated for PKa inhibition in whole plasma, in which FXII was activated with either dextran sulfate (DXS) or polyphosphate (PolyP)[151,152] (Table 2.9).

Table 2.9. Whole plasma model biological activity of **91** against PKa

Human PKa IC_{50} (nM)[a] Geomean			
1 min	10 min	1 h	2 h
90.9	6.1	0.33	0.29
Human DXS whole plasma IC_{50} (6.25 ug/mL) (nM)[a] Geomean			
5 min	30 min	1 h	2 h
482	432	529	443
Human PolyP whole plasma IC_{50} (1000ug/mL) (nM)[a] Geomean			
5 min	30 min	1 h	2 h
86.8	130	129	174

[a]Data are expressed as mean of 2 experiments, where each experimental curve was performed in triplicate.

91 showed inhibitory activity against PKa in both DXS and PolyP plasma models. As expected, the IC_{50} potency observed in either whole plasma model was significantly lower than for the isolated enzyme assay, both due to the higher enzyme concentration in the whole plasma experiments and the presence of other enzymes and components of plasma capable of interfering with PKa binding.

Additionally, no covalent binding was observed by examination of IC_{50} values across all time points. This could potentially reflect the instability of **91** and its known tendency to deborylate under a variety of conditions. In the case of the PolyP model, potency was seen to decrease over the 2 hour time course, suggesting possible protodeborylation of **91.**

For further elucidation, **91** was evaluated for IC_{50} against PKa in isolated enzyme assays at PKa concentration reflecting that found in blood plasma. PKa concentration was adjusted to 100 nM concentration in the isolated enzyme assay for comparison against the whole plasma model (Table 2.10).

Table 2.10. Biological activity of **91** and **31** at 100 nM PKa concentration

Example	**PKa IC_{50} @ 100 nM concentration (nM)[a]**		
	1 min	10 min	120 min
91	353	135	25
31	198	143	19

[a]Data are expressed as mean of 2 experiments, where each experimental curve was performed in triplicate.

Data from Table 2.10 shows that **91** acts as a covalent inhibitor at higher PKa concentrations in an isolated enzyme assay, suggesting that the integrity of **91** may have been affected within the whole plasma assays. Covalent control **31** showed comparable PKa binding to **91** at each time point.

2.2.3 Crystallography

To elucidate structural information and gain further validation of covalent binding of **91** to PKa, X-Ray Crystallography was used to image **91** within the PKa active site (Figure 2.6). Crystallographic data were produced by Paul McEwan and Lungelo Mandyoli at Evotec Ltd. Crystals of the bound enzyme-inhibitor complex were grown using a soak method according to the procedure of Tang *et al*.[70]

Unfortunately, **91** decomposed *via* protodeborylation during the crystallography protocol, perhaps due to the use of an acidic buffer medium used in the crystallisation procedure, in line with the observed method. Nonetheless, a crystal structure of deborylated analogue **106** was produced and provided insight into its binding pose in the PKa active site.

106 can be seen bridging the S1 and S4 pockets of PKa, π-stacking interactions are visible between the central pyrazole core and His_{57} as well as between the P4 pyrazole and Tyr_{174}. Importantly, the image shows Ser_{195} placed in the proximity of the benzylic carbon extending from the P1 aryl group, suggesting that covalent interaction may be able to take place between Ser_{195} and the boronate warhead in the corresponding α-amidoboronate analogue.

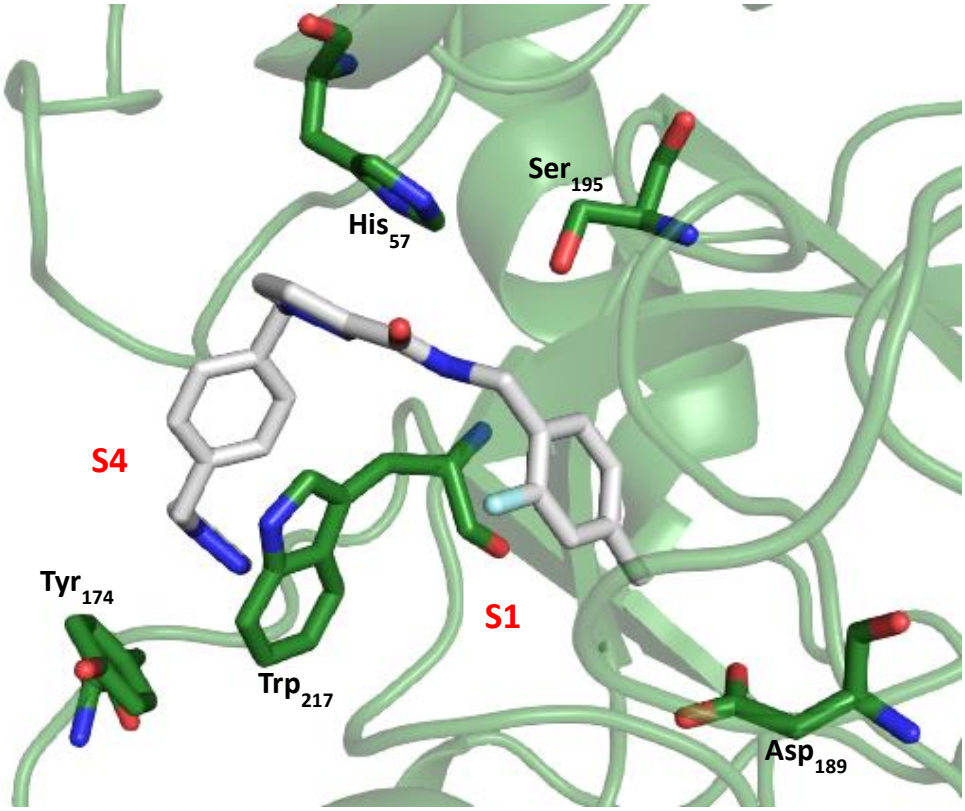

Figure 2.6. Crystal structure of **106** bound to PKa active site with labelling of S1 and S4 binding sites.

2.2.4 Buffer Stability Study

It has been noted that the α-amidoboronate compounds described in this chapter are prone to hydrolysis and protodeborylation under acidic aqueous conditions. This brought into question their stability in phosphate buffered saline (PBS), and by extension, their integrity within isolated enzyme assay conditions. It had been previously hypothesised that these compounds were hydrolysing within the isolated enzyme assays to release the corresponding boronic acids as the active binding species.

To investigate this hypothesis and assess stability, a PBS solution was made in D_2O and was acidified to physiological pH (pH = 7.4) using 20 % DCl in D_2O, in order to monitor any possible decomposition by ^1H NMR.

^1H NMR of the original sample of **95** in DMSO showed the pinacol ester protons as a two signals at δ = 0.90, 0.99 ppm due to the diastereotopicity of the pinacol protons of **95** (Figure 2.7).

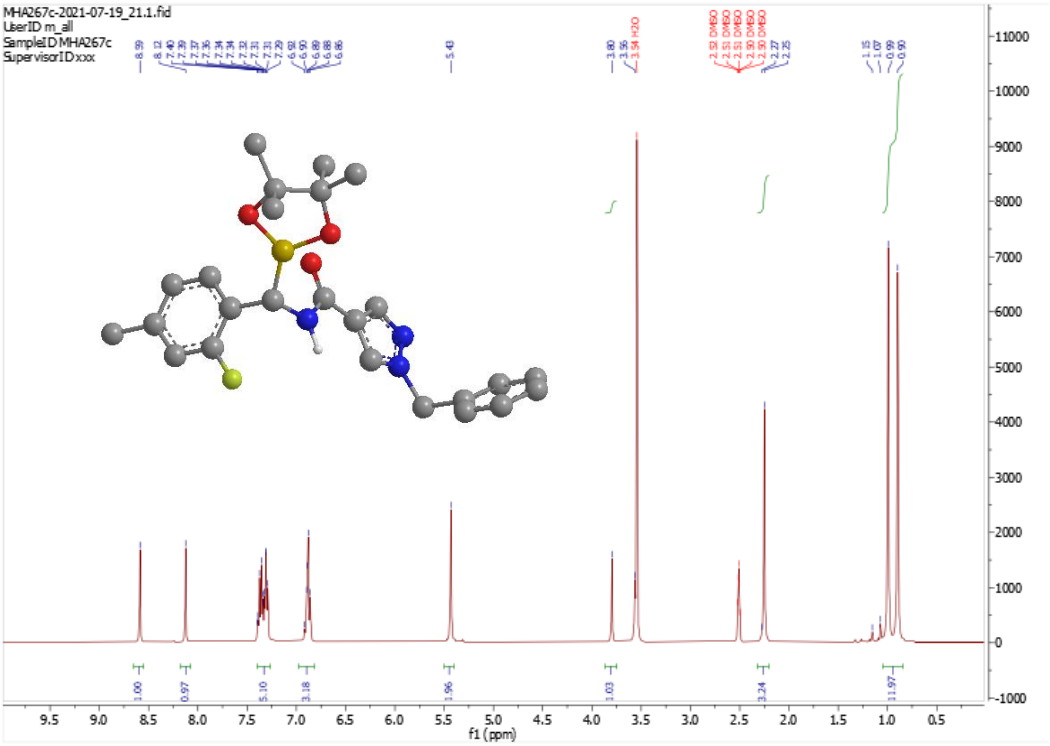

Figure 2.7. ^1H NMR spectrum of **95** in deuterated DMSO including MMFF94 energy-minimised model of **95** created in Chem3D.

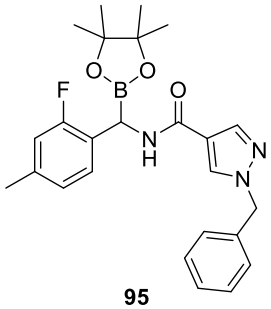

95

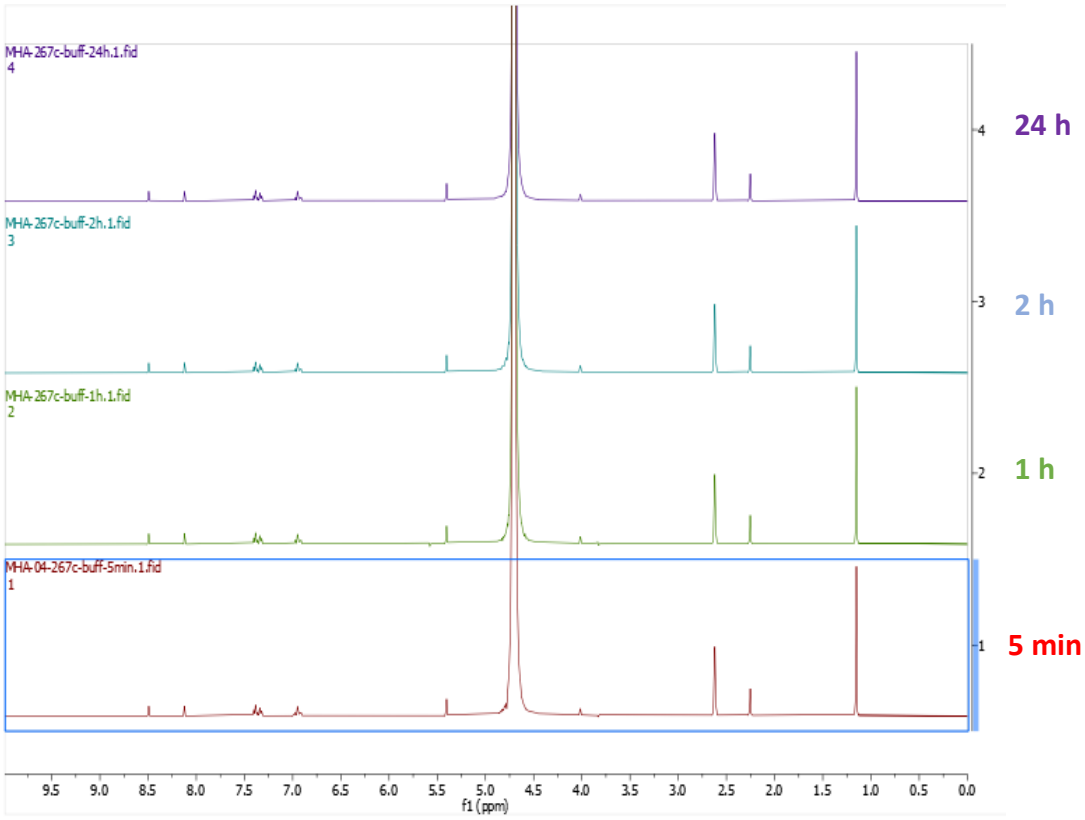

Figure 2.8. ^{1}H NMR spectra of **95** in deuterated PBS buffer over multiple time points

95 (0.5 mg) was dissolved in the D_2O buffer medium (0.4 mL) and DMSO (0.1 mL) to aide solubility, before monitoring by ^{1}H NMR at various time points to establish whether any chemical modification was taking place by reference of the observed chemical shifts (Figure 2.8).

Interestingly, examination of the shift of the pinacol protons in PBS buffer at 5 minutes showed only one signal at δ = 1.2 ppm, suggesting rapid cleavage and

release of pinacol (Scheme 2.14). This argument is further supported by comparison of the ^{1}H NMR profile of isolated pinacol, which includes a 12H singlet at around δ = 1.2 ppm.[153,154] Furthermore, a change in chemical shift of the methyne proton (BC-*H*) is seen from δ 3.80 in DMSO to δ 4.07 in deuterated PBS, further supporting the hypothesis of pinacol ester hydrolysis.

No overall change in the ^{1}H NMR profile of **95** was observed over the course of 24 hours, suggesting no further decomposition is occurring in PBS buffer solution.

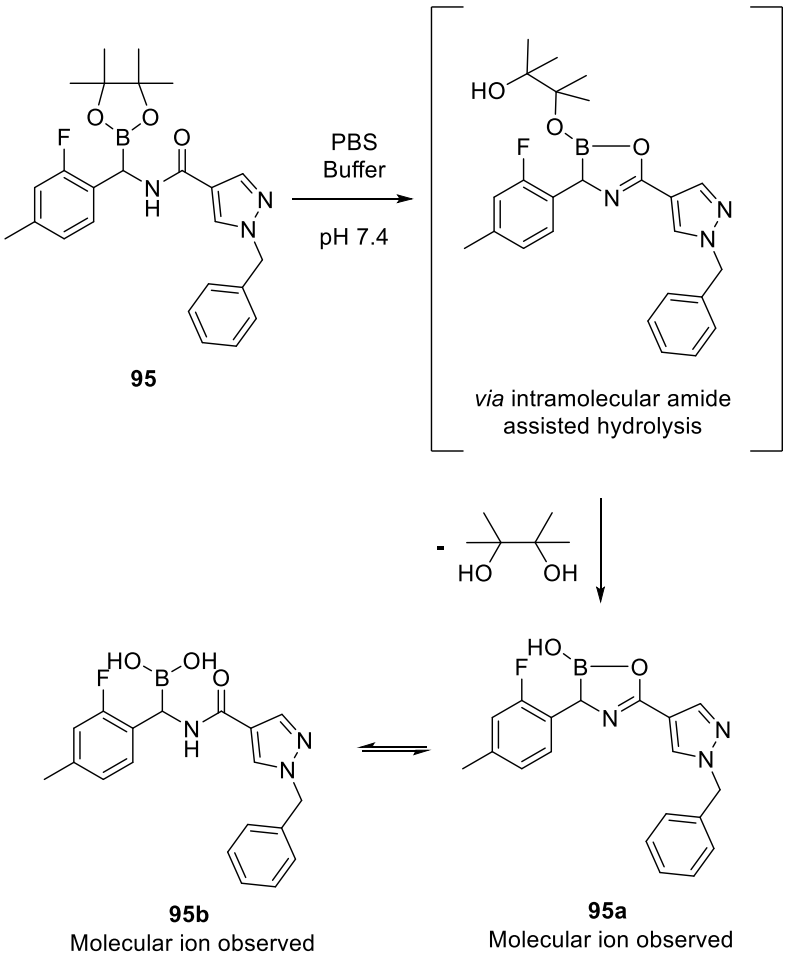

Scheme 2.14. Proposed pathway for pinacol hydrolysis of **95** in PBS buffer system.

By extension, it is probable that all α-amidoboronate analogues **91-96** exhibit pinacol ester hydrolysis in PBS buffer. This theory was further investigated through *in silico* modelling, the corresponding (*S*)-boronic acid of key compound **91** was docked into a PKa model to give assessment of the potential binding pose of the boronic acid derivative **91a** (Figure 2.9)

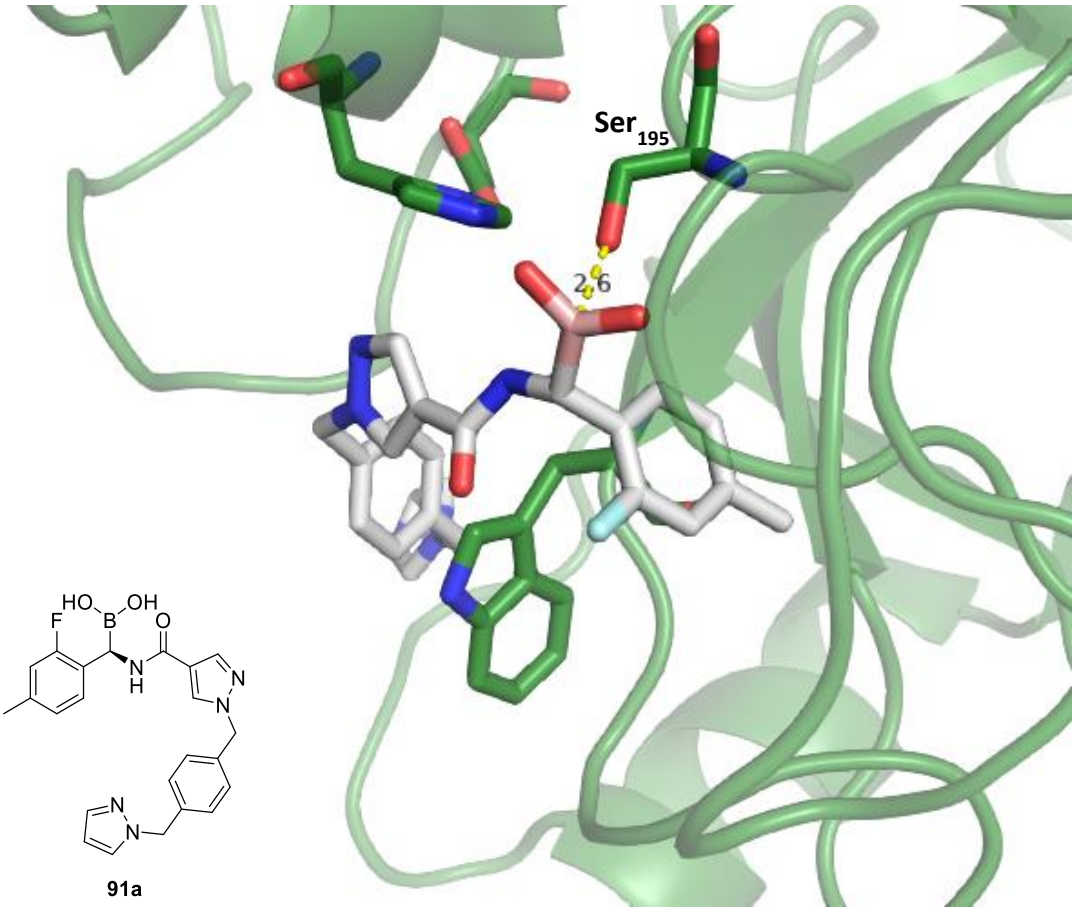

Figure 2.9. Docking of boronic acid derivate **91a** in PKa mutant model (Ala_{195}) from PDB 6O1S created in Openeye using FRED docking programme.

Visual inspection of the docking image of the (*S*)-boronic acid derivate **91a** in PKa shows close positioning of the nucleophilic oxygen atom of Ser_{195} to the boron centre. This suggests that a productive covalent interaction could take place between PKa and **91a**.

Docking of the corresponding (*R*)-enantiomer showed projection of the boronic acid group away from Ser_{195} suggesting that the (*S*)-enantiomer is the more active of the two possible stereoisomers.

No binding pose could be established for pinacol boronate **91**, suggesting that the boronic acid is likely the active species.

2.3 Conclusions

A series of highly potent α-amidoboronate covalent inhibitors of PKa was synthesised *via* a Matteson homologation sequence. Covalent inhibition was characterised through kinetic assessment of IC_{50} values over various time courses up to 24 hours, jump dilution assays, which showed **91** did not wash out from the PKa binding site, matching the profile of known PKa covalent inhibitor **31**, and comparison of IC_{50} data with that of noncovalent matched pairs. Additionally, compounds from this series were selected for evaluation against FXIa, all of which showed >1000-fold selectivity towards PKa.

Subjection of **91** to further evaluation in the form of a whole plasma IC_{50} assay showed no sign of covalent inhibition, suggesting possible decomposition of **91** under the assay conditions. The tendency of **91** to decompose was also reflected in the crystallographic analysis where decomposition was observed, producing a crystal structure of noncovalent matched pair **106**. NMR evaluation of the chemical stability of **95** in a deuterated PBS medium showed possible cleavage of the boronic ester to the corresponding boronic acid, suggesting that the boronic acid is generated within the assay medium as the active species. This assertion was supported by molecular docking simulations showing close positioning of the putative boronic acid relative to Ser_{195}.

2.4 Experimental

2.4.1 Methods and Materials

HPLC grade and analytical grade chemicals and solvents were purchased from the standard suppliers and were used without further purification. Sigma Aldrich supplied high-grade silica, 60 Å, 230-400 mesh, for flash chromatography, and deuterated solvents (Chloroform-*d*, Methanol-d_4, DMSO-d_6, Acetone-d_6) were purchased from Sigma Aldrich. Reactions were monitored by thin-layer chromatography (TLC) on commercially available silica pre-coated aluminium-backed plates (Merck Kieselgel 60 F254). Visualization was under UV light (254 nm and 366 nm), and where necessary staining with ninhydrin, potassium permanganate dips. NMR spectra were recorded with a Bruker AV(III) 400 NMR spectrometer. ^{1}H NMR was recorded at 400.13 MHz, and ^{13}C NMR was recorded at 101.6 MHz. Deuterated solvents used for the preparation of NMR samples were $CDCl_3$, MeOD-d_4, acetone-d_6 or DMSO-d_6. Chemical shifts (δ) are reported in ppm with reference to the chemical shift of the deuterated solvent. Coupling constants (*J*) are recorded in hertz, and the signal multiplicities are described by the following: s, singlet; d, doublet; t, triplet; td, triplet of doublets; q, quartet; br, broad singlet; m, multiplet; dd, doublet of doublets; ddd, double doublet of doublets; dt, doublet of triplets; p, pentet. NMR data was processed using MestReNova version 10.0.2. For the analysis of reaction mixtures and isolated compounds a Shimadzu UFLCXR HPLC was used, equipped with a Biosystems MDS SCIEX API2000 ESI+ MS. The column was a Gemini 3 µm C18 110 Å, LC column 50

x 2 nm. As eluent a mixture was used of MeCN and H_2O, containing 0.1% formic acid. Samples were run using a gradient of 1:19 v/v to 19:1 v/v over either 5 or 15 minutes, with a flowrate of 0.5 mL/min. UV absorption was detected at 254 nm and 220 nm. Preparative RP-HPLC was performed on a Waters 2767 sample manager coupled to Waters 2525 binary-gradient module and a Waters 2457 dual-wavelength absorbance detector. The column used was a Phenomenex Gemini-NX (5 µm, 110 Å, C18, 150 × 21 mm) at ambient temperature. The flow rate was 25 mL/min, and UV detection was at 254 nm. Mobile phases were solvent A, 0.1% TFA in water, and solvent B, acetonitrile, degassed by helium bubble and sonication, respectively. HRMS was done on a Bruker microTOF II mass spectrometer using electrospray ionization (ESI-TOF) operating in the positive mode. Adducts within errors of ±10 ppm were reported.

Biochemical evaluation of inhibitors was performed by Edward Duckworth, Freya Pinckney and Adrian Mogg at Kalvista Pharmaceuticals Ltd. Inhibition of PKa and FXIIa catalytic activity was assessed by monitoring the cleavage of fluorescent substrate H-D-Pro-Phe-Arg-AFC using the Tecan Spark 20M fluorometer. Compound IC_{50} values were determined as the concentration of inhibitor that provided half maximal inhibition. The length of inhibitor/enzyme preincubation was varied to indicate if compounds displayed slow binding kinetics.

All dissociation experiments were performed in buffer containing 100 mM Tris-HCl, 0.5 mM EDTA, 0.1% BSA pH 8. PKa enzyme (6.25 nM) and inhibitors were pre-incubated together using a concentration of inhibitor that generated a resulting EI complex ≥ 96% of the total enzyme concentration. After 10 min, the solution

was rapidly diluted 62.5-fold. This resulted in an enzyme concentration of 0.1 nM and an inhibitor concentration well below the IC50 with the concentration of the EI complex approximately ≤ 10%-15%. This solution was immediately transferred to an assay plate containing the fluorescent substrate (Pro-Phe-Arg-AFC) at a concentration ~10x Km in order to limit re-entrance of the inhibitor after dissociation from the enzyme. Change in fluorescence signal was then monitored over 10 min.

2.4.2 General Procedures

Representative General Procedure for Synthesis of Boronic Esters (74a-c):

To a solution of boronic acid (4 mmol) and pinacol (4 mmol) in dichloromethane (10 mL) was added anhydrous $MgSO_4$ (0.8 mmol). The resulting solution was stirred at room temperature for 16 hours, after which, it was filtered, and the filtrate concentrated *in vacuo* to afford the boronic ester which was used without further purification.

Representative General Procedure for Preparation of Aminoboronate HCl salts (77a-c)[140]:

To a -78 ^oC cooled solution of dichloromethane (33.0 mmol) and aryl pinacol boronate (6.61 mmol) in THF (20 mL) was added *n*-butyl lithium (6.61 mmol), the reaction mixture was allowed to stir for 16 hours, during which it warmed to ambient temperature. The reaction mixture was then re-cooled to -78 ^oC and was allowed to stir for 16 hours, after which, the solvent was removed *in vacuo*, the residue was dissolved in hexane (50 mL) and passed through celite. The resulting filtrate was concentrated *in vacuo* and redissolved in diethyl ether (15 mL). This solution was then stirred at -78 ^oC before careful addition of hydrochloric acid (10 mL, 19.82 mmol) (4M in dioxane). The solution was allowed to stir for 30 min and then stood at rt for 2h, leading to precipitation of the desired compound, which was washed by decantation with cold Et_2O and collected by filtration.

Representative General Procedure for Amide Coupling of Aminoboronate HCl salts (90-96):

To a stirring, ice-cooled solution of aminoboronate salt (0.17 mmol), carboxylic acid (0.17 mmol) and HATU (0.19 mmol) in MeCN (2 mL) was added DIPEA (0.51 mmol). The ice-bath was removed, and the reaction mixture was stirred at rt for a period of 3 hours. Upon completion, the solvent was removed *in vacuo* and the residue was purified by C18-prep-HPLC (10-90% MeCN in H_2O) and lyophilised to dryness to afford the title compounds.

Representative General Procedure for Amide Coupling of Benzylamines (102-109):

To a stirring solution of carboxylic acid (0.16 mmol), HATU (0.16 mmol) and DIPEA (0.48 mmol) in MeCN (2 mL) was added substituted benzylamine (0.16 mmol). The reaction mixture was allowed to stir at room temperature for 1 hour, after which the solvent was removed *in vacuo* and the crude residue was purified by flash chromatography (0-10% MeOH in DCM) to afford the title compounds.

2.4.3 Chemical Characterisation

Methyl 2-amino-2-(3-chlorophenyl)acetate (66)

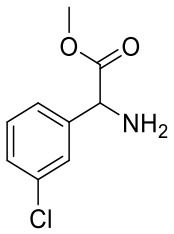

To a room temperature, stirring solution of 3-chlorophenyl glycine (2.00 g, 10.0 mmol) in methanol (20 mL), was added thionyl chloride (0.73 mL, 10.0 mmol). The reaction mixture was heated to reflux and stirred for 16 hours. The resulting solution was concentrated *in vacuo* to afford a residue which was dissolved in ethyl acetate (25 mL) and washed with water (3 x 25 mL) and brine (25 mL). The combined organics were dried over $MgSO_4$, filtered, and evaporated to dryness to afford the title compound as a colourless oil which was used without further purification (1.76 g, 88 %). ^{1}H NMR (400 MHz, MeOD-*d*$_4$) δ 7.86 (s, 1H, Ar-*H*), 7.65 (d, *J* = 8.2 Hz, 1H, Ar-*H*), 7.32 (m, 2H, Ar-*H*), 5.41 (s, 1H, C=OC-*H*), 3.86 (s, 3H, -C*H*$_3$) ^{13}C NMR (101 MHz, MeOD-*d*$_4$) δ 168.1, 157.2, 155.2, 155.0, 153.8, 151.1, 150.1, 87.1, 55.2 LCMS (ESI+) m/z calcd for $C_9H_{10}ClNO_2$ = 199.0, found 200.0 [M+H]

Methyl 2-(1-benzyl-1*H*-pyrazole-4-carboxamido)-2-(3-chlorophenyl)acetate (68)

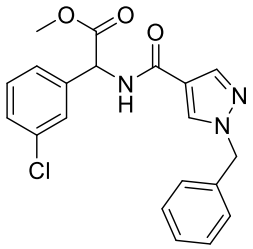

66 (100 mg, 0.50 mmol), **67** (101 mg, 0.50 mmol), EDC (78 mg, 0.50 mmol) and HOBt (68 mg, 0.50 mmol) were charged into a reaction vessel, to which was added anhydrous DMF (2 mL). The reaction mixture was stirred at room temperature for 5 minutes before the addition of DIPEA (0.26 mL, 1.50 mmol). The reaction mixture continued to stir for 16 hours, following which it was diluted with ethyl acetate (25 mL) and washed with 3 x 100 mL portions of water. The resulting organics were then washed with 2.0 M aqueous HCl (10 mL), 2.0 M aqueous NaOH (10 mL) and then brine (10 mL). The combined organics were dried over $MgSO_4$, filtered, and evaporated to dryness *in vacuo*. The resulting residue was purified by silica gel flash chromatography, eluting with 30-50 % EtOAc in petroleum ether, to afford the title compound as a pale yellow oil (123 mg, 64%) ^{1}H NMR (400 MHz, MeOD-d_4) δ 8.44 (s, 1H, Ar-*H*), 8.21 (s, 1H, Ar-*H*), 8.01 (s, 1H, Ar-*H*), 7.52 – 7.24 (m, 8H, Ar-*H*), 5.68 (s, 1H, C=OC-*H*), 5.36 (s, 2H, -CH_2), 4.87 (s, 3H, -OCH_3) ^{13}C NMR (101 MHz, MeOD-d_4) δ 171.0, 163.2, 139.3, 137.3, 136.0, 134.8, 134.1, 131.9, 130.0, 129.4, 128.5, 128.5, 127.9, 127.6, 117.5, 56.2, 55.6, 51.8 LCMS (ESI+) m/z calcd for $C_{20}H_{18}ClN_3O_3$ = 383.1, found 384.4 [M+H]

2-(1-Benzyl-1*H*-pyrazole-4-carboxamido)-2-(3-chlorophenyl)acetic acid (69)

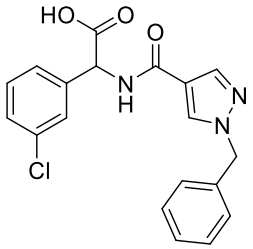

68 (100 mg, 0.26 mmol) was dissolved in EtOH/H_2O (1:5) (5 mL) and NaOH (100 mg, 2.5 mmol) was added. The reaction mixture was stirred at 50 ^oC for 3 hours, after which it was acidified to pH 1-2, forming a precipitate which was collected and dried *in vacuo* to afford the title compound as a white solid (74 mg, 77%) ^1H NMR (400 MHz, MeOD-d_4) δ 8.77 (s, 1H, Ar-*H*), 8.40 (s, 1H, Ar-*H*), 8.00 (s, 1H, Ar-*H*), 7.54 – 7.52 (m, 1H, Ar-*H*), 7.45 – 7.39 (m, 3H, Ar-*H*), 7.37 – 7.34 (m, 2H, Ar-*H*), 7.28 – 7.25 (m, 2H, Ar-*H*), 5.60 (s, 1H, C=OC-*H*), 5.36 (s, 2H, -CH_2) ^{13}C NMR (101 MHz, MeOD-d_4) δ 172.0, 161.9, 141.3, 140.2, 139.8, 137.3, 134.3, 133.5, 132.5, 130.8, 129.1, 128.3, 128.3, 127.4, 118.2, 56.0, 55.6 LCMS (ESI+) m/z calcd for $C_{19}H_{13}ClN_3O_3$ = 369.1, found 370.1 [M+H]

(4,4,5,5-Tetramethyl-1,3,2-dioxaborolan-2-yl)methanamine hydrochloride (72)[155]

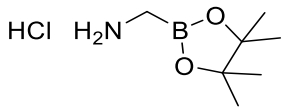

To a -78 °C stirring solution of bromomethyl boronic acid pinacol ester (1.00 g, 4.55 mmol) was added lithium HMDS (1.0 M solution in THF) (4.55 mL, 4.55 mmol). The solution was stirred for 16 hours, allowing warming to room temperature, following which the reaction mixture was concentrated *in vacuo*, dissolved in cyclohexane, and filtered through celite. The filtrate was concentrated *in vacuo* to yield a clear oil which was dissolved in ether (20 mL), cooled to -78 °C and acidified with 4N HCl in dioxane (3 mL). This mixture was stirred for 2 hours, leading to the formation of a precipitate which was collected and dried to yield the title compound as a white solid (448 mg, 58%). ^{1}H NMR (400 MHz, DMSO-d_6) δ 6.53 (s, 2H, -NH_2), 5.47 (s, 2H, -CH_2), 1.12 (s, 12H, -CH_3) ^{13}C NMR (101 MHz, DMSO-d_6) 76.6, 52.4, 38.9 LCMS (ESI+) m/z calcd for $C_7H_{16}BClNO_2$ = 193.1, found 158.1 [M-Cl]

((2-(1-benzyl-1*H*-pyrazole-4-carboxamido)-2-(3-chlorophenyl)acetamido)methyl)boronic acid (73)

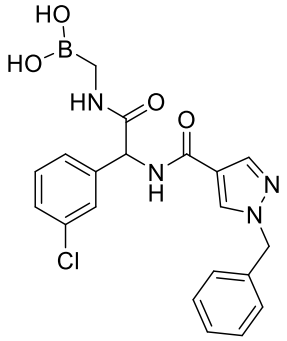

69 (100 mg, 0.27 mmol), **72** (60 mg, 0.27 mmol) and HATU (103 mg, 0.27 mmol) were dissolved in anhydrous DMF (2 mL), the reaction mixture was cooled to 0 °C before addition of DIPEA (0.14 mL, 0.81 mmol). The reaction mixture was allowed to stir for 3 hours whilst warming to room temperature, following which, the solvent was removed *in vacuo,* the resulting residue was dissolved in DMSO (2 mL), loaded onto a Puriflash C18 12g cartridge and purified in acetonitrile in water (10 – 90%). The acetonitrile was removed *in vacuo* and the resulting aqueous solution was lyophilised to dryness to afford the title compound as a white solid (41 mg, 36%). ^{1}H NMR (400 MHz, DMSO-d_6); δ 8.39 (s, 1H, Ar-*H*), 7.98 (s, 1H, Ar-*H*), 7.53 – 7.50 (m, 1H, Ar-*H*), 7.42 – 7.29 (m, 6H, Ar-*H*), 7.28 – 7.24 (m, 2H, Ar-*H*), 5.64 (s, 1H, C=OC-*H*), 5.33 (s, 2H, -CH_2), 2.73 – 2.51 (m, 2H, -CH_2) ^{13}C NMR (101 MHz, DMSO-d_6) δ 169.7, 161.8, 142.1, 139.9, 137.3, 136.2 133.3, 132.5, 130.5, 129.1, 128.3, 127.8, 126.8, 125.3 118.4, 56.1, 55.6, 47.5 LCMS (ESI+) m/z calcd for $C_{22}H_{20}BClN_4O_4$ = 426.1, found 427.3 [M+H].

Ethyl 1-(4-(chloromethyl)benzyl)-1*H*-pyrazole-4-carboxylate (83)

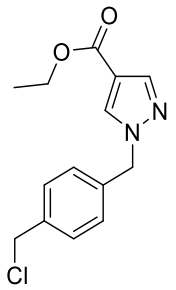

To an ice-cooled solution of (4-(chloromethyl)phenyl)methanol (1000 mg, 6.39 mmol), Ethyl 1H-pyrazole-4-carboxylate (984 mg, 7.02 mmol) and Triphenylphosphine (2512 mg, 9.58 mmol), was added diisopropyl diazene-1,2-dicarboxylate (DIAD) (1937 mg, 9.58 mmol). The resulting solution was allowed to stir for 1 hour under ice-cooling and then for a further 2 hours at room temperature. Upon completion, the reaction mixture was concentrated *in vacuo* and the resulting residue purified on silica (0-70 % EtOAc in hexanes), to afford the title compound as a white solid. (1.56g, 88 %) ^{1}H NMR (400 MHz, DMSO-d_6) δ 8.47 (s, 1H, Ar-*H*), 7.87 (s, 1H, Ar-*H*), 7.42 (d, *J* = 7.9 Hz, 2H, Ar-*H*), 7.28 (d, *J* = 7.9 Hz, 2H, Ar-*H*), 5.38 (s, 2H, -CH_2), 4.74 (s, 2H, -CH_2), 4.21 (q, *J* = 7.1 Hz, 2H, -OCH_2), 1.26 (t, *J* = 7.1 Hz, 3H, -CH_3). ^{13}C NMR (101 MHz, $CDCl_3$) δ = 162.9, 141.3, 137.8, 135.6, 132.7, 129.2, 128.3, 115.6, 56.0, 45.6, 21.9, 14.3. LCMS (ESI+) m/z calcd for $C_{14}H_{15}ClN_2O_2$ = 278.1, found 279.2 [M+H].

Ethyl 1-(4-((1*H*-pyrazol-1-yl)methyl)benzyl)-1*H*-pyrazole-4-carboxylate (86)[57]

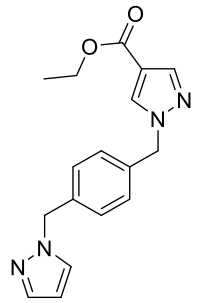

To a stirring ice-cooled solution of **83** (1000 mg, 3.59 mmol) and pyrazole (489 mg, 7.18 mmol) was added Sodium hydride (60% in mineral oil) (258 mg, 10.76 mmol). The reaction mixture was then heated to 80ºC and stirred for 2 hours. Upon completion, the mixture was diluted with DCM, filtered through celite and concentrated *in vacuo*. The resulting residue was purified by on silica (0-10% MeOH in DCM) to yield the title compound as a white solid. (887 mg, 80%). ^{1}H NMR (400 MHz, $CDCl_3$) δ = 7.97 (s, 1H, Ar-*H*), 7.78 (s, 1H, Ar-*H*), 7.43 (d, *J* = 2.2 Hz, 1H, Ar-*H*), 7.39 (d, *J* = 2.2 Hz, 1H, Ar-*H*), 7.11– 7.09 (m, 4H, Ar-*H*), 6.27 (t, *J* = 2.2 Hz, 1H, Ar-*H*), 5.34 (s, 2H, -C*H*$_2$), 5.29 (s, 2H, -C*H*$_2$) 3.21 (q, *J* = 4.3 Hz, 2H, -OC*H*$_2$), 2.89 (t, *J* = 4.3 Hz, 3H, -C*H*$_3$) ^{13}C NMR (101 MHz, $CDCl_3$) δ = 163.4, 140.9, 140.2, 138.0, 133.2, 132.3, 129.1, 128.0, 127.5, 114.5, 106.1, 56.1, 55.3, 24.3, 21.8. LCMS (ESI+) m/z calcd for $C_{17}H_{18}N_4O_2$ = 310.1, found 311.1 [M+H].

1-(4-((1*H*-pyrazol-1-yl)methyl)benzyl)-1*H*-pyrazole-4-carboxylic acid (87)[57]

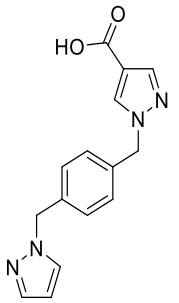

86 (500 mg, 1.61 mmol) and NaOH (322 mg, 8.06 mmol) were dissolved in THF/H_2O (10 mL/2 mL). The mixture was warmed to 50 ^oC for 3 hours, after which it was concentrated *in vacuo*, diluted with H_2O (20 mL) and acidified to pH 1. The acidified aqueous layer was extracted with ethyl acetate (3 x 20 mL) and the combined organics washed with brine and dried over $MgSO_4$ before concentration *in vacuo*. The resulting residue was purified by flash chromatography (0-10% MeOH in DCM) to afford the title compound as a white solid. (296 mg, 65%). ^1H NMR (400 MHz, DMSO-d_6) δ = 12.21 (br, 1H, -COO*H*), 7.97 (s, 1H, Ar-*H*), 7.89 (s, 1H, Ar-*H*), 7.56 (d, *J* = 2.2 Hz, 1H, Ar-*H*), 7.39 (d, *J* = 2.2 Hz, 2H, Ar-*H*), 7.25 – 7.12 (m, 4H, Ar-*H*), 6.29 (t, *J* = 2.2 Hz, 2H, Ar-*H*), 5.34 (s, 2H, -CH_2), 5.29 (s, 2H, -CH_2). ^{13}C NMR (101 MHz, DMSO-d_6) δ = 166.9, 141.9, 141.3, 139.7, 137.2, 135.0, 133.3, 132.7, 129.5, 128.5, 128.2, 114.9, 106.2, 56.1, 55.4. LCMS (ESI+) m/z calcd for $C_{15}H_{14}N_4O_2$ = 282.1, found 283.3 [M+H].

Ethyl 1-(4-((2-oxopyridin-1(2*H*)-yl)methyl)benzyl)-1*H*-pyrazole-4-carboxylate (84)[57]

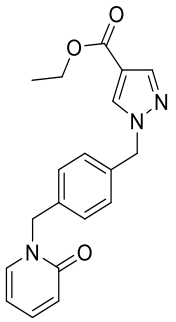

83 (1000 mg, 3.59 mmol) and pyridin-2-ol (341 mg, 3.59 mmol) were dissolved in DMF (10 mL) at room temperature, NaH (60% dispersion in mineral oil) (258 mg, 10.76 mmol) was added and the mixture was stirred at 50°C for 12h. Upon completion, the inhomogeneous reaction mixture was filtered, concentrated *in vacuo* and purified by flash chromatography (0-10% MeOH in DCM) to afford the title compound as a white solid. (786 mg, 65%). ^{1}H NMR (400 MHz, DMSO-d_6) δ = 8.01 (s, 1H, Ar-*H*), 7.83 (s, 1H, Ar-*H*), 7.80 (ddd, *J* = 6.7, 2.0, 0.7 Hz, 1H, Ar-*H*), 7.45 (ddd, 1H, *J* = 9.2, 6.7, 2.0 Hz), 7.41 – 7.25 (m, 4H, Ar-*H*), 6.60 (ddd, *J* = 9.2, 1.4, 0.7 Hz, 1H, Ar-*H*), 6.15 (td, *J* = 6.7, 1.4 Hz, 1H, Ar-*H*), 5.28 (s, 2H, -CH_2), 5.13 (s, 2H, -CH_2), 4.27 (q, *J* = 4.1 Hz, 2H, -OCH_2), 1.32 (t, *J* = 4.1 Hz, 3H, -CH_3). ^{13}C NMR (101 MHz, DMSO-d_6) δ 162.9, 162.6, 141.3, 139.5, 137.3, 136.8, 135.2, 132.7, 128.7, 128.4, 121.3, 115.6, 106.3, 60.2, 56.0, 51.6, 50.2. LCMS (ESI+) m/z calcd for $C_{19}H_{19}N_3O_3$ = 337.1, found 338.3 [M+H].

1-(4-((2-Oxopyridin-1(2*H*)-yl)methyl)benzyl)-1*H*-pyrazole-4-carboxylic acid (85)[57]

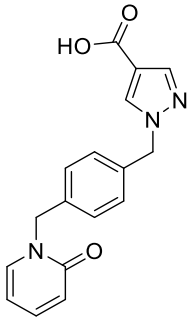

For method, see **87**. White solid. (532 mg, 64 %) ^{1}H NMR (400 MHz, DMSO-d_6) δ 12.33 (br, 1H, -COO*H*), 8.36 (s, 1H, Ar-*H*), 7.79 (s, 1H, Ar-*H*), 7.77 (ddd, *J* = 6.7, 2.0, 0.6 Hz, 1H, Ar-*H*), 7.41 (ddd, *J* = 8.9, 6.7, 2.0 Hz, 1H, Ar-*H*), 7.29 – 7.21 (m, 4H, Ar-*H*), 6.40 (ddd, *J* = 8.9, 1.1, 0.6 Hz, 1H, Ar-*H*), 6.22 (td, *J* = 6.7, 1.1 Hz, 1H, Ar-*H*), 5.33 (s, 2H, -CH_2), 5.07 (s, 2H, CH_2). ^{13}C NMR (101 MHz, DMSO-d_6) δ 163.1, 160.8, 140.2, 139.5, 138.5, 136.5, 135.4, 133.2, 127.5, 127.3, 119.3, 114.4, 104.9, 54.1, 50.2 LCMS (ESI+) m/z calcd for $C_{17}H_{15}N_3O_3$ = 309.1, found 310.2 [M+H]

3-(Methoxymethyl)-1-(4-((2-oxopyridin-1(2*H*)-yl)methyl)benzyl)-1*H*-pyrazole-4-carboxylic acid (88)

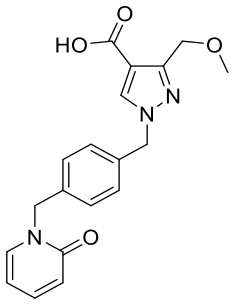

Off white solid. ^{1}H NMR (400 MHz, DMSO-d_6) δ 12.27 (br, 1H, -COO*H*) 8.32 (s, 1H, -Ar-*H*), 7.76 (ddd, *J* = 6.7, 2.1, 0.7 Hz, 1H, Ar-*H*), 7.41 (ddd, *J* = 8.9, 6.7, 2.1 Hz, 1H, Ar-*H*), 7.31 – 7.21 (m, 4H, Ar-*H*), 6.41 (ddd, *J* = 8.9, 1.4, 0.7 Hz, 1H, Ar-*H*), 6.22 (td, *J* = 6.7, 1.4 Hz, 1H, Ar-*H*), 5.30 (s, 2H -CH_2), 5.08 (s, 2H, -CH_2), 4.51 (s, 2H, -CH_2), 3.23 (s, 3H, -CH_3). ^{13}C NMR (101 MHz, DMSO-d_6) δ 164.4, 161.9, 150.5, 140.6, 139.5, 137.6, 136.4, 135.6, 128.5, 128.4, 120.3, 113.1, 106.0, 66.0, 58.0, 55.1, 51.3. LCMS (ESI+) m/z calcd for $C_{19}H_{19}N_3O_4$ = 353.1, found 354.2 [M+H] *Obtained from the compound library of Kalvista Pharmaceuticals Ltd.

3-(Methoxymethyl)-1-(4-((4-methyl-1*H*-pyrazol-1-yl)methyl)benzyl)-1*H*-pyrazole-4-carboxylic acid (89)

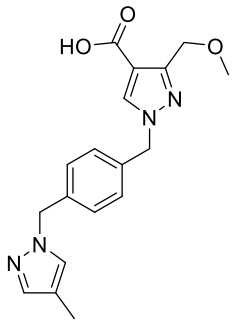

Off white solid. ^{1}H NMR (400 MHz, DMSO-d_6) δ 12.25 (br, 1H, -COO*H*) 8.32 (s, 1H, Ar-*H*), 7.26 – 7.21 (m, 4H, Ar-*H*), 7.20 – 7.16 (m, 2H, Ar-*H*), 5.29 (s, 2H, -CH_2), 5.21 (s, 2H, -CH_2), 4.50 (s, 2H, -CH_2), 3.23 (s, 3H, -OCH_3), 1.98 (s, 3H, -CH_3). ^{13}C NMR (101 MHz, DMSO-d_6) δ 164.4, 150.5, 139.7, 138.2, 136.4, 135.6, 129.2, 128.4, 128.2, 115.7, 113.0, 66.0, 58.0, 55.1, 54.8, 12.3 *Obtained from the compound library of Kalvista Pharmaceuticals Ltd.

2-(3-chlorophenyl)-4,4,5,5-tetramethyl-1,3,2-dioxaborolane (74a)[156]

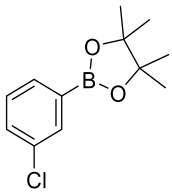

Colourless oil. (1430 mg, 99%) ^{1}H NMR (400 MHz, DMSO-d_6) δ 7.81 (d, *J* = 0.9 Hz, 1H, Ar-*H*), 7.75 (d, *J* = 6.8 Hz, 1H, Ar-*H*), 7.49 (dd, *J* = 6.8, 0.9 Hz, 1H, Ar-*H*), 7.34 (t, *J* = 6.8 Hz, 1H, Ar-*H*) 1.40 (s, 12H, -C*H*$_3$) ^{13}C NMR (101 MHz, DMSO-d_6) δ 137.1, 137.0, 134.3, 132.2, 131.9, 129.8, 85.0, 26.1 LCMS (ESI+) m/z calcd for $C_{12}H_{16}BClO_2$ = 238.1, found 239.1 [M+H]

2-(3-Chloro-2-fluorophenyl)-4,4,5,5-tetramethyl-1,3,2-dioxaborolane (74c)[157]

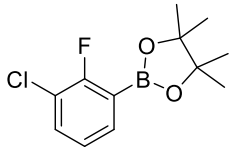

White solid. (1310 mg, quant.) ^{1}H NMR (400 MHz, DMSO-d_6) δ 7.63 – 7.60 (m, 1H, Ar-*H*), 7.53 – 7.50 (m, 1H, Ar-*H*), 7.11 (t, *J* = 7.6 Hz, 1H, Ar-*H*), 1.36 (s, 12H, -C*H*$_3$) ^{13}C NMR (101 MHz, DMSO-d_6) δ 163.1, 130.7, 133.1, 127.7, 125.7, 120.8, 88.4, 24.8 LCMS (ESI+) m/z calcd for $C_{12}H_{15}BClFO_2$ = 256.1, found = 257.1 [M+H]

2-(2-fluoro-4-methylphenyl)-4,4,5,5-tetramethyl-1,3,2-dioxaborolane (74b)[158]

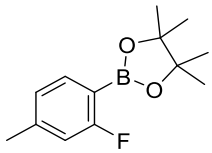

Colourless solid. (1540 mg, quant.) ^{1}H NMR (400 MHz, DMSO-*d*$_6$) δ 7.53 (s, 1H, Ar-*H*), 7.03 (d, *J* = 7.5 Hz, 1H, Ar-*H*), 6.97 (d, *J* = 7.5 Hz, 1H, Ar-*H*), 1.29 (s, 12H, -C*H*$_3$). ^{13}C NMR (101 MHz, DMSO-*d*$_6$) δ 168.2, 165.8, 145.1, 136.9, 125.3, 116.3, 84.0, 25.1, 21.4 LCMS (ESI+) m/z calcd for $C_{13}H_{18}BFO_2$ = 236.1, found 237.1 [M+H]

(3-Chlorophenyl)(4,4,5,5-tetramethyl-1,3,2-dioxaborolan-2-yl)methanamine hydrochloride (77a)

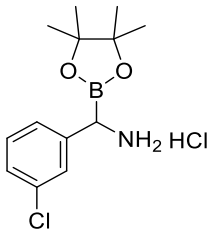

White solid. (509 mg, 40%, 3 steps) ^{1}H NMR (400 MHz, DMSO-*d*$_6$) δ 8.55 (s, 1H, Ar-*H*), 7.46 – 7.43 (m, 3H, Ar-*H*), 4.06 – 3.90 (m, 1H, BC-*H*), 2.36, (br, 2H, -*NH*$_2$), 1.26 (s, 6H, -C*H*$_3$), 1.13 (s, 6H, -C*H*$_3$). ^{13}C NMR (101 MHz, DMSO-*d*$_6$), δ 135.2, 132.9, 130.5, 130.1, 129.1, 123.5, 85.3, 66.8, 24.9 LCMS was not obtained due to compound decomposition on HPLC column.

(3-Chloro-2-fluorophenyl)(4,4,5,5-tetramethyl-1,3,2-dioxaborolan-2-yl)methanamine hydrochloride (77c)

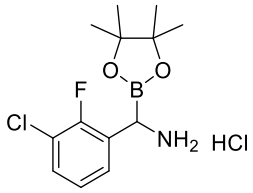

White solid (38 mg, 7%, 3 steps), ^{1}H NMR (400 MHz, DMSO-d_6) δ 7.71 – 7.49 (m, 3H, Ar-*H*), 4.16 (s, 1H, BC-*H*), 2.44 (br, 2H, -NH_2), 1.32 (s, 6H, -CH_3), 1.24 – 1.20 (m, 6H, -CH_3). ^{13}C NMR (101 MHz, DMSO-d_6) δ 161.1, 131.4, 128.6, 126.6, 125.4, 120.1, 88.5, 65.4, 24.0. LCMS was not obtained due to compound decomposition on HPLC column.

(2-Fluoro-4-methylphenyl)(4,4,5,5-tetramethyl-1,3,2-dioxaborolan-2-yl)methanamine hydrochloride (77b)

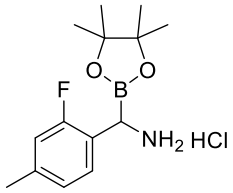

White solid. (250 mg, 20%, 3 steps) ^{1}H NMR (400 MHz, DMSO-d_6) δ 8.46 (s, 1H, Ar-*H*), 7.69 – 7.45 (m, 1H, Ar-*H*), 7.45 – 7.32 (m, 1H, Ar-*H*), 4.12 – 3.93 (m, 1H, BC-*H*), 2.30 (br, 2H, -NH_2), 1.37 (s, 6H, -CH_3), 1.18 (s, 6H, -CH_3). ^{13}C NMR (101 MHz, DMSO-d_6) δ 161.4, 141.1, 131.2, 125.8, 120.2, 116.4, 85.3, 66.7, 24.8, 21.0. LCMS was not obtained due to compound decomposition on HPLC column.

1-Benzyl-*N*-((3-chlorophenyl)(4,4,5,5-tetramethyl-1,3,2-dioxaborolan-2-yl)methyl)-1*H*-pyrazole-4-carboxamide (78)

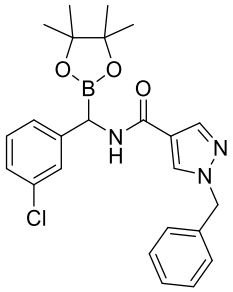

White solid (86 mg, 56%) ^{1}H NMR (400 MHz, MeOD-d_4) δ 8.44 (s, 1H, Ar-*H*), 8.13 (s, 1H, Ar-*H*), 7.43 – 7.31 (m, 5H, Ar-*H*), 7.19 – 7.12 (m, 3H, Ar-*H*), 7.09 – 7.03 (m, 1H, Ar-*H*), 5.44 (s, 2H, -C*H*$_2$), 2.98 (s, 1H, BC-*H*), 1.12 (s, 6H, -C*H*$_3$), 0.96 (s, 6H, -C*H*$_3$) ^{13}C NMR (101 MHz, MeOD-d_4) δ 168.0, 143.9, 139.9, 138.7, 135.6, 133.6, 131.5, 129.1, 128.6, 128.1, 127.7, 125.9, 125.2, 124.5, 109.9, 80.3, 55.9, 24.0. LCMS (ESI+) m/z calcd for $C_{24}H_{27}BClN_3O_3$ = 452.1, found 452.2 [M+H]

((1-Benzyl-1*H*-pyrazole-4-carboxamido)(3-chlorophenyl)methyl)boronic acid (79)[132]

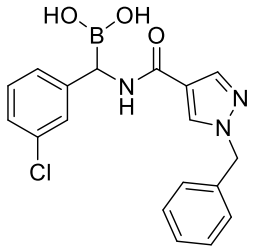

78 (50 mg, 0.11 mmol) and pentylboronic acid (63 mg, 0.55 mmol) were stirred in methanol/cyclohexane (1:1) (4 mL). 3N aqueous HCl (2 mL) was added, and the mixture was stirred at room temperature for 16 hours. Upon completion, the reaction mixture was washed with cyclohexane (3 x 5 mL) and the water/methanol layer was collected and concentrated *in vacuo* at room temperature. The resulting residue was dissolved in 2N aqueous NaOH (2 mL) and re-concentrated *in vacuo* at room temperature. The remaining material was dissolved in DMSO (1 mL) and loaded onto a 12g Puriflash C18 cartridge and purified, eluting with 10 – 90% acetonitrile in water. The resulting aqueous fractions were lyophilised to dryness to afford the title compound as a white solid (9 mg, 23%). ^{1}H NMR (400 MHz, DMSO-d_6) δ 8.74 (s, 1H, Ar-*H*), 8.38 (s, 1H, Ar-*H*), 7.67 – 7.60 (m, 3H, Ar-*H*), 7.42 – 7.32 (m, 5H, Ar-*H*), 7.12 – 7.09 (m, 1H, Ar-*H*), 5.51 (s, 2H, -CH_2), 4.33 (s, 1H, BC-*H*) ^{13}C NMR (101 MHz, DMSO-d_6) δ 158.8, 153.2, 142.7, 136.9, 136.5, 134.9, 134.3, 130.4, 129.2, 129.1, 128.6, 128.5, 122.3, 107.1, 56.0, 55.5. LCMS was not obtained due to compound decomposition on HPLC column.

1-(4-((1*H*-pyrazol-1-yl)methyl)benzyl)-*N*-((3-chlorophenyl)(4,4,5,5-tetramethyl-1,3,2-dioxaborolan-2-yl)methyl)-1*H*-pyrazole-4-carboxamide (90)

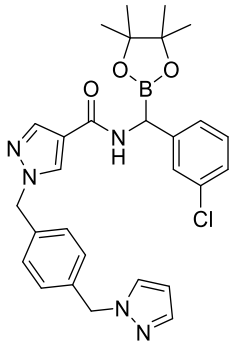

White solid (6 mg, 23%). ^{1}H NMR (400 MHz, MeOD-d_4) δ 8.45 (s, 1H, Ar-*H*), 8.14 (s, 1H, Ar-*H*), 7.72 (d, *J* = 2.2 Hz, 1H, Ar-*H*), 7.55 (d, *J* = 2.2 Hz, 1H, Ar-*H*), 7.38 – 7.22 (m, 4H, Ar-*H*), 7.19 – 7.12 (m, 3H, Ar-*H*), 7.10 – 7.03 (m, 1H, Ar-*H*), 6.37 (t, *J* = 2.2 Hz, 1H, Ar-*H*), 5.45 (s, 2H, -CH_2), 5.39 (s, 2H, -CH_2), 3.83 (s, 1H, BC-*H*), 1.17 (s, 6H, -CH_3), 1.05 (s, 6H, -CH_3). ^{13}C NMR (101 MHz, MeOD-d_4) δ 170.1, 144.0, 139.7, 138.5, 136.7, 136.5, 134.1, 132.0, 129.9, 129.5, 128.4, 128.1, 127.1, 126.5, 126.1, 111.9, 104.5, 88.5, 58.8, 58.5, 55.5, 24.1 LCMS (ESI+) m/z calcd for $C_{28}H_{31}BClN_5O_3$ = 531.2, found 532.2 [M+H]

1-(4-((1*H*-Pyrazol-1-yl)methyl)benzyl)-*N*-((2-fluoro-4-methylphenyl)(4,4,5,5-tetramethyl-1,3,2-dioxaborolan-2-yl)methyl)-1*H*-pyrazole-4-carboxamide (91)

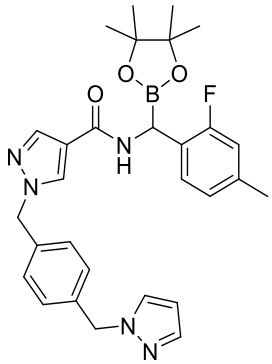

White solid (15 mg, 22%). ^{1}H NMR (400 MHz, DMSO-d_6) δ 8.58 (s, 1H, Ar-*H*), 8.11 (s, 1H, Ar-*H*), 7.80 (d, *J* = 2.1 Hz, 1H, Ar-*H*), 7.45 (d, *J* = 2.1 Hz, 1H, Ar-*H*), 7.27 (d, *J* = 8.2 Hz, 2H, Ar-*H*), 7.21 (d, *J* = 8.2 Hz, 2H, Ar-*H*), 6.91 – 6.85 (m, 3H, Ar-*H*), 6.26 (t, *J* = 2.1 Hz, 1H, Ar-*H*), 5.41 (s, 2H, -CH_2), 5.31 (s, 2H, -CH_2), 3.79 (s, 1H, BC-*H*), 2.26 (s, 3H, Ar-CH_3), 1.05 (s, 6H, -CH_3), 0.90 (s, 6H, -CH_3). ^{13}C NMR (101 MHz, DMSO-d_6) δ 167.3, 140.3, 139.5, 138.0, 136.7, 136.6, 136.1, 134.3, 133.7, 130.6, 128.6, 128.3, 126.8, 124.8, 110.5, 105.9, 103.9, 79.5, 76.0, 55.4, 54.8, 25.6, 25.3. ^{19}F NMR (377 MHz, DMSO) δ -119.7 (dd, *J* = 12.0, 6.7 Hz). LCMS (ESI+) m/z calcd for $C_{29}H_{33}BFN_5O_3$ = 529.3, found 530.3 [M+H]. HRMS m/z calcd for $[C_{29}H_{34}BFN_5O_3]^+$, 530.2739, found 530.2744 [M+H]

_N_-((2-Fluoro-4-methylphenyl)(4,4,5,5-tetramethyl-1,3,2-dioxaborolan-2-yl)methyl)-1-(4-((2-oxopyridin-1(2_H_)-yl)methyl)benzyl)-1_H_-pyrazole-4-carboxamide (92)

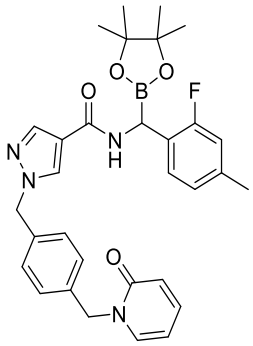

White solid, (2 mg, 3%). ^{1}H NMR (400 MHz, MeOD-d_4) δ 8.43 (s, 1H, Ar-*H*), 7.80 (s, 1H, Ar-*H*), 7.69 (ddd, *J* = 6.8, 2.1, 0.7 Hz, 1H, Ar-*H*), 7.53 (ddd, *J* = 9.0, 6.8, 2.1 Hz, 1H, Ar-*H*), 7.35 – 7.30 (m, 5H, Ar-*H*), 7.27 – 7.23 (m, 2H, Ar-*H*), 6.58 (ddd, *J* = 9.0, 1.4, 0.7 Hz, 1H, Ar-*H*), 6.40 (td, *J* = 6.8, 1.4 Hz, 1H, Ar-*H*), 5.32 (s, 2H, -CH_2), 5.20 (s, 2H, -CH_2), 3.00 (s, 3H, Ar-CH_3), 2.83 (s, 1H, BC-*H*), 1.08 (s, 6H, -CH_3), 1.03 (s, 6H, -CH_3). ^{13}C NMR (101 MHz, MeOD-d_4) δ 168.9, 163.2, 147.2, 140.9, 140.7, 138.4, 136.5, 136.4, 135.0, 132.4, 128.0, 127.9, 127.8, 126.9, 122.1, 119.5, 117.2, 110.6, 107.5, 74.4, 63.7, 54.8, 51.6, 25.1 23.6. LCMS (ESI+) m/z calcd for $C_{31}H_{34}BFN_4O_4$ = 556.3, found 557.5 [M+H].

***N*-((2-Fluoro-4-methylphenyl)(4,4,5,5-tetramethyl-1,3,2-dioxaborolan-2-yl)methyl)-3-(methoxymethyl)-1-(4-((2-oxopyridin-1(2*H*)-yl)methyl)benzyl)-1*H*-pyrazole-4-carboxamide (93)**

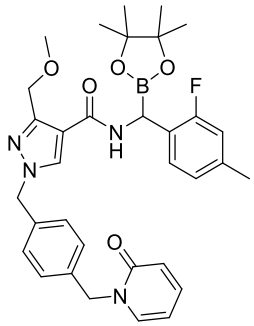

White solid, (12 mg, 18%) ^{1}H NMR (400 MHz, DMSO-d_6) δ 8.63 (s, 1H, Ar-*H*), 7.86 (ddd, *J* = 6.6, 2.1, 0.9 Hz, 1H, Ar-*H*), 7.50 (ddd, *J* = 9.1, 6.6, 2.1 Hz, 1H, Ar-*H*), 7.35 – 7.26 (m, 3H, Ar-*H*), 7.03 – 6.92 (m, 4H, Ar-*H*), 6.49 (ddd, *J* = 9.1, 1.3, 0.9 Hz, 1H, Ar-*H*), 6.32 (td, *J* = 6.6, 1.3 Hz, 1H, Ar-*H*), 5.48 (s, 2H, -CH_2), 5.32 (s, 2H, -CH_2), 5.17 (s, 2H, -OCH_2), 4.16 (s, 3H, -OCH_3), 3.35 (s, 3H, Ar-CH_3), 2.91, (s, 1H, BC-*H*), 1.10 (s, 6H, -CH_3), 0.99 (s, 6H, -CH_3). ^{13}C NMR (101 MHz, DMSO-d_6) δ 169.7, 162.2, 159.3, 150.5, 140.3, 137.6, 136.4, 134.6, 133.5, 129.0, 128.8, 128.4, 127.0, 126.5, 124.1, 117.0, 115.4, 112.0, 106.2, 88.7, 67.2, 59.0, 58.3, 52.5, 50.9, 25.4, 21.2. LCMS (ESI+) m/z calcd for $C_{33}H_{38}BFN_4O_5$ = 600.3, found = 601.2 [M+H].

***N*-((2-fluoro-4-methylphenyl)(4,4,5,5-tetramethyl-1,3,2-dioxaborolan-2-yl)methyl)-3-(methoxymethyl)-1-(4-((4-methyl-1*H*-pyrazol-1-yl)methyl)benzyl)-1*H*-pyrazole-4-carboxamide (94)**

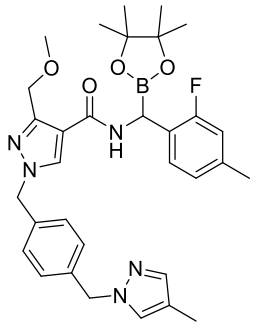

White solid, (1 mg, 9%). ^{1}H NMR (400 MHz, Acetone-d_6) δ 8.50 (s, 1H, Ar-*H*), 7.47 (s, 1H, Ar-*H*), 7.35 (d, *J* = 8.2 Hz, 2H, Ar-*H*), 7.31 (s, 1H, Ar-*H*), 7.27 (d, *J* = 8.2 Hz, 2H, Ar-*H*), 7.25 – 7.21 (m, 3H, Ar-*H*), 5.45 (s, 2H, -CH_2), 5.28 (s, 2H, -CH_2), 5.21 (s, 2H, -OCH_2), 4.19 (s, 3H, -OCH_3), 3.34 (s, 1H, BC-*H*), 2.89 (s, 3H, Ar-CH_3), 2.29 (s, 3H, Ar-CH_3), 1.07 (s, 6H, -CH_3), 0.99 (s, 6H, -CH_3). LCMS (ESI+) m/z calcd for $C_{32}H_{39}BFN_5O_4$ = 587.3, found = 588.4 [M+H]

*^{13}C NMR not obtained due to insufficient material quantity

1-Benzyl-*N*-((2-fluoro-4-methylphenyl)(4,4,5,5-tetramethyl-1,3,2-dioxaborolan-2-yl)methyl)-1*H*-pyrazole-4-carboxamide (95)

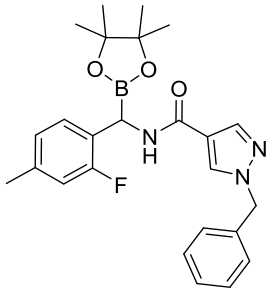

White solid (37 mg, 41%). ^{1}H NMR (400 MHz, DMSO-d_6) δ 8.59 (s, 1H, Ar-*H*), 8.12 (s, 1H, Ar-*H*), 7.44 (m, 5H, Ar-*H*), 7.02 – 6.80 (m, 3H, Ar-*H*), 5.43, (s, 2H, -CH_2), 3.80 (s, 1H, BC-*H*), 2.25 (s, 3H, Ar-CH_3), 0.99 (s, 6H, -CH_3), 0.90 (s, 6H, -CH_3) ^{13}C NMR (101 MHz, DMSO-d_6) δ 167.3, 158.8, 140.3, 136.8, 134.2, 129.2, 128.5, 128.4, 127.4, 126.7, 124.8, 115.6, 115.4, 110.4, 79.6, 60.7, 55.7, 25.5, 20.8. LCMS (ESI+) m/z calcd for $C_{25}H_{29}BFN_3O_3$ = 449.2, found 450.4 [M+H].

1-Benzyl-*N*-((3-chloro-2-fluorophenyl)(4,4,5,5-tetramethyl-1,3,2-dioxaborolan-2-yl)methyl)-1*H*-pyrazole-4-carboxamide (96)

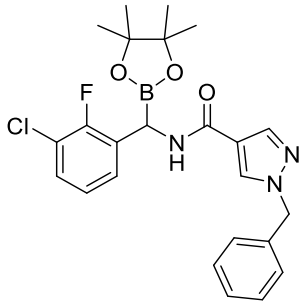

White solid (47 mg, 40%). ^{1}H NMR (400 MHz, DMSO-d_6) δ 8.61 (s, 1H, Ar-*H*), 8.14 (s, 1H, Ar-*H*), 7.50 – 7.43 (m, 5H, Ar-*H*), 7.38 – 7.34 (m, 3H, Ar-*H*), 5.43 (s, 2H, -CH_2), 3.66 (s, 1H, BC-*H*), 0.99 (s, 6H, -CH_3), 0.89 (s, 6H, -CH_3). ^{13}C NMR (101 MHz, DMSO-d_6) δ 169.9, 144.4, 138.5, 135.7, 133.7, 132.2, 129.3, 128.6, 127.5, 126.4, 125.7, 125.2, 124.0, 112.3, 77.2, 57.3, 50.6, 24.6. LCMS (ESI+) m/z calcd for $C_{24}H_{26}BClFN_3O_3$ = 469.2, found 470.2 [M+H]

1-(4-((1*H*-pyrazol-1-yl)methyl)benzyl)-*N*-(3-chlorobenzyl)-1*H*-pyrazole-4-carboxamide (102)

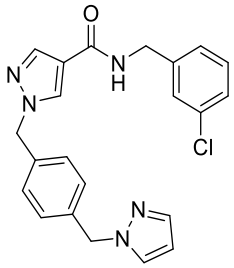

Off white solid (16 mg, 67%). ^{1}H NMR (400 MHz, DMSO-d_6) δ 8.65 (br, 1H, -N*H*), 8.25 (d, *J* = 0.8 Hz, 1H, Ar-*H*), 7.89 (d, *J* = 0.8 Hz, 1H, Ar-*H*), 7.80 (dd, *J* = 2.3, 0.7 Hz, 1H, Ar-*H*), 7.44 (dd, *J* = 2.3, 0.7 Hz, 1H, Ar-*H*), 7.37 – 7.28 (m, 4H, Ar-*H*), 7.26 – 7.22 (m, 3H, Ar-*H*), 7.21 – 7.16 (m, 1H, Ar-*H*), 6.25 (t, *J* = 2.3 Hz, 1H, Ar-*H*), 5.32 (s, 2H, -CH_2), 5.31 (s, 2H, -CH_2) 4.40 – 4.36 (m, 2H, -CH_2). ^{13}C NMR (101 MHz, DMSO-d_6) δ 161.1, 141.9, 138.4, 138.2, 136.8, 135.5, 132.3, 131.0, 129.6, 129.5, 127.4, 127.2, 126.4, 126.1, 125.3, 117.8, 104.9, 59.2, 54.1, 53.7. LCMS (ESI+) m/z calcd for $C_{22}H_{20}ClN_5O$ = 405.1, found 406.1 [M+H]

***N*-(3-Chlorobenzyl)-1-(4-((2-oxopyridin-1(2*H*)-yl)methyl)benzyl)-1*H*-pyrazole-4-carboxamide (103)**

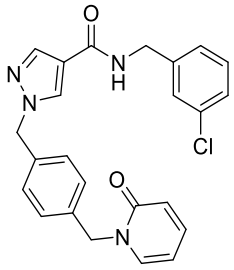

White solid (100 mg, 89%) ^{1}H NMR (400 MHz, DMSO-d_6) δ 8.66 (br, 1H, -N*H*), 8.26 (d, *J* = 0.8 Hz, 1H, Ar-*H*), 7.90 (d, *J* = 0.8 Hz, 1H, Ar-*H*), 7.76 (ddd, *J* = 6.8, 2.1, 0.7 Hz, 1H, Ar-*H*), 7.41 (ddd, *J* = 8.9, 6.8, 2.1 Hz, 1H, Ar-*H*), 7.37 – 7.30 (m, 3H, Ar-*H*), 7.29 – 7.22 (m, 5H, Ar-*H*), 6.40 (ddd, *J* = 8.9, 1.4, 0.7 Hz, 1H, Ar-*H*), 6.22 (td, *J* = 6.8, 1.4 Hz, 1H, Ar-*H*), 5.32 (s, 2H, -CH_2), 5.07 (s, 2H, -CH_2), 4.41 – 4.33 (m, 2H, -CH_2). ^{13}C NMR (101 MHz, DMSO-d_6) δ 161.2, 160.8, 141.9, 139.5, 138.5, 138.2, 136.5, 135.5, 132.3, 131.0, 129.6, 127.5, 127.3, 126.4, 126.1, 125.3, 119.3, 117.8, 104.9, 54.1, 50.2, 40.8. LCMS (ESI+) m/z calcd for $C_{24}H_{21}ClN_4O_2$ = 432.1, found 433.2 [M+H].

1-(4-((1*H*-Pyrazol-1-yl)methyl)benzyl)-*N*-(2-fluoro-4-methylbenzyl)-1*H*-pyrazole-4-carboxamide (106)

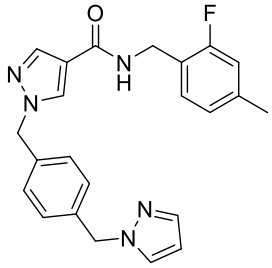

White solid (8 mg, 34%) ^{1}H NMR (400 MHz, DMSO-d_6) δ 8.54 (br, 1H, -N*H*), 8.25 (s, 1H, Ar-*H*), 7.89 (s, 1H, Ar-*H*), 7.80 (d, *J* = 2.3 Hz, 1H, Ar-*H*), 7.44 (d, *J* = 2.3 Hz, 1H, Ar-*H*), 7.23 (d, *J* = 8.2 Hz, 2H, Ar-*H*), 7.21 – 7.16 (m, 3H, Ar-*H*), 7.02 – 6.93 (m, 2H, Ar-*H*), 6.25 (t, *J* = 2.3 Hz, 1H, Ar-*H*), 5.31 (s, 4H, -CH_2), 4.42 – 4.33 (m, 2H, -CH_2), 2.28 (s, 3H, Ar-CH_3).^{13}C NMR (101 MHz, DMSO-d_6) δ 162.1, 139.5, 137.9, 136.6, 132.0, 130.6, 129.9, 128.5, 128.2, 125.3, 125.3, 123.6, 123.4, 118.9, 116.0, 115.8, 105.9, 56.5, 55.2, 54.8, 22.3. LCMS (ESI+) m/z calcd for $C_{23}H_{22}FN_5O$ = 403.2, found 404.1 [M+H].

***N*-(2-fluoro-4-methylbenzyl)-1-(4-((2-oxopyridin-1(2*H*)-yl)methyl)benzyl)-1*H*-pyrazole-4-carboxamide (107)**

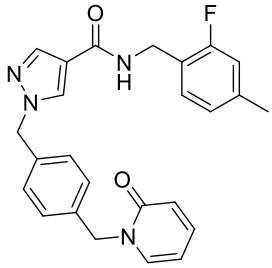

Off white solid (88 mg, 83%) ^{1}H NMR (400 MHz, DMSO-d_6) δ 8.53 (br, 1H, -N*H*), 8.25 (s, 1H, Ar-*H*), 7.89 (s, 1H, Ar-*H*), 7.76 (ddd, *J* = 6.8, 2.1, 0.7 Hz, 1H, Ar-*H*), 7.41 (ddd, *J* = 8.9, 6.8, 2.1 Hz, 1H, Ar-*H*), 7.26 (d, *J* = 8.3 Hz, 2H, Ar-*H*), 7.23 (d, *J* = 8.3 Hz, 2H, Ar-*H*), 7.21 – 7.17 (m, 1H, Ar-*H*), 7.01 – 6.93 (m, 2H, Ar-*H*), 6.40 (ddd, *J* = 8.9, 1.4, 0.7 Hz, 1H, Ar-*H*), 6.22 (td, *J* = 6.8, 1.4 Hz, 1H, Ar-*H*), 5.31 (s, 2H, -CH_2), 5.07 (s, 2H, -CH_2), 4.42 – 4.35 (m, 2H, -CH_2), 2.28 (s, 3H, Ar-CH_3).^{13}C NMR (101 MHz, DMSO-d_6) δ 161.1, 160.8, 139.5, 138.5, 138.2, 138.1, 136.5, 135.5, 130.9, 128.8, 127.3, 124.2, 122.5, 122.4, 119.3, 117.8, 114.9, 114.7, 104.9, 54.1, 50.2, 34.9, 19.9. LCMS (ESI+) m/z calcd for $C_{25}H_{23}FN_4O_2$ = 430.2, found 431.1 [M+H]

***N*-(3-Chlorobenzyl)-3-(methoxymethyl)-1-(4-((2-oxopyridin-1(2*H*)-yl)methyl)benzyl)-1*H*-pyrazole-4-carboxamide (104)**

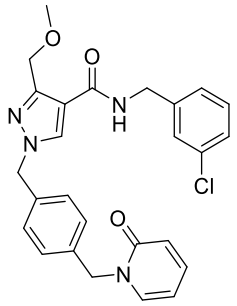

Off white solid (80 mg, 74%) ^{1}H NMR (400 MHz, DMSO-d_6) δ 8.49, (br, 1H, N*H*), 8.44 (s, 1H, Ar-*H*), 8.25 (s, 1H, Ar-*H*), 7.76 (ddd, *J* = 6.8, 2.1, 0.8 Hz, 1H, Ar-*H*), 7.41 (ddd, *J* = 9.3, 6.8, 2.1 Hz, 1H, Ar-*H*), 7.38 – 7.30 (m, 4H, Ar-*H*), 7.30 – 7.28 (m, 1H, Ar-*H*), 7.27 – 7.22 (m, 3H, Ar-*H*), 6.40 (ddd, *J* = 9.3, 1.4, 0.8 Hz, 1H, Ar-*H*), 6.22 (td, *J* = 6.8, 1.4 Hz, 1H, Ar-*H*), 5.29 (s, 2H, -CH_2), 5.07 (s, 2H, -CH_2), 4.54 (s, 2H, -OCH_2), 4.42 – 4.38 (m, 2H, -CH_2), 3.21 (s, 3H, -OCH_3). ^{13}C NMR (101 MHz, DMSO-d_6) δ 161.7, 160.8, 147.5, 141.7, 139.5, 138.5, 136.5, 135.4, 132.4, 131.8, 129.6, 127.5, 127.3, 126.4, 125.3, 119.3, 115.3, 112.6, 104.9, 65.5, 56.8, 54.1, 50.2, 41.0. LCMS (ESI+) m/z calcd for $C_{26}H_{25}ClN_4O_3$ = 476.2, found 477.1 [M+H]

***N*-(3-chlorobenzyl)-3-(methoxymethyl)-1-(4-((4-methyl-1*H*-pyrazol-1-yl)methyl)benzyl)-1*H*-pyrazole-4-carboxamide (105)**

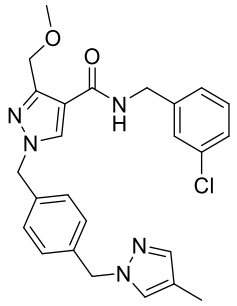

Off white solid (35 mg, 53%). ^{1}H NMR (400 MHz, DMSO-d_6) δ 8.49 (br, 1H, -N*H*), 8.41 (s, 1H, Ar-*H*), 7.47 (s, 1H, Ar-*H*), 7.35 (s, 1H, Ar-*H*), 7.23 – 7.19 (m, 4H, Ar-*H*), 7.18 – 7.14 (m, 1H, Ar-*H*), 7.03 – 6.93 (m, 3H, Ar-*H*), 5.28 (s, 2H, -CH_2), 5.21 (s, 2H, -CH_2), 4.52 (s, 2H, -OCH_2), 4.40 – 4.35 (m, 2H, -CH_2), 2.28 (s, 3H, -OCH_3), 1.98 (s, 3H, Ar-CH_3). ^{13}C NMR (101 MHz, DMSO-d_6) δ 161.7, 147.6, 141.7, 138.7, 137.0, 135.4, 132.4, 131.9, 129.6, 128.1, 127.4, 127.2, 126.4, 126.1, 125.3, 115.3, 114.6, 65.5, 56.8, 54.1, 53.7, 41.0, 37.7. LCMS (ESI+) m/z calcd for $C_{25}H_{26}ClN_5O_2$ = 463.2, found 464.2 [M+H]

***N*-(2-fluoro-4-methylbenzyl)-3-(methoxymethyl)-1-(4-((2-oxopyridin-1(2*H*)-yl)methyl)benzyl)-1*H*-pyrazole-4-carboxamide (108)**

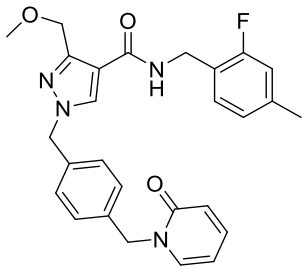

White solid (80 mg, 79%) ^{1}H NMR (400 MHz, DMSO-d_6) δ 8.49 (br, 1H, -N*H*), 8.36 (s, 1H, Ar-*H*), 7.76 (ddd, *J* = 6.8, 2.1, 0.7 Hz, 1H, Ar-*H*), 7.41 (ddd, *J* = 9.1, 6.8, 2.1 Hz, 1H, Ar-*H*), 7.31 – 7.15 (m, 4H, Ar-*H*), 7.05 – 6.93 (m, 3H, Ar-*H*), 6.40 (ddd, *J* = 9.1, 1.4, 0.7 Hz, 1H, Ar-*H*), 6.22 (td, *J* = 6.8, 1.4 Hz, 1H, Ar-*H*), 5.29 (s, 2H, -CH_2), 5.07 (s, 2H, -CH_2), 4.53 (s, 2H, -OCH_2), 4.38 – 4.35 (m, 2H, -CH_2), 3.21 (s, 3H, -OCH_3), 2.28 (s, 3H, Ar-CH_3). ^{13}C NMR (101 MHz, DMSO-d_6) δ 162.6, 161.8, 148.4, 140.6, 139.6, 137.6, 136.5, 133.2, 130.0, 128.5, 128.4, 125.4, 123.4, 123.3, 120.3, 116.5, 116.0, 115.8, 106.0, 66.6, 57.8, 55.1, 51.3, 38.1, 21.0 LCMS (ESI+) m/z calcd for $C_{27}H_{27}FN_4O_3$ = 474.2, found 475.2 [M+H]

***N*-(2-fluoro-4-methylbenzyl)-3-(methoxymethyl)-1-(4-((4-methyl-1*H*-pyrazol-1-yl)methyl)benzyl)-1*H*-pyrazole-4-carboxamide (109)**

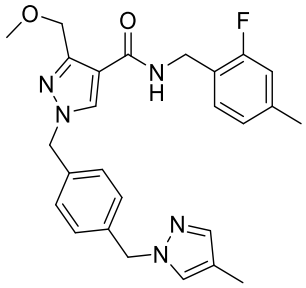

White solid (15 mg, 45%) ^{1}H NMR (400 MHz, DMSO-d_6) δ 8.47 (br, 1H, -N*H*), 8.24 (s, 1H, Ar-*H*), 7.52 (s, 1H, Ar-*H*), 7.38 (s, 1H, Ar-*H*), 7.27 – 7.21 (m, 4H, Ar-*H*), 7.20 – 7.16 (m, 1H, Ar-*H*), 7.09 – 6.94 (m, 2H, Ar-*H*), 5.28 (s, 2H, -CH_2), 5.21 (s, 2H, -CH_2), 4.52 (s, 2H, -OCH_2), 4.40 – 4.35 (m, 2H, -CH_2), 3.20 (s, 3H, -OCH_3), 2.28 (s, 3H, Ar-CH_3), 1.98 (s, 3H, Ar-CH_3). ^{13}C NMR (101 MHz, DMSO-d_6) δ 162.6, 148.3, 139.7, 139.5, 139.4, 138.1, 136.4, 133.2, 130.7, 129.2, 128.5, 128.2, 125.3, 123.4, 116.5, 116.0, 115.8, 66.6, 57.8, 55.2, 54.7, 42.2, 36.3, 21.0 LCMS (ESI+) m/z calcd for $C_{26}H_{28}FN_5O_2$ = 461.2, found 462.3 [M+H].

Chapter 3

Chapter 3: Synthesis and Biological Evaluation of β-Ketoboronates as Inhibitors of Plasma Kallikrein

3.1 Introduction

Classically the synthesis of boronic esters and boronates has been achieved *via* the reaction of hard organometallic reagents with borate esters or through hydroboration strategies, however issues arise with these methods due to limited substrate scope and high air and moisture sensitivity.[159,160]

Since the discovery of the Suzuki-Miyaura coupling reaction,[161–163] the importance of boronates and boronic acids in organic synthesis has increased significantly, and by extension the development of further methodologies for the synthesis of boronates. Notably, the Miyaura borylation established a catalytic route for the conversion of aryl halides to aryl boronates under relatively mild conditions[164,165] (Scheme 3.1).

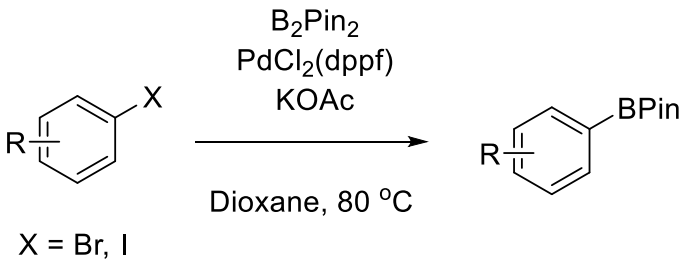

Scheme 3.1. Miyaura borylation conditions

Following this discovery, numerous other methods for catalytic borylation have been explored to accommodate a greater range of substrates and conditions, examples of which include the borylation of olefins. Of these methods, those mediated by copper-boryl species have been shown to enable mild reaction conditions, good functional group tolerance and low cost of the metal catalyst.[166] The first examples of copper mediated borylation include those of Miyaura *et al* and Hosomi *et al*[167,168] (Scheme 3.2).

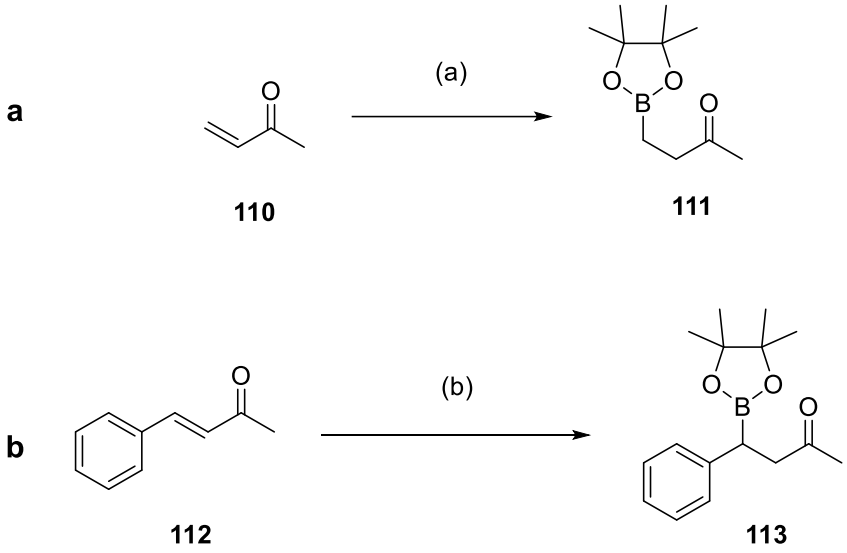

Scheme 3.2. **a** CuCl-mediated borylation of α,β-enones by Miyaura *et al.* **b** Borylation of α,β-enones using a Cu(I)-phosphine mixture catalyst by Hosomi *et al*. Reagents and conditions **(a)** B_2Pin_2, CuCl (10 mol%, KOAc (10 mol%), DMF, rt, 16 h **(b)** B_2Pin_2, $Cu(OTf)_2.C_6H_6$ (10 mol%), PBu_3 (10 mol%) DMF, rt, 24 h

Both examples from Scheme 3.2 show the use of a diboron reagent as a means of transferring boronates onto α,β-unsaturated ketones. Diborons are particularly effective in catalytic borylations due to elongation of the boron-boron bond upon

coordination of a ligating group, enabling facile transfer of a boronate onto the catalyst, generating a copper-boryl species.[169]

Further examples of Cu-borylation chemistry were reported by Yun *et al*, in which a copper-diphosphine catalyst is generated *in situ* to enable borylation, it was also found that the use of alcohol additives dramatically accelerated rate of reaction and yield by promoting protonation of the Cu-BPin-olefin complex to release the desired boronate product[170] (Scheme 3.3).

114 **115**

95%

Scheme 3.3. Cu-borylation accelerated by alcohol additive by Yun *et al.* Reagents and conditions **(a)** CuCl (1 mol %), DPEPhos (3 mol%), NaO^{t}Bu (3 mol%), B_2Pin_2, MeOH, THF, rt, 14 h.

This work showed excellent borylation yields as well as diverse functional group tolerance. It had been previously noted that phosphine based ligands such as XantPhos and DPEPhos were able to increase the reactivity of copper-hydride species, leading to speculation over their effects on borylation of α,β-unsaturated carbonyls.[170]

Mechanistically, this reaction is believed to proceed *via* the formation of a precatalyst from the ligation of NaO^tBu with CuCl, subsequent displacement of the $-O^tBu$ ligand with DPEPhos occurs, enabling generation of a copper-boryl species which undergoes conjugate addition to the α,β-unsaturated carbonyl, followed by protonation of the organocopper species **117**/**118** to release the boronate product **115** (Figure 3.1).

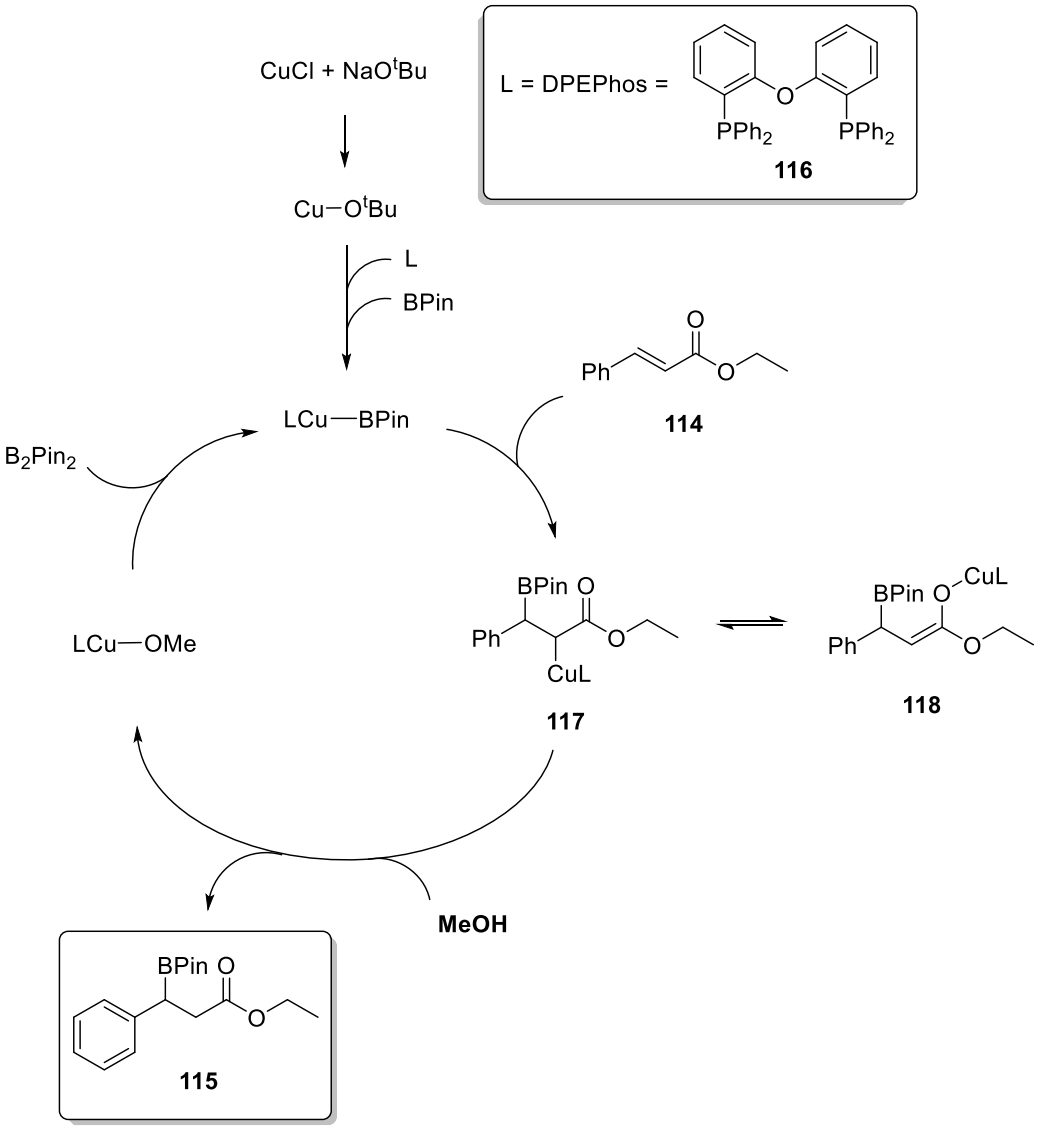

Figure 3.1. Proposed mechanism of Cu-borylation reported by Yun *et al.*[170]

3.1.1 Summary

Borylation of α-β-unsaturated carbonyls has been well explored as a viable method for the synthesis of carbon-boron bonds, demonstrating potential for high yields and good functional group tolerance. Application of this methodology in the synthesis of PKa inhibitors was explored, intending to create stable analogues of compounds described in Chapter 2 *via* circumnavigation of the amide functional group.

3.2 Results and Discussion

3.2.1 Synthetic Chemistry

The chemistry reported by Yun *et al*[170] was tested on chalcone **119** to assess compatibility with biaryl-enone systems (Scheme 3.4).

119 **120**

Scheme 3.4. Cu-catalysed borylation of chalcone. Reagents and conditions (a) CuCl (1 mol%), NaO^{t}Bu (3 mol%), DPEPhos (3 mol%), B_2Pin_2, MeOH, THF, rt, 24 h, 77%.

Borylation of chalcone proceeded well and the borylation product was separated on silica gel, suggesting greater acid stability that the α-amidoboronates described in Chapter 2. Additionally, cleavage of the boronic ester was attempted under mild aqueous conditions (2M HCl in THF), as well as reduction of the ketone in an effort to produce an internal borocycle, however these efforts were unsuccessful. In the case of the boronic ester cleavage, strong acidic conditions were eventually used to attempt boronic ester hydrolysis (20% TFA in CH_2Cl_2), forcing deborylation. As for the attempted ketone reduction, no success was observed with reagents such as $NaBH_4$, DIBAL-H and $LiAlH_4$, possibly due to their hard anions forming an adduct with the boronate.

Further synthetic efforts were directed towards the synthesis of an enone scaffold analogous to those described in Chapter 2 for the application Cu-borylation chemistry (Scheme 3.5). 1,4-dibromoxylene **121** was reacted with a stochiometric quantity of pyrazole in the presence of NaH to afford **122**, which was subjected similar conditions with 1H-4-acetylpyrazole to yield **123**. Aldol condensation of **123** with substituted benzaldehydes gave compounds **124a** and **124b**.

Subjection of **124a** and **124b** to the Cu-borylation conditions of Yun *et al* provided boronates **125a** and **125b** (Scheme 3.6). Further attempts to cleave the pinacol ester under acidic or basic conditions to afford the corresponding boronic acid were unsuccessful due to protodeborylation. The reluctance of **125a-b** to cleave under mild aqueous conditions may reflect the increased stability of the boronic esters of these compounds relative to **91-96** due to the absence of amide

functionality, preventing the formation of an intramolecular cyclic boronate adduct (see **Chapter 2**, Scheme 2.14).

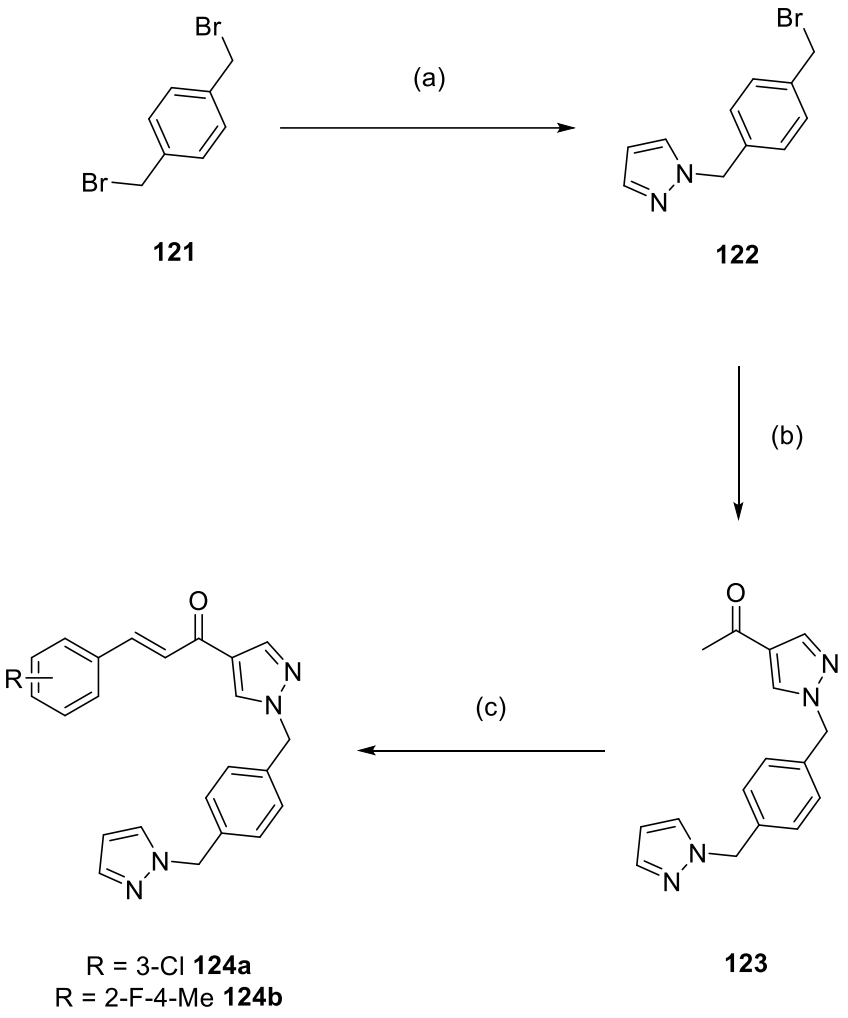

Scheme 3.5. Synthesis of α,β-unsaturated ketone precursor for borylation. Reagents and conditions (a) pyrazole, NaH, THF, 0 °C – rt, 1 h, 50% (b**)** 1-(1*H*-Pyrazol-4-yl)ethenone, NaH, THF, 0 – 50 °C, 2 h, 63% (c) 3 chlorobenzaldehyde or 2-fluoro-4-methylbenzaldeyde, NaOH, MeOH, rt, 3 h, 70-81%.

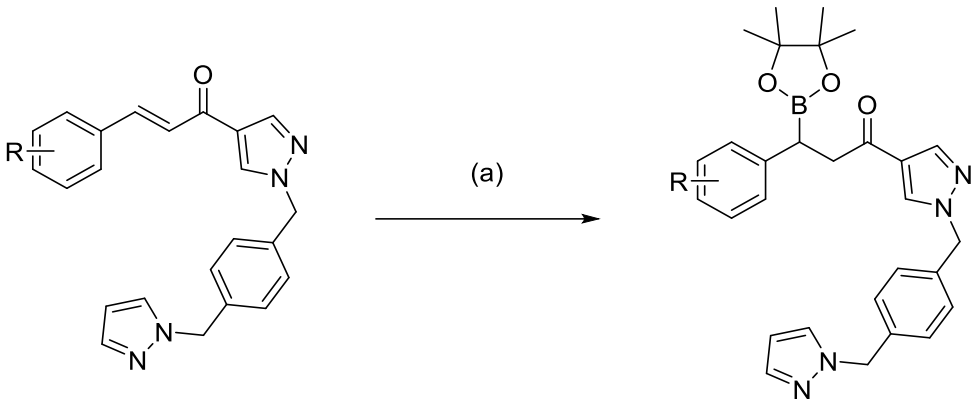

R = 3-Cl **124a**
R = 2-F-4-Me **124b**

R = 3-Cl **125a**
R = 2-F-4-Me **125b**

Scheme 3.6. Borylation of α,β-unsaturated carbonyls **124a** and **124b**. Reagents and conditions (a) CuCl (1 mol%), NaO^{t}Bu (3 mol%), DPEPhos (3 mol%), B_2Pin_2, MeOH, THF, rt, 16 h, 34-56%.

Diboron compounds **126**-**128** were also subjected to the same conditions, attempting to study the effect of different boronic esters on the properties of these boronate compounds, however attempts were unsuccessful due to rapid decomposition of the product upon forming, observed by LCMS (Figure 3.2).

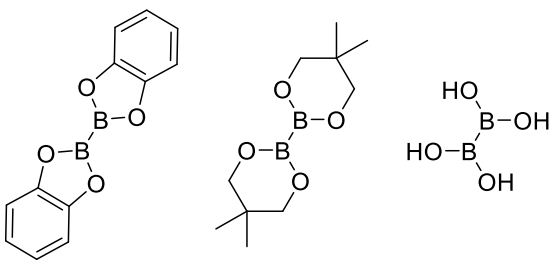

126 **127** **128**

Figure 3.2. Structures of diboron compounds **126-128**.

Further to the synthesis of boronates, the possibility of installing other functional groups that could potentially act as covalent warheads was explored for scaffolds **124a** and **124b.** For instance, the installation of a nitrile group was achieved *via* reaction of **124a** and **124b** with TMSCN, CsF and H_2O, as originally reported by Yang and Chen[171] (Scheme 3.7).

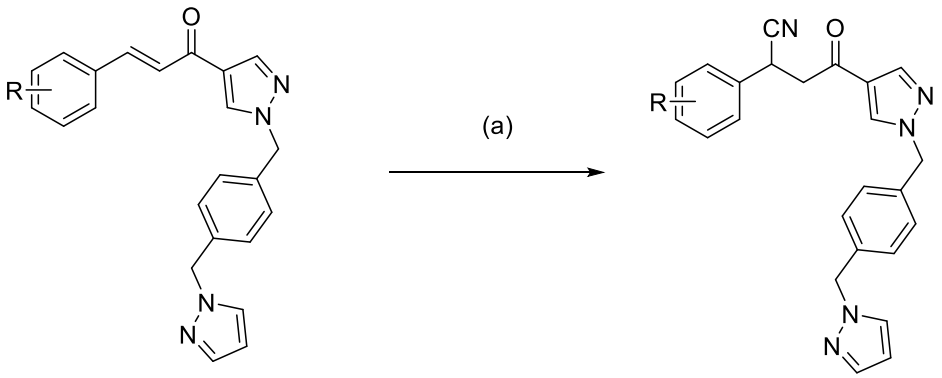

R = 3-Cl **124a**
R = 2-F-4-Me **124b**

R = 3-Cl **129a**
R = 2-F-4-Me **129b**

Scheme 3.7. Cyanation of **124a** and **124b**. Reagents and condition (a) TMSCN, CsF, H_2O, dioxane, 100 ^oC, 16 h, 78-82%.

Mechanistically, it is proposed that this reaction proceeds *via* transition state **124c**, followed by conjugate addition of CN and generation of silyl-enol species **129c**, liberating CsF. Conversion of **129c** to its keto form is driven by the presence of water to give β-ketonitriles **129a-b** (Figure 3.3).

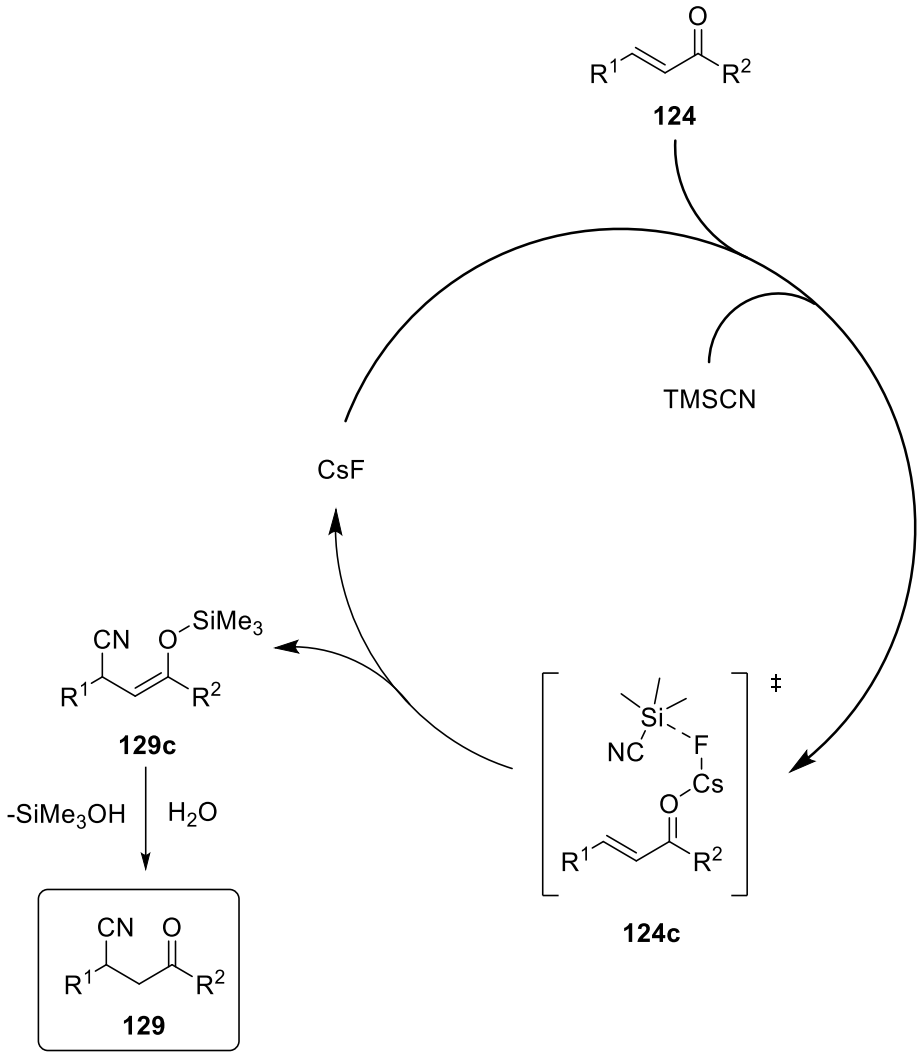

Figure 3.3. Proposed mechanism for CsF-catalysed cyanation of enones by Yang and Chen.[171]

Subsequent efforts were made to install trifluoromethyl ketone and sulfonyl fluoride warheads onto **124a** and **124b**, however these attempts proved to be unsuccessful.[172,173]

3.2.2 Pharmacology

3.2.2.1 Evaluation of Inhibitor Potency

Compounds **124a**, **124b**, **129a** and **129b** were subjected to the same IC_{50} assay as described in Section 2.2.2 for assessment of PKa binding. (Table 3.1).

Table 3.1. Biological activity of **124a-129b** against PKa

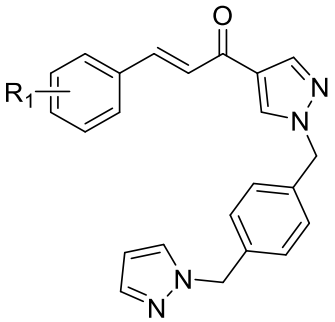

R_1 = 3-Cl **124a**
R_1 = 2-F-4-Me **124b**

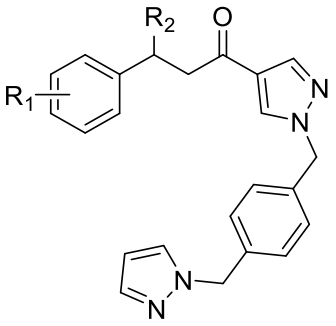

R_1 = 3-Cl, R_2 = BPin **125a**
R_1 = 2-F-4-Me, R_2 = BPin **125b**
R_1 = 3-Cl, R_2 = CN **129a**
R_1 = 2-F-4-Me, R_2 = CN **129b**

Example	**PKa IC_{50} (nM)**[a]		
	1 min	10 min	1 h
124a	>400000	>400000	>400000
124b	98089	7263	5975
125a	1534	2173	2637
125b	41.1	40.7	33.9
129a	22320	18859	21786
129b	223	90.2	33.2

[a]Data are expressed as mean of 2 experiments, where each experimental curve was performed in triplicate.

Enone **124a** showed no observable PKa binding, whereas **124b** showed mild PKa inhibition, possibly acting as a covalent inhibitor as a decrease in IC_{50} value was shown over the 3 time points. Boronate **125a** displayed modest PKa inhibition with no evidence of covalent binding. Interestingly, boronate **125b** showed greatly enhanced potency (~40 nM) in comparison to **125a** (~2000 nM), however similarly, no evidence of covalent binding was seen from the IC_{50} data.

Nitrile **129a** showed weak PKa inhibition with no change in binding seen over the time points. Interestingly, modification of the P1 group in **129b** showed roughly 100-fold enhancement in potency at 1 min incubation time and continued to show increase in IC_{50} potency over each time point, indicative of covalent binding.

Extended time course analysis up to 24 hours of **125b** confirmed the lack of exhibition of covalent binding due to no significant change in IC_{50} over the 24 hour period (Table 3.2).

Table 3.2. Extended time course biological evaluation of **125b** against PKa.

Example	**PKa IC_{50} (nM)[a]**			
	1 min	2 h	5 h	24 h
125b	27.6	16.4	35.6	22.5

[a]Data are expressed as mean of 2 experiments, where each experimental curve was performed in triplicate.

3.2.2.2 Jump dilution assays

Confirmation of noncovalent binding and characterisation of binding reversibility for compounds **125a** and **125b** was determined through subjection to a jump dilution assay (described in Section 2.2.2.2) (Figure 3.4).

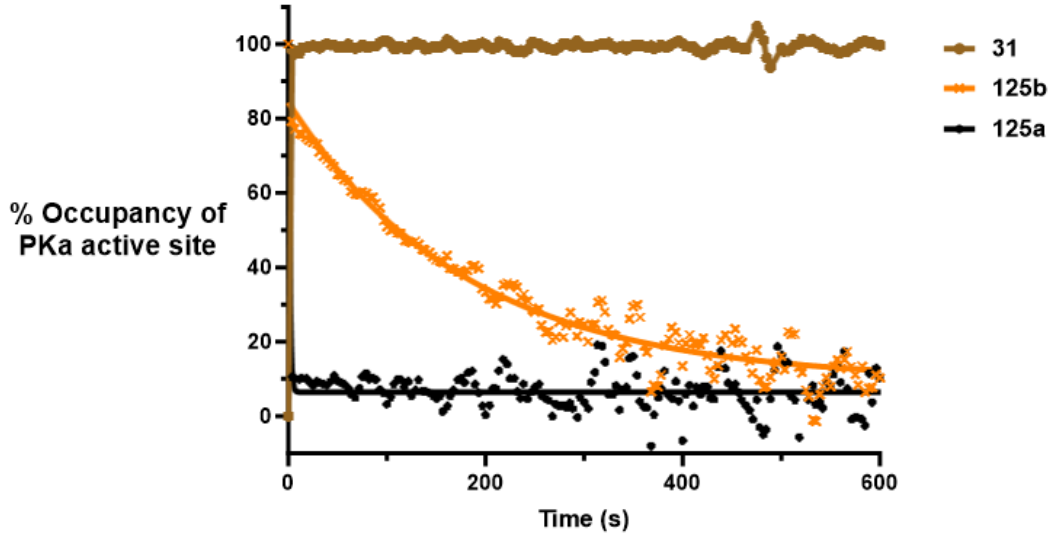

Figure 3.4. Jump dilution dissociation curves of **125a** and **125b**.

Interestingly, whilst both boronates showed reversible binding concomitant with noncovalent inhibition, **125b** acted as a slow off-rate inhibitor whereas **125a** demonstrated instantaneous equilibrium dissociation from PKa upon dilution. The 2-fluoro-4-methylphenyl P1 group demonstrates stronger S1 binding with respect to 3-chlorophenyl, partially due to displacement of a water molecule bound to Asp_{189} in the S1 site by the *p*-methyl group. Furthermore, it has been considered that the *o*-fluoro- atom may undergo a hydrogen bonding interaction with Lys_{192} at the edge of the S1 site.[174]

3.3 Conclusions

Biological evaluation of boronates **125a-b** demonstrated inhibition of PKa, in the case of **125b** a vast improvement in potency was observed from variation of the 3-chlorophenyl P1 group to 2-Fluoro-4-Methylphenyl, however covalent inhibition was not observed in either instance.

Transformation of enones **124a-b** to the corresponding β-cyanoketones **129a-b** was achieved, **129a** showed modest noncovalent activity in PKa, whereas **129b** showed good potency and covalent inhibition by examination of IC_{50} value over the measured time points. Whilst further work could not be carried out to investigate the potential of these β-cyanoketones, the collected data represents promise for these compounds to be explored in the future.

3.4 Experimental

3.4.1 Materials and Methods

Materials and methods relevant to chemical synthesis and pharmacology have been described in Section 2.4.1.

3.4.2 General Procedures

Representative General Procedure for Borylation of Enones 119, 124a and 124b:[170]

CuCl (0.5 mg, 0.004 mmol), DPEPhos (6 mg, 0.01 mmol) and NaO^tBu (1.1 mg, 0.01 mmol) were added to a microwave vial which was sealed and purged with nitrogen. Anhydrous THF (0.5 mL) was added, and the suspension was stirred for 30 minutes. B_2Pin_2 (36 mg, 0.14 mmol) in 0.5 mL anhydrous THF was then added, and the mixture was stirred for a further 10 minutes before addition of enone (50 mg, 0.12 mmol) and methanol (8 mg, 82 µL, 0.24 mmol) in 1 mL anhydrous THF. The reaction mixture was allowed to stir at room temperature for 16 hours under nitrogen, after which, it was filtered through celite, concentrated *in vacuo* and purified by silica gel flash chromatography (20 – 50 % EtOAc in cyclohexane) to afford the product as a colourless oil, which was lyophilised to produce a white solid.

Representative General Procedure for Cyanation of Enones 124a and 124b:

124a or **124b** (100 mg, 0.3 mmol), caesium fluoride (5 mg, 0.03 mmol), and distilled water (22 µL, 1.25 mmol) were dissolved in dioxane (3 mL). TMSCN (0.1 mL, 0.69 mmol) was added, and the reaction mixture heated to 100 ^{o}C for 16 hours. Upon completion, the solvent was removed *in vacuo* and the residue was purified by silica gel flash chromatography (30 – 50 % EtOAc in cyclohexane) to afford the product as a white solid.

3.4.3 Chemical Characterisation

1,3-diphenyl-3-(4,4,5,5-tetramethyl-1,3,2-dioxaborolan-2-yl)propan-1-one (120)

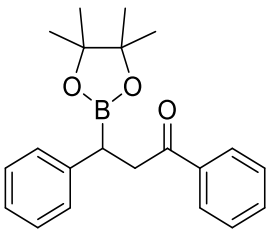

Colourless oil (124 mg, 67%) ^{1}H NMR (400 MHz, $CDCl_3$) δ 7.58 – 7.52 (m, 5H, Ar-*H*), 7.43 – 7.37 (m, 5H, Ar-*H*), 3.43 (dd, *J* = 9.0, 5.9 Hz, 1H, BC-*H*), 2.81 (dd, *J* = 16.0, 9.0 Hz, 1H, C=OCH_a), 2.69 (dd, *J* = 16.0, 5.9 Hz, 1H, C=OCH_b), 1.21 (s, 12H) ^{13}C NMR (101 MHz, $CDCl_3$) δ 200.1, 140.2, 137.0, 132.9, 130.0, 129.0, 128.6, 127.5, 125.9, 88.3, 35.9, 33.1, 24.7 LCMS (ESI+) m/z calcd for $C_{21}H_{25}BO_3$ = 336.2, found 337.1 [M+H].

1-(4-(bromomethyl)benzyl)-1*H*-pyrazole (122)[175]

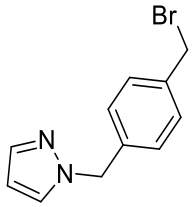

To an ice-cooled, stirring solution of 1,4-bis(bromomethyl)benzene (1056 mg, 4.0 mmol) and pyrazole (272 mg, 4.0 mmol) in THF (30 mL), was added NaH (60% dispersion in mineral oil) (176 mg, 2.2 mmol). The reaction mixture was allowed to warm to room temperature over 2 hours. Upon completion, the reaction mixture was quenched with water, concentrated *in vacuo* and partitioned between EtOAc and water. The aqueous layer was extracted with EtOAc (3 x 40 mL), the organics were combined, washed with brine, dried over $MgSO_4$, filtered, and concentrated *in vacuo*. The resulting residue was purified by flash column chromatography (10 % EtOAc in cyclohexane) to afford the title compound. White solid (716 mg, 72%). ^{1}H NMR (400 MHz, $CDCl_3$) δ 7.58 (d, *J* = 2.0 Hz, 1H, Ar-*H*), 7.42 (d, *J* = 2.0 Hz, 1H, Ar-*H*), 7.39 (d, *J* = 7.9 Hz, 2H, Ar-*H*), 7.19 (d, *J* = 7.9 Hz, 2H, Ar-*H*), 6.31 (t, *J* = 2.0 Hz, 1H, Ar-*H*), 5.34 (s, 2H, -C*H*$_2$), 4.49 (s, 2H, -C*H*$_2$). ^{13}C NMR (101 MHz, $CDCl_3$) δ 140.1, 139.7, 135.6, 130.1, 129.7, 128.7, 127.6, 58.9, 37.6. LCMS (ESI+) m/z calcd for $C_{11}H_{11}BrN_2$ = 250.0, found 251.1 [M+H].

1-(1-(4-((1*H*-pyrazol-1-yl)methyl)benzyl)-1*H*-pyrazol-4-yl)ethan-1-one (123)

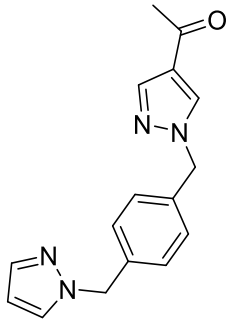

To an ice-cooled, stirring solution of 1-(4-(bromomethyl)benzyl)-1H-pyrazole (500 mg, 2.0 mmol) and 1-(1H-pyrazol-4-yl)ethan-1-one (264 mg, 2.4 mmol) in THF (15 mL) was added NaH (60% dispersion in mineral oil) (120 mg, 3.0 mmol). The solution was heated to 50 ^{o}C for a period of 3 hours, after which it was concentrated *in vacuo* and partitioned between EtOAc and water. The aqueous layer was extracted with EtOAc (3 x 20 mL), the organics were combined, washed with brine, dried over $MgSO_4$, filtered, and concentrated *in vacuo*. The resulting residue was purified by flash column chromatography (30 – 50 % EtOAc in cyclohexane) to afford the title compound. White solid (353 mg, 63%). ^{1}H NMR (400 MHz, DMSO-d_6) δ 8.51 (s, 1H, Ar-*H*), 7.92 (s, 1H, Ar-*H*), 7.80 (d, *J* = 2.2 Hz, 1H, Ar-*H*), 7.45 (d, *J* = 2.2 Hz, 1H, Ar-*H*), 7.25 (d, *J* = 8.0 Hz, 2H, Ar-*H*), 7.19 (d, *J* = 8.0 Hz, 2H, Ar-*H*), 6.26 (t, *J* = 2.2 Hz, 1H, Ar-*H*), 5.34 (s, 2H, -CH_2), 5.31 (s, 2H, -CH_2), 2.35 (s, 3H, -CH_3). ^{13}C NMR (101 MHz, DMSO-d_6) δ 192.0, 140.6, 139.5, 138.0, 136.4, 134.0, 132.0, 131.9, 130.6, 124.3, 105.9, 55.2, 54.8, 28.3. LCMS (ESI+) m/z calcd for $C_{16}H_{16}N_4O$ = 280.1, found 281.1 [M+H].

(*E*)-1-(1-(4-((1*H*-pyrazol-1-yl)methyl)benzyl)-1*H*-pyrazol-4-yl)-3-(3-chlorophenyl)prop-2-en-1-one (124a)

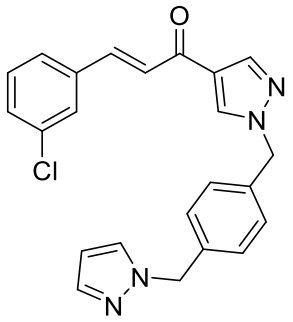

1-(1-(4-((1*H*-pyrazol-1-yl)methyl)benzyl)-1*H*-pyrazol-4-yl)ethan-1-one (100 mg, 0.36 mmol), 3-chlorobenzaldehyde (51 mg, 0.04 mL, 0.36 mmol) and NaOH (29 mg, 0.72 mmol) were dissolved in MeOH. The mixture was allowed to stir at room temperature for 16 hours, after which the reaction mixture was concentrated *in vacuo* and the residue partitioned between EtOAc and water. The aqueous layer was extracted with EtOAc (3 x 20 mL), the organics were combined, washed with brine, dried over $MgSO_4$, filtered, and concentrated *in vacuo*. The resulting residue was purified by flash column chromatography (30 – 50 % EtOAc in cyclohexane) to afford the title compound. White solid (117 mg, 81%). ^{1}H NMR (400 MHz, DMSO-d_6) δ 8.47 (s, 1H, Ar-*H*), 8.11 (s, 1H, Ar-*H*), 8.00 (d, *J* = 2.3 Hz, 1H, Ar-*H*), 7.80 (d, *J* = 2.3 Hz, 1H, Ar-*H*), 7.77 (dd, *J* = 6.2, 1.8 Hz, 1H, Ar-*H*), 7.51 – 7.47 (m, 2H, Ar-*H*), 7.44 (d, *J* = 1.8 Hz, 1H, Ar-*H*), 7.27 (d, *J* = 8.0 Hz, 2H, Ar-*H*), 7.21 (d, *J* = 8.0 Hz, 2H, Ar-*H*), 7.18 (d, *J* = 15.7 Hz, 1H, C=OC*H*CH), 7.02 (d, *J* = 15.7 Hz, 1H, C=OCHC*H*), 6.26 (t, *J* = 2.3 Hz, 1H, Ar-*H*), 5.38 (s, 2H, -CH_2), 5.32 (s, 2H, -CH_2). ^{13}C NMR (101 MHz, DMSO-d_6) δ 188.5, 145.3, 139.7, 139.5, 137.1, 135.5, 130.9, 129.5, 129.3, 128.3, 128.2, 125.3, 124.0, 124.0, 119.4, 117.0, 116.8, 106.1, 67.8, 56.0, 55.5. LCMS (ESI+) m/z calcd for $C_{23}H_{19}ClN_4O$ = 402.1, found 403.0 [M+H]

(*E*)-1-(1-(4-((1*H*-pyrazol-1-yl)methyl)benzyl)-1*H*-pyrazol-4-yl)-3-(2-fluoro-4-methylphenyl)prop-2-en-1-one (124b)

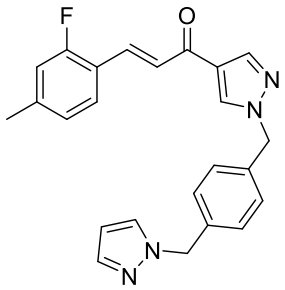

1-(1-(4-((1*H*-pyrazol-1-yl)methyl)benzyl)-1*H*-pyrazol-4-yl)ethan-1-one (100 mg, 0.36 mmol), 2-fluoro-4-methylbenzaldehyde (50 mg, 0.04 mL, 0.36 mmol) and NaOH (29 mg, 0.72 mmol) were dissolved in MeOH. The mixture was allowed to stir at room temperature for 16 hours, after which the reaction mixture was concentrated *in vacuo* and the residue partitioned between EtOAc and water. The aqueous layer was extracted with EtOAc (3 x 20 mL), the organics were combined, washed with brine, dried over $MgSO_4$, filtered, and concentrated *in vacuo*. The resulting residue was purified by flash column chromatography (30 – 50 % EtOAc in cyclohexane) to afford the title compound. White solid (101 mg, 70%). ^{1}H NMR (400 MHz, $CDCl_3$) δ 8.08 (s, 1H, Ar-*H*), 8.00 (s, 1H, Ar-*H*), 7.57 (d, *J* = 2.3 Hz, 1H, Ar-*H*), 7.42 (d, *J* = 2.3 Hz, 1H, Ar-*H*), 7.31 – 7.25 (m, 4H, Ar-*H*), 7.25 – 7.20 (m, 3H, Ar-*H*), 7.01 (d, *J* = 11.8 Hz, 1H, C=OC*H*CH), 6.96 (d, *J* = 11.8 Hz, 1H, C=OCHC*H*), 6.31 (t, *J* = 2.3 Hz, 1H, Ar-*H*), 5.36 – 5.33 (s, 4H, -CH_2), 2.40 (s, 3H, Ar-CH_3). ^{13}C NMR (101 MHz, $CDCl_3$) δ 183.5, 143.1, 143.0, 140.8, 139.8, 137.3, 136.3, 135.9, 134.9, 132.2, 129.7, 129.4, 128.5, 125.4, 125.1, 124.8, 116.9, 116.7, 106.1, 56.2, 55.4, 21.4. LCMS (ESI+) m/z calcd for $C_{24}H_{21}FN_4O$ = 400.2, found 401.2 [M+H]

1-(1-(4-((1*H*-pyrazol-1-yl)methyl)benzyl)-1*H*-pyrazol-4-yl)-3-(3-chlorophenyl)-3-(4,4,5,5-tetramethyl-1,3,2-dioxaborolan-2-yl)propan-1-one (125a)

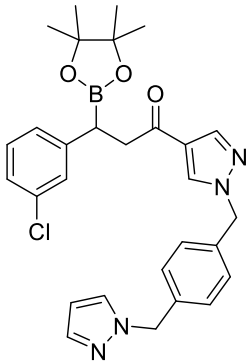

White solid (35 mg, 56 %) ^{1}H NMR (400 MHz, MeOD-*d*$_4$) δ 8.31 (s, 1H, Ar-*H*), 7.97 (s, 1H, Ar-*H*), 7.68 (d, *J* = 2.3 Hz, 1H, Ar-*H*), 7.52 (d, *J* = 2.3 Hz, 1H, Ar-*H*), 7.28 – 7.22 (m, 3H, Ar-*H*), 7.21 – 7.17 (m, 4H, Ar-*H*), 7.17 – 7.12 (m, 1H, Ar-*H*), 6.33 (t, *J* = 2.3 Hz, 1H, Ar-*H*), 5.34 (s, 4H, -C*H*$_2$), 3.33 (dd, *J* = 17.9, 10.3 Hz, 1H, C=OC*H*$_a$), 3.23 (dd, *J* = 17.9, 5.6 Hz, 1H, C=OC*H*$_b$), 2.67 (dd, *J* = 10.3, 5.6 Hz, 1H, BC-*H*), 1.23 (s, 6H, -C*H*$_3$), 1.21 (s, 6H, -C*H*$_3$). ^{13}C NMR (101 MHz, MeOD-*d*$_4$) δ 194.5, 144.2, 140.0, 139.2, 137.2, 135.7, 133.8, 133.1, 130.3, 129.5, 128.0, 127.9, 127.7, 126.4, 125.3, 123.2, 105.6, 83.5, 74.4, 55.2, 54.5, 43.2, 23.7 LCMS (ESI+) m/z calcd for $C_{29}H_{32}BClN_4O_3$ = 530.2, found 531.2 [M+H]

1-(1-(4-((1*H*-pyrazol-1-yl)methyl)benzyl)-1*H*-pyrazol-4-yl)-3-(2-fluoro-4-methylphenyl)-3-(4,4,5,5-tetramethyl-1,3,2-dioxaborolan-2-yl)propan-1-one (125b)

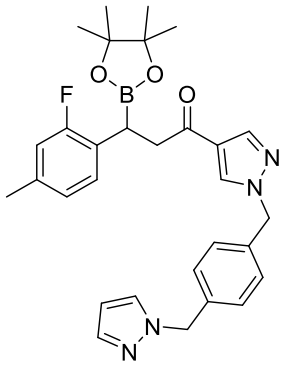

White solid (22 mg, 34 %). ^{1}H NMR (400 MHz, MeOD-d_4) δ 8.28 (s, 1H, Ar-*H*), 7.93 (s, 1H, Ar-*H*), 7.68 (d, *J* = 2.3 Hz, 1H, Ar-*H*), 7.52 (d, *J* = 2.3 Hz, 1H, Ar-*H*), 7.25 (d, *J* = 8.0 Hz, 2H, Ar-*H*), 7.20 (d, *J* = 8.0 Hz, 2H, Ar-*H*), 7.16 – 7.11 (m, 1H, Ar-*H*), 6.89 – 6.80 (m, 2H, Ar-*H*), 6.33 (t, *J* = 2.2 Hz, 1H, Ar-*H*), 5.35 (s, 2H, -CH_2), 5.34 (s, -CH_2), 3.32 (dd, *J* = 17.2, 9.2 Hz, 1H, C=OCH_a) 3.13 (dd, *J* = 17.2, 6.1 Hz, 1H, C=OCH_b), 2.92 (dd, *J* = 9.2, 6.1 Hz, 1H, BC-*H*), 2.28 (s, 3H, Ar-CH_3), 1.23 (s, 6H, -CH_3), 1.21 (s, 6H, -CH_3). ^{13}C NMR (101 MHz, MeOD-d_4) δ 194.8, 139.9, 139.1, 137.6, 137.2, 135.7, 133.0, 130.3, 129.8, 127.9, 127.6, 125.3, 124.4, 123.3, 115.3, 115.1, 105.6, 83.5, 74.4, 55.1, 54.5, 42.2, 23.5, 19.5. LCMS (ESI+) m/z calcd for $C_{30}H_{34}BFN_4O_3$ = 528.3, found 529.3 [M+H]

4-(1-(4-((1*H*-pyrazol-1-yl)methyl)benzyl)-1*H*-pyrazol-4-yl)-2-(3-chlorophenyl)-4-oxobutanenitrile (129a)

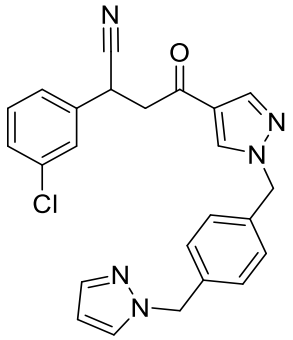

White solid (15 mg, 82%). ^{1}H NMR (400 MHz, MeOD-d_4) δ 8.34 (s, 1H, Ar-*H*), 7.99 (s, 1H, Ar-*H*), 7.68 (d, *J* = 2.4 Hz, 1H, Ar-*H*), 7.52 (d, *J* = 2.4 Hz, 1H, Ar-*H*), 7.48 – 7.44 (m, 1H, Ar-H), 7.43 – 7.32 (m, 3H, Ar-*H*), 7.25 (d, *J* = 8.1 Hz, 2H, Ar-*H*), 7.20 (d, *J* = 8.0 Hz, 2H, Ar-*H*), 6.33 (t, *J* = 2.4 Hz, 1H, Ar-*H*), 5.34 (s, 4H, -CH_2), 4.57 (dd, *J* = 8.4, 5.9 Hz, 1H, NCC-*H*), 3.61 (dd, *J* = 17.6, 8.4 Hz, 1H, C=OCH_a), 3.44 (dd, *J* = 17.6, 5.9 Hz, 1H, C=OCH_b). ^{13}C NMR (101 MHz, MeOD-d_4) δ 189.6, 140.0, 139.2, 137.8, 137.3, 135.6, 134.5, 133.3, 130.3, 129.3, 128.0, 127.9, 127.6, 127.5, 125.8, 122.9, 120.1, 105.6, 55.2, 54.5, 44.2, 31.1. LCMS (ESI+) m/z calcd for $C_{24}H_{20}ClN_5O$ = 429.1, found = 430.1 [M+H].

4-(1-(4-((1*H*-pyrazol-1-yl)methyl)benzyl)-1*H*-pyrazol-4-yl)-2-(2-fluoro-4-methylphenyl)-4-oxobutanenitrile (129b)

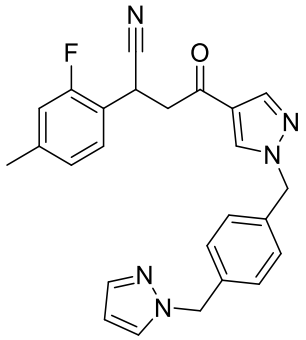

White solid (13 mg, 78%). ^{1}H NMR (400 MHz, MeOD-d_4) δ 8.31 (s, 1H), 7.93 (s, 1H), 7.70 (d, *J* = 2.3 Hz, 1H), 7.52 (d, *J* = 2.3 Hz, 1H), 7.34 (d, *J* = 8.1 Hz, 2H), 7.27 (d, *J* = 8.1 Hz, 3H), 7.14 – 7.10 (m, 1H), 6.92 – 6.86 (m, 2H), 6.32 (t, *J* = 2.3 Hz, 1H), 5.39 (s, 2H, -CH_2), 5.37 (s, 2H, -CH_2), 4.54 (dd, *J* = 8.6, 6.1 Hz, 1H, NCC-*H*), 3.10 (dd, *J* = 17.6 Hz, 6.1 Hz, 1H, C=OCH_a), 2.96 (dd, *J* = 9.2, 6.1 Hz, 1H, C=OCH_b), 2.35 (s, 3H, Ar-CH_3). ^{13}C NMR (101 MHz, MeOD-d_4) δ 190.1, 139.6, 139.3, 137.9, 137.2, 136.6, 134.8, 130.3, 129.8, 127.9, 127.6, 125.3, 125.1, 123.7, 120.5, 115.2, 112.0, 105.6, 58.1, 57.9, 40.5, 26.3, 19.8. LCMS (ESI+) m/z calcd for $C_{25}H_{22}FN_5O$ = 427.2, found = 428.3 [M+H]

Chapter 4

Chapter 4: Conclusions and Future Direction

4.1 Key Findings

The α-amidobenzylboronate compounds that have been the focus of **Chapter 2** represent an interesting new example of PKa-targeting covalent inhibitors arising from installation of a boronate warhead onto active PKa scaffolds targeting the P1 and P4 binding sites. Covalent inhibition was characterised through kinetic assessment of IC_{50} values over various time courses up to 24 hours, (**91** IC_{50} = 70 pM at 24 hours), jump dilution assays, which showed **91** did not wash out from the PKa binding site, matching the profile of known PKa covalent inhibitor **31**, and comparison of IC_{50} data with that of noncovalent matched pairs. Additionally, compounds from this series were selected for evaluation against FXIa and FXIIa, all of which showed >1000-fold selectivity towards PKa.

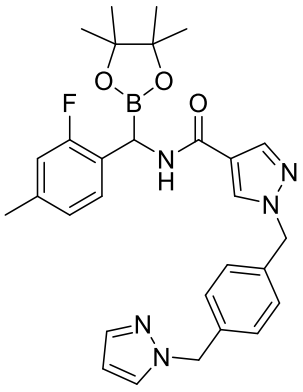

91

Subjection of **91** to further evaluation in the form of a whole plasma IC_{50} assay showed no sign of covalent inhibition, suggesting possible decomposition of **91** under the assay conditions. The tendency of **91** to decompose was also reflected in the crystallographic analysis where decomposition was observed, producing a crystal structure of noncovalent matched pair **106**.

NMR evaluation of the chemical stability of **95** in a deuterated PBS medium showed possible decomposition to the boronic acid as the mechanism of inhibition, which was supported by *in silico* modelling.

Chemical stability being a key limitation of these compounds, efforts to produce more stable analogues would be a consideration for any further work to be undertaken. Stability issues notwithstanding, this class of compounds proves the possibility of obtaining highly potent covalent boronate inhibitors of PKa, representing advancement towards the development of covalent modulators of PKa as HAE therapies.

Chapter 3 discussed the synthesis and biological evaluation of β-ketoboronates synthesised *via* catalytic borylation of unsaturated ketones. Whilst these compounds showed some inhibitory activity against PKa, no evidence of covalent inhibition was observed. Interestingly, the installation of a nitrile warhead to unsaturated ketone precursor **124b** to give **129b** showed reasonable covalent activity in PKa (IC_{50} = 33 nM at 1 hour), and therefore its analogues should be explored further along with the possibility of installing other serine-targeting covalent warheads.

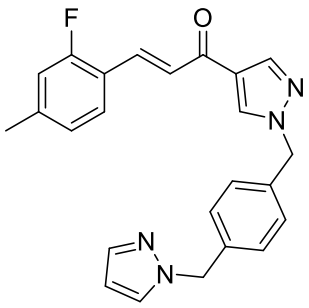

124b

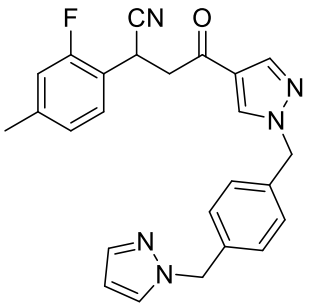

129b

4.2 Future direction

4.2.1 α-Amidobenzylboronates

Despite showing great promise by evaluation of sheer potency, these compounds remain limited by their chemical stability, particularly towards acidic environments. Prior efforts to increase the stability of chemically labile boronates include the incorporation of intramolecular borocycles. For example, vaborbactam **127**, a β-lactamase inhibitor features an α-amidoboronate functionality and incorporates a cyclic boronic ester, enhancing stability (Figure 4.1).[176,177]

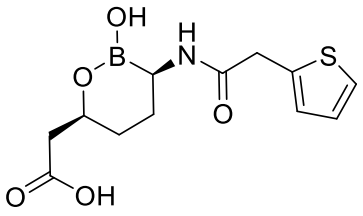

127

Figure 4.1. Structure of vaborbactam.

Incorporation of similar cyclic boronic esters into α-amidoboronates from **Chapter 2** may enhance compound stability and enable access to a stable cyclic hemiboronic acid (Scheme 4.1).

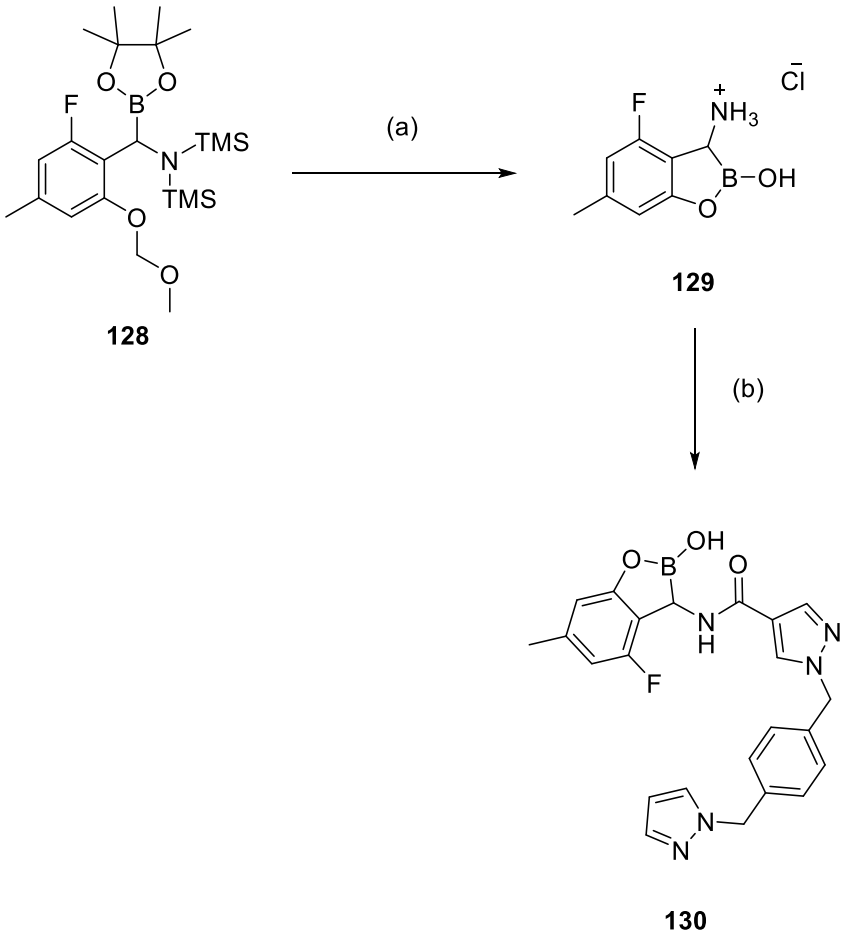

128 **129** **130**

Scheme 4.1. Proposed synthesis of cyclic boronic ester α-amidobenzylboronate analogues. Reagents and conditions: (a) 4N HCl in dioxane, Et_2O, -78 °C **(b)** RCOOH, HATU, DIPEA, MeCN, 0 °C - rt

Using a 6-substituted methoxymethyl ether (OMOM) arylboronic ester and applying the Matteson homologation sequence used in the synthesis of

compounds **91-96** may allow access to silylated amine **128**, global deprotection of the TMS and MOM groups under acidic conditions and amidation of the corresponding cyclic α-aminoboronate **129** may enable access to cyclic α-amidobenzylboronates such as **130**, with potential enhanced stability relative to **91-96** due to tethering of the boron centre to the P1 aryl system.

Hoppe *et al* first reported the synthesis of α-carbamoylboronates as a precursor in the synthesis of enantioenriched secondary alcohols using (-)sparteine as a chiral reagent (Scheme 4.2).[178]

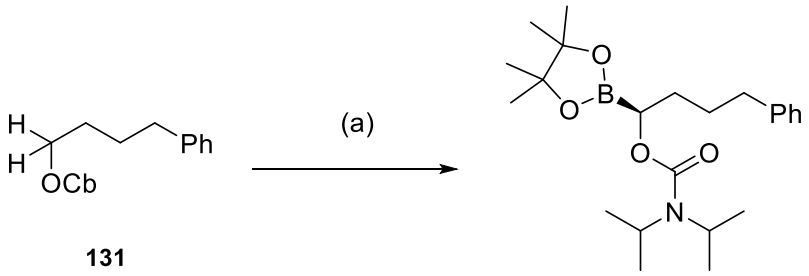

131 **132**

Scheme 4.2. Synthesis of α-carbamoylboronates by Hoppe *et al.* Reagents and conditions: (a) 1) ^{s}BuLi, (-) sparteine 2) B(O^{i}Pr)$_3$ 3) pinacol, *p*-TsOH, $MgSO_4$, Et_2O, -78 °C

Lithiation of the α-carbamoyl position of **131** enables complexation with (-) sparteine and subsequent displacement of triisopropyl borate, followed by treatment with pinacol to trap pinacol boronic ester **132.**

This methodology may be used to synthesise carbamoyl analogues of **91-96** with the possibility of enantiospecificity through the use of sparteine as a chiral reagent (Scheme 4.3).[179–181]

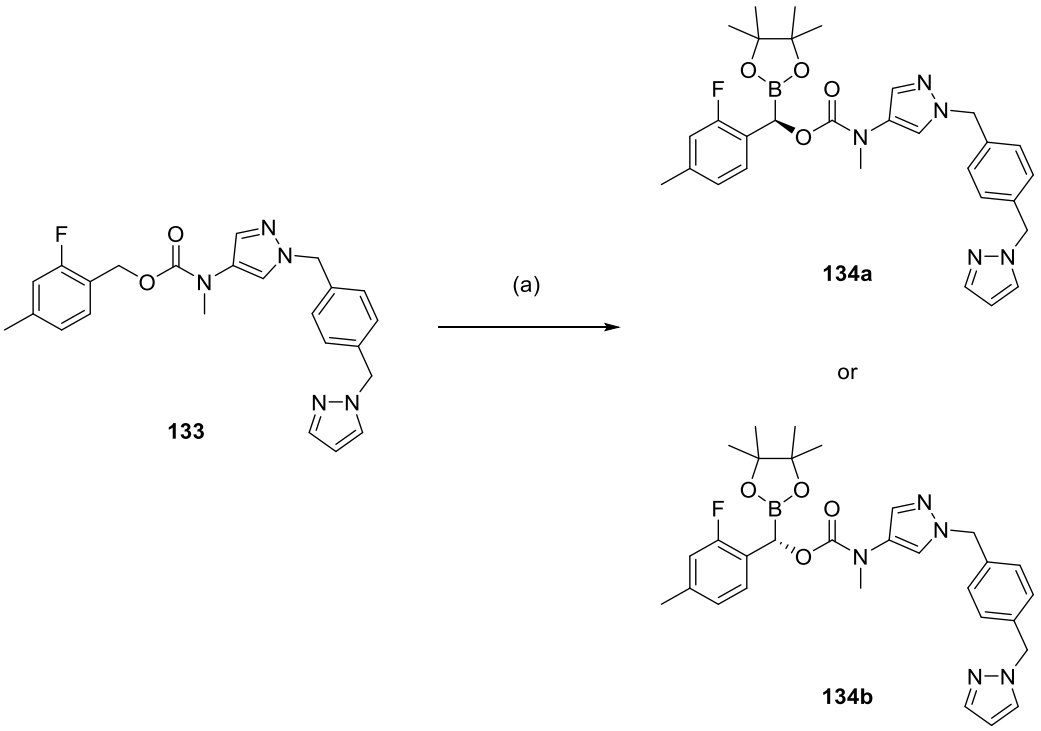

Scheme 4.3. Proposed synthesis of α- carbamoylbenzylboronates *via* a lithiation-borylation procedure. Reagents and conditions: (a) **)** 1) ^{s}BuLi, (-) sparteine or (+) sparteine 2) B(O^{i}Pr)$_3$ 3) pinacol, *p*-TsOH, $MgSO_4$, Et_2O, -78 ^{o}C

The application of this lithiation-borylation methodology on an *N*-methylated carbamoyl scaffold such as **133** may allow for enantioselective borylation and a more robust synthetic procedure than the Matteson homologation sequence described in **Chapter 2**, enabling synthesis of more analogues and installation of a variety of boronic esters.

4.2.2 β-Ketobenzylboronates

Despite showing improved chemical stability relative to compounds **91-96**, β-ketoboronates **125a** and **125b** showed no sign of covalent inhibition in PKa. Interestingly, β-ketonitrile **129b** showed appreciable activity in PKa and demonstrated binding kinetics consistent with that of a covalent inhibitor over the measured time points. Accordingly, the scope of this inhibitor should be explored through variation of P1 and P4 groups to maximise inhibitor activity. Furthermore, the use of basic P1 groups is not precluded in the case of nitriles, enabling wider functional group tolerance (Figure 4.2).

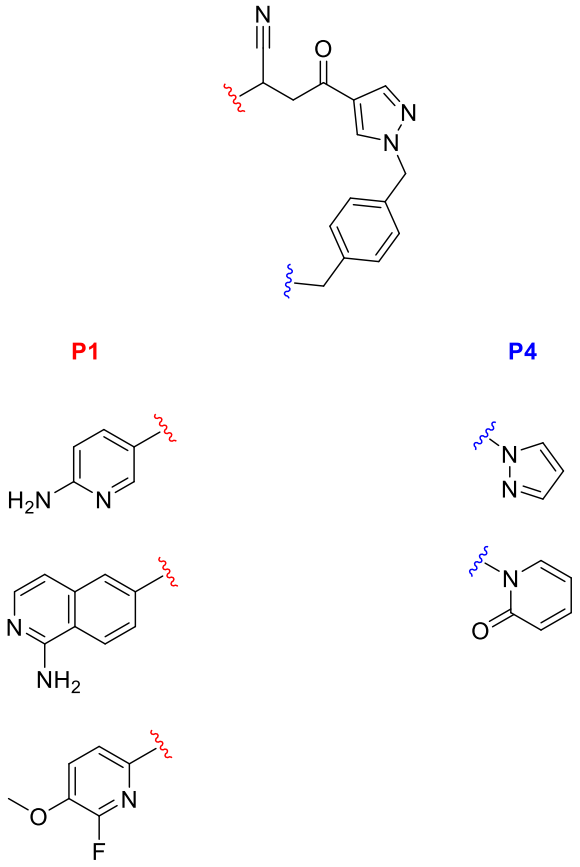

Figure 4.2. Proposed SAR exploration of β-ketonitriles

Further to the use of nitriles as covalent warheads, the use of acyl groups was explored, however this work was not completed due to time constraint. A synthesis was devised enabling access to a α-hydroxy- species **137**, which in principle could be acylated, carbamylated, sulfonylated, amongst other transformations. (Scheme 4.4).

135 was synthesised *via* displacement of **122** with pyrazole-4-carbaldehyde, subsequent aldol condensation of **135** with 2-fluoro-4-methyl acetophenone gave **136** which was selectively reduced with DIBAL-H to yield the corresponding alcohol **137**. Various conditions were explored towards the installation of functional groups which may be transferred onto Ser_{195} of PKa, however no conditions that were trialled enabled the intended transformations. As a result, further work should include optimisation of these conditions and exploration of the chemistry of the hydrogenated counterpart of **137**.

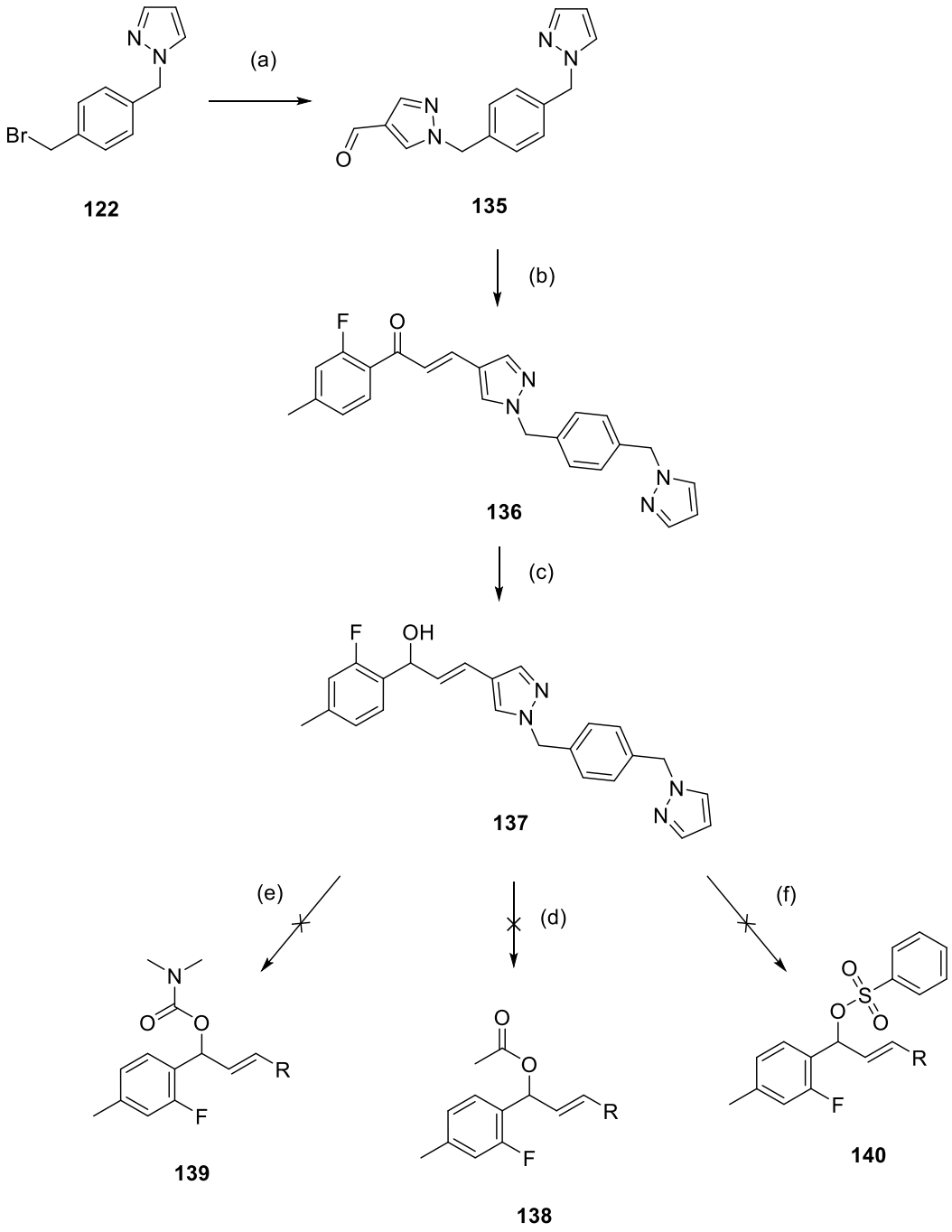

***Scheme* 4.4.** Synthesis and attempted transformation of α-hydroxy- species **137**. Reagents and conditions: (a) 1H-pyrazole-4-carbaldehyde, NaH, THF, 0 °C (b) 2-Fluoro-4-methylacetophenone, NaOH, MeOH, rt (c) DIBAL-H, THF, 0 °C – rt (d) Ac_2O, pyridine, DMAP, rt (e) *N,N*-Dimethylcarbamyl chloride, NaH, DMF, 0°C – rt (e) Phenylsulfonyl chloride, NaH, DMF, 0 °C – rt.

Chapter 5

Chapter 5: References

(1) Nzeako, U. C.; Frigas, E.; Tremaine, W. J. Hereditary Angioedema: A Broad Review for Clinicians. *Arch. Intern. Med.* **2001**, *161* (20), 2417–2429. https://doi.org/10.1001/archinte.161.20.2417.

(2) Han, E. D.; MacFarlane, R. C.; Mulligan, A. N.; Scafidi, J.; Davis, A. E. Increased Vascular Permeability in C1 Inhibitor-Deficient Mice Mediated by the Bradykinin Type 2 Receptor. *J. Clin. Invest.* **2002**, *109* (8), 1057–1063. https://doi.org/10.1172/JCI200214211.

(3) Donaldson, V. H.; Evans, R. R. A Biochemical Abnormality in Hereditary Angioneurotic Edema. *Am. J. Med.* **1963**, *35* (1), 37–44. https://doi.org/10.1016/0002-9343(63)90162-1.

(4) Davis, A. E. Biological Effects of C1 Inhibitor. *Drug News Perspect.* **2004**, *17* (7), 439–446. https://doi.org/10.1358/dnp.2004.17.7.863703.

(5) Zuraw, B. L.; Herschbach, J. Detection of C1 Inhibitor Mutations in Patients with Hereditary Angioedema. *J. Allergy Clin. Immunol.* **2000**, *105* (3), 541–546. https://doi.org/10.1067/mai.2000.104780.

(6) Bork, K.; Barnstedt, S. E.; Koch, P.; Traupe, H. Hereditary Angioedema with Normal C1-Inhibitor Activity in Women. *Lancet* **2000**, *356* (9225), 213–217. https://doi.org/10.1016/S0140-6736(00)02483-1.

(7) Di Cera, E. Serine Proteases. *IUBMB Life* **2009**, *61* (5), 510–515. https://doi.org/10.1002/iub.186.

(8) Rawlings, N. D.; Barrett, A. J. MEROPS: The Peptidase Database. *Nucleic Acids Res.* **1999**, *34* (1), 270–272. https://doi.org/10.1093/nar/27.1.325.

(9) Hedstrom, L. Serine Protease Mechanism and Specificity. *Chem. Rev.* **2002**, *102* (12), 4501–4524. https://doi.org/10.1021/cr000033x.

(10) Schmaier, A. H. The Kallikrein-Kinin and the Renin-Angiotensin Systems Have a Multilayered Interaction. *Am. J. Physiol. - Regul. Integr. Comp. Physiol.* **2003**, *285* (1), 1–13. https://doi.org/10.1152/ajpregu.00535.2002.

(11) Hooley, E.; McEwan, P. A.; Emsley, J. Molecular Modeling of the Prekallikrein Structure Provides Insights into High-Molecular-Weight Kininogen Binding and Zymogen Activation. *J. Thromb. Haemost.* **2007**, *5* (12), 2461–2466. https://doi.org/10.1111/j.1538-7836.2007.02792.x.

(12) Bourdet, B.; Pécher, C.; Minville, V.; Jaafar, A.; Allard, J.; Blaes, N.; Girolami, J. P.; Tack, I. Distribution and Expression of B2-Kinin Receptor on Human Leukocyte Subsets in Young Adults and Elderly Using Flow Cytometry. *Neuropeptides* **2010**, *44* (2), 155–161. https://doi.org/10.1016/j.npep.2009.12.005.

(13) Chen, L.; Deng, H.; Cui, H.; Fang, J.; Zuo, Z.; Deng, J.; Li, Y.; Wang, X.; Zhao,

L. Inflammatory Responses and Inflammation-Associated Diseases in Organs. *Oncotarget* **2018**, *9* (6), 7204–7218. https://doi.org/10.18632/oncotarget.23208.

(14) Shen, J. kang; Zhang, H. tao. Function and Structure of Bradykinin Receptor 2 for Drug Discovery. *Acta Pharmacol. Sin.* **2023**, *44*, 489–498. https://doi.org/10.1038/s41401-022-00982-8.

(15) Madeddu, P.; Emanueli, C.; El-Dahr, S. Mechanisms of Disease: The Tissue Kallikrein-Kinin System in Hypertension and Vascular Remodeling. *Nat. Clin. Pract. Nephrol.* **2007**, *3* (4), 208–221. https://doi.org/10.1038/ncpneph0444.

(16) Wojciak-Stothard, B.; Ridley, A. J. Rho GTPases and the Regulation of Endothelial Permeability. *Vascul. Pharmacol.* **2002**, *39* (4), 187–199. https://doi.org/10.1016/S1537-1891(03)00008-9.

(17) Heestermans, M.; Naudin, C.; Mailer, R. K.; Konrath, S.; Klaetschke, K.; Jämsä, A.; Frye, M.; Deppermann, C.; Pula, G.; Kuta, P.; Friese, M. A.; Gelderblom, M.; Sickmann, A.; Preston, R. J. S.; Nofer, J. R.; Rose-John, S.; Butler, L. M.; Salomon, O.; Stavrou, E. X.; Renné, T. Identification of the Factor XII Contact Activation Site Enables Sensitive Coagulation Diagnostics. *Nat. Commun.* **2021**, *12* (5596), 4374–4387. https://doi.org/10.1038/s41467-021-25888-7.

(18) Schmaier, A. H. The Contact Activation and Kallikrein/Kinin Systems: Pathophysiologic and Physiologic Activities. *J. Thromb. Haemost.* **2016**, *14* (1), 28–39. https://doi.org/10.1111/jth.13194.

(19) Renné, T.; Pozgajová, M.; Grüner, S.; Schuh, K.; Pauer, H. U.; Burfeind, P.; Gailani, D.; Nieswandt, B. Defective Thrombus Formation in Mice Lacking Coagulation Factor XII. *J. Exp. Med.* **2005**, *202* (2), 271–281. https://doi.org/10.1084/jem.20050664.

(20) Cochrane, C. G.; Revak, S. D.; Wuepper, K. D. Activation of Hageman Factor in Solid and Fluid Phases: A Critical Role of Kallikrein. *J. Exp. Med.* **1973**, *138* (6), 1564–1583. https://doi.org/10.1084/jem.138.6.1564.

(21) Moreau, M. E.; Garbacki, N.; Molinaro, G.; Brown, N. J.; Marceau, F.; Adam, A. The Kallikrein-Kinin System: Current and Future Pharmacological Targets. *J. Pharmacol. Sci.* **2005**, *99* (1), 6–38. https://doi.org/10.1254/jphs.SRJ05001X.

(22) Shariat-Madar, Z.; Schmaier, A. H. The Plasma Kallikrein/Kinin and Renin Angiotensin Systems in Blood Pressure Regulation in Sepsis. *J. Endotoxin Res.* **2004**, *10* (1), 3–13. https://doi.org/10.1179/096805104225003807.

(23) Li, H. H. Self-Administered C1 Esterase Inhibitor Concentrates for the Management of Hereditary Angioedema: Usability and Patient Acceptance. *Patient Prefer. Adherence* **2016**, *10* (10), 1727–1737. https://doi.org/10.2147/PPA.S86379.

(24) Farkas, H.; Varga, L. Human Plasma-Derived, Nanofiltered, C1-Inhibitor Concentrate (Cinryze®), a Novel Therapeutic Alternative for the Management of Hereditary Angioedema Resulting from C1-Inhibitor Deficiency. *Biol. Ther.* **2012**, *2* (1), 2–4. https://doi.org/10.1007/s13554-012-0002-5.

(25) Yang, W. H.; Li, H. H.; Chase, C.; Moldovan, D.; Grivcheva-Panovska, V.; Harper, J. R.; Relan, A.; Riedl, M. A. Recombinant Human C1 Inhibitor (RHC1INH) Is Efficacious and Well Tolerated As Prophylaxis for Prevention of Hereditary Angioedema (HAE) Attacks: A Randomized, Phase 2 Trial. *J. Allergy Clin. Immunol.* **2017**, *139* (2), 231–236. https://doi.org/10.1016/j.jaci.2016.12.744.

(26) Hock, F. J.; Wirth, K.; Albus, U.; Linz, W.; Gerhards, H. J.; Wiemer, G.; Henke, S.; Breipohl, G.; König, W.; Knolle, J.; Schölkens, B. A. Hoe 140 a New Potent and Long Acting Bradykinin-antagonist: In Vitro Studies. *Br. J. Pharmacol.* **1991**, *102* (3), 769–773. https://doi.org/10.1111/j.1476-5381.1991.tb12248.x.

(27) Cicardi, M.; Banerji, A.; Bracho, F.; Malbrán, A.; Rosenkranz, B.; Riedl, M.; Bork, K.; Lumry, W.; Aberer, W.; Bier, H.; Bas, M.; Greve, J.; Hoffmann, T. K.; Farkas, H.; Reshef, A.; Ritchie, B.; Yang, W.; Grabbe, J.; Kivity, S.; Kreuz, W.; Levy, R. J.; Luger, T.; Obtulowicz, K.; Schmid-Grendelmeier, P.; Bull, C.; Sitkauskiene, B.; Smith, W. B.; Toubi, E.; Werner, S.; Anné, S.; Björkander, J.; Bouillet, L.; Cillari, E.; Hurewitz, D.; Jacobson, K. W.; Katelaris, C. H.; Maurer, M.; Merk, H.; Bernstein, J. A.; Feighery, C.; Floccard, B.; Gleich, G.; Hébert, J.; Kaatz, M.; Keith, P.; Kirkpatrick, C. H.; Langton, D.; Martin, L.; Pichler, C.; Resnick, D.; Wombolt, D.; Fernández Romero, D. S.; Zanichelli, A.; Arcoleo, F.; Knolle, J.; Kravec, I.; Dong, L.; Zimmermann, J.; Rosen, K.; Fan, W.-T. T.; Romero, D. S. F.; Zanichelli, A.; Arcoleo, F.; Knolle, J.; Kravec, I.; Dong, L.; Zimmermann, J.; Rosen, K.; Fan, W.-T. T. Icatibant, a New Bradykinin-Receptor Antagonist, in Hereditary Angioedema. *N. Engl. J. Med.* **2010**, *363* (6), 532–541. https://doi.org/10.1056/nejmoa0906393.

(28) Floccard, B.; Hautin, E.; Bouillet, L.; Coppere, B.; Allaouchiche, B. An Evidence-Based Review of the Potential Role of Icatibant in the Treatment of Acute Attacks in Hereditary Angioedema Type i and II. *Core Evid.* **2012**, *7*, 105–114. https://doi.org/10.2147/CE.S24743.

(29) Félétou, M.; Martin, C. A. E.; Molimard, M.; Naline, E.; Germain, M.; Thurieau, C.; Fauchère, J. L.; Canet, E.; Advenier, C. In Vitro Effects of HOE 140 in Human Bronchial and Vascular Tissue. *Eur. J. Pharmacol.* **1995**, *274* (1), 57–64. https://doi.org/10.1016/0014-2999(94)00709-G.

(30) Caballero, T.; Baeza, M. L.; Cabañas, R.; Campos, A.; Cimbollek, S.; Gómez-Traseira, C.; González-Quevedo, T.; Guilarte, M.; Jurado-Palomo, J.; Larco, J. I.; López-Serrano, M. C.; López-Trascasa, M.; Marcos, C.; Muñoz-Caro, J. M.; Pedrosa, M.; Prior, N.; Rubio, M.; Sala-Cunill, A. Consensus Statement on the Diagnosis, Management, and Treatment of Angioedema Mediated by Bradykinin. Part II. Treatment, Follow-up, and Special Situations. *J.*

Investig. Allergol. Clin. Immunol. **2011**, *21* (6), 422–441.

(31) Lunn, M.; Banta, E. Ecallantide for the Treatment of Hereditary Angiodema in Adults. *Clin. Med. Insights Cardiol.* **2011**, *5* (5), 49–54. https://doi.org/10.4137/CMC.S4434.

(32) Craig, T. J.; Li, H. H.; Riedl, M.; Bernstein, J. A.; Lumry, W. R.; MacGinnitie, A. J.; Stolz, L. E.; Biedenkapp, J.; Chyung, Y. Characterization of Anaphylaxis After Ecallantide Treatment of Hereditary Angioedema Attacks. *J. Allergy Clin. Immunol. Pract.* **2015**, *3* (2), 206-212.e4. https://doi.org/10.1016/j.jaip.2014.09.001.

(33) Cicardi, M.; Levy, R. J.; McNeil, D. L.; Li, H. H.; Sheffer, A. L.; Campion, M.; Horn, P. T.; Pullman, W. E. Ecallantide for the Treatment of Acute Attacks in Hereditary Angioedema. *N. Engl. J. Med.* **2010**, *363* (6), 523–531. https://doi.org/10.1056/nejmoa0905079.

(34) Bernstein, J. A.; Qazi, M. Ecallantide: Its Pharmacology, Pharmacokinetics, Clinical Efficacy and Tolerability. *Expert Rev. Clin. Immunol.* **2010**, *6* (1), 29–39. https://doi.org/10.1586/eci.09.60.

(35) Craig, T.; Zuraw, B.; Longhurst, H.; Cicardi, M.; Bork, K.; Grattan, C.; Katelaris, C.; Sussman, G.; Keith, P. K.; Yang, W.; Hébert, J.; Hanzlikova, J.; Staubach-Renz, P.; Martinez-Saguer, I.; Magerl, M.; Aygören-Pürsün, E.; Farkas, H.; Reshef, A.; Kivity, S.; Neri, S.; Crisan, I.; Caballero, T.; Baeza, M. L.; Hernandez, M. D.; Li, H.; Lumry, W.; Bernstein, J. A.; Hussain, I.; Anderson, J.; Schwartz, L. B.; Jacobs, J.; Manning, M.; Levy, D.; Riedl, M.; Christiansen, S.; Feuersenger, H.; Pragst, I.; Mycroft, S.; Pawaskar, D.; Jacobs, I. Long-Term Outcomes with Subcutaneous C1-Inhibitor Replacement Therapy for Prevention of Hereditary Angioedema Attacks. *J. Allergy Clin. Immunol. Pract.* **2019**, *7* (6), 1792–1802. https://doi.org/10.1016/j.jaip.2019.01.054.

(36) Agostoni, A.; Aygören-Pürsün, E.; Binkley, K. E.; Blanch, A.; Bork, K.; Bouillet, L.; Bucher, C.; Castaldo, A. J.; Cicardi, M.; Davis, A. E.; De Carolis, C.; Drouet, C.; Duponchel, C.; Farkas, H.; Fáy, K.; Fekete, B.; Fischer, B.; Fontana, L.; Füst, G.; Giacomelli, R.; Gröner, A.; Erik Hack, C.; Harmat, G.; Jakenfelds, J.; Juers, M.; Kalmár, L.; Kaposi, P. N.; Karádi, I.; Kitzinger, A.; Kollár, T.; Kreuz, W.; Lakatos, P.; Longhurst, H. J.; Lopez-Trascasa, M.; Martinez-Saguer, I.; Monnier, N.; Nagy, I.; Németh, É.; Nielsen, E. W.; Nuijens, J. H.; O'Grady, C.; Pappalardo, E.; Penna, V.; Perricone, C.; Perricone, R.; Rauch, U.; Roche, O.; Rusicke, E.; Späth, P. J.; Szendei, G.; Takács, E.; Tordai, A.; Truedsson, L.; Varga, L.; Visy, B.; Williams, K.; Zanichelli, A.; Zingale, L. Hereditary and Acquired Angioedema: Problems and Progress: Proceedings of the Third C1 Esterase Inhibitor Deficiency Workshop and Beyond. *J. Allergy Clin. Immunol.* **2004**, *114* (3), 51–131. https://doi.org/10.1016/j.jaci.2004.06.047.

(37) Zuraw, B. L.; Busse, P. J.; White, M.; Jacobs, J.; Lumry, W.; Baker, J.; Craig, T.; Grant, J. A.; Hurewitz, D.; Bielory, L.; Cartwright, W. E.; Koleilat, M.;

Ryan, W.; Schaefer, O.; Manning, M.; Patel, P.; Bernstein, J. A.; Friedman, R. A.; Wilkinson, R.; Tanner, D.; Kohler, G.; Gunther, G.; Levy, R.; McClellan, J.; Redhead, J.; Guss, D.; Heyman, E.; Blumenstein, B. A.; Kalfus, I.; Frank, M. M. Nanofiltered C1 Inhibitor Concentrate for Treatment of Hereditary Angioedema. *N. Engl. J. Med.* **2010**, *363* (6), 513–522. https://doi.org/10.1056/nejmoa0805538.

(38) Cicardi, M.; Castelli, R.; Zingale, L. C.; Agostoni, A. Side Effects of Long-Term Prophylaxis with Attenuated Androgens in Hereditary Angioedema: Comparison of Treated and Untreated Patients. *J. Allergy Clin. Immunol.* **1997**, *99* (2), 194–196. https://doi.org/10.1016/S0091-6749(97)70095-2.

(39) Al-Badr, A. A. Danazol. *Profiles Drug Subst. Excipients Relat. Methodol.* **2022**, *47*, 149–326. https://doi.org/10.1016/bs.podrm.2021.10.005.

(40) Nieschlag, E.; Behre, H. M.; Nieschlag, S. Andrology: Male Reproductive Health and Dysfunction. *Androl. Male Reprod. Heal. Dysfunct.* **2010**, 79–83. https://doi.org/10.1007/978-3-540-78355-8.

(41) Drouet, C.; Désormeaux, A.; Robillard, J.; Ponard, D.; Bouillet, L.; Martin, L.; Kanny, G.; Moneret-Vautrin, D. A.; Bosson, J. L.; Quesada, J. L.; López-Trascasa, M.; Adam, A. Metallopeptidase Activities in Hereditary Angioedema: Effect of Androgen Prophylaxis on Plasma Aminopeptidase P. *J. Allergy Clin. Immunol.* **2008**, *121* (2), 429–433. https://doi.org/10.1016/j.jaci.2007.10.048.

(42) Xu, Y.; Zhi, Y. Long-Term Prophylaxis of Hereditary Angioedema with Danazol. *Chin. Med. J. (Engl).* **2022**, *135* (21), 2642–2643. https://doi.org/10.1097/CM9.0000000000002144.

(43) Maurer, M.; Magerl, M.; Betschel, S.; Aberer, W.; Ansotegui, I. J.; Aygören-Pürsün, E.; Banerji, A.; Bara, N. A.; Boccon-Gibod, I.; Bork, K.; Bouillet, L.; Boysen, H. B.; Brodszki, N.; Busse, P. J.; Bygum, A.; Caballero, T.; Cancian, M.; Castaldo, A.; Cohn, D. M.; Csuka, D.; Farkas, H.; Gompels, M.; Gower, R.; Grumach, A. S.; Guidos-Fogelbach, G.; Hide, M.; Kang, H. R.; Kaplan, A. P.; Katelaris, C.; Kiani-Alikhan, S.; Lei, W. Te; Lockey, R.; Longhurst, H.; Lumry, W. R.; MacGinnitie, A.; Malbran, A.; Martinez Saguer, I.; Matta, J. J.; Nast, A.; Nguyen, D.; Nieto-Martinez, S. A.; Pawankar, R.; Peter, J.; Porebski, G.; Prior, N.; Reshef, A.; Riedl, M.; Ritchie, B.; Rafique Sheikh, F.; Smith, W. B.; Spaeth, P. J.; Stobiecki, M.; Toubi, E.; Varga, L. A.; Weller, K.; Zanichelli, A.; Zhi, Y.; Zuraw, B.; Craig, T. The International WAO/EAACI Guideline for the Management of Hereditary Angioedema—The 2021 Revision and Update. *Allergy Eur. J. Allergy Clin. Immunol.* **2022**, *77* (7), 1961–1990. https://doi.org/10.1111/all.15214.

(44) Cicardi, M.; Bork, K.; Caballero, T.; Craig, T.; Li, H. H.; Longhurst, H.; Reshef, A.; Zuraw, B.; Aberer, W.; Aygören-Pürsün, E.; Banerji, A.; Bjorkander, J.; Boccon-Gibod, I.; Bouillet, L.; Grenoble, F.; Bova, M.; Bowen, T.; Calgary, C.; Branco, F. M.; Bygum, A.; Caballero, T.; Cancian, M.; Castel-Branco, M. G.; de Carolis, C.; Mihály, E.; Fabiani, J.; Farkas, H.; Gompels, M.; Gower,

R.; Groffik, A.; Grumach, A.; Guillarte, M.; Hack, E.; Hernandez, L. M.; Kaplan, A.; Lara, A.; Leibovich, I.; Li, H.; Lock, B.; Lumry, W.; Malbran, A.; Martinez-Saguer, I.; Matta, C.; Maurer, M.; Moldovan, D.; Montinaro, V.; Nieto, S.; Nordenfelt, P.; Obtulovicz, K.; Perricone, R.; Prior, N.; Riedl, M.; Rodrigues do, V.; Savoca, C.; Spaeth, P.; Staubach-Renz, P.; Stobiecki, M.; Triggiani, M.; Vacchini, R.; Varga, L.; Zanichelli, A.; Zarchi, K.; Zeerleder, S.; Zingale, L. Evidence-Based Recommendations for the Therapeutic Management of Angioedema Owing to Hereditary C1 Inhibitor Deficiency: Consensus Report of an International Working Group. *Allergy Eur. J. Allergy Clin. Immunol.* **2012**, *67* (2), 147–157. https://doi.org/10.1111/j.1398-9995.2011.02751.x.

(45) Tabatabaei A. P-185: A Clinical Randomized Single Blind Trial of Medical Therapies for Menorrhagia Using Ibuprofen and Tranexamic Acid. *Int J Fertil Steril* **2013**, *136* (1), 1–2.

(46) Gompels, M. M.; Lock, R. J.; Abinun, M.; Bethune, C. A.; Davies, G.; Grattan, C.; Fay, A. C.; Longhurst, H. J.; Morrison, L.; Price, A.; Price, M.; Watters, D. C1 Inhibitor Deficiency: Consensus Document. *Clin. Exp. Immunol.* **2005**, *139* (3), 379–394. https://doi.org/10.1111/j.1365-2249.2005.02726.x.

(47) Longhurst, H. J.; Tarzi, M. D.; Ashworth, F.; Bethune, C.; Cale, C.; Dempster, J.; Gompels, M.; Jolles, S.; Seneviratne, S.; Symons, C.; Price, A.; Edgar, D. C1 Inhibitor Deficiency: 2014 United Kingdom Consensus Document. *Clin. Exp. Immunol.* **2015**, *180* (3), 475–483. https://doi.org/10.1111/cei.12584.

(48) Cai, J.; Ribkoff, J.; Olson, S.; Raghunathan, V.; Al-Samkari, H.; DeLoughery, T. G.; Shatzel, J. J. The Many Roles of Tranexamic Acid: An Overview of the Clinical Indications for TXA in Medical and Surgical Patients. *Eur. J. Haematol.* **2020**, *102* (4), 79–87. https://doi.org/10.1111/ejh.13348.

(49) Horiuchi, T.; Hide, M.; Yamashita, K.; Ohsawa, I. The Use of Tranexamic Acid for On-Demand and Prophylactic Treatment of Hereditary Angioedema—A Systematic Review. *J. Cutan. Immunol. Allergy* **2018**, *1* (4), 126–138. https://doi.org/10.1002/cia2.12029.

(50) Kenniston, J. A.; Faucette, R. R.; Martik, D.; Comeau, S. R.; Lindberg, A. P.; Kopacz, K. J.; Conley, G. P.; Chen, J.; Viswanathan, M.; Kastrapeli, N.; Cosic, J.; Mason, S.; DiLeo, M.; Abendroth, J.; Kuzmic, P.; Ladner, R. C.; Edwards, T. E.; TenHoor, C.; Adelman, B. A.; Nixon, A. E.; Sexton, D. J. Inhibition of Plasma Kallikrein by a Highly Specific Active Site Blocking Antibody. *J. Biol. Chem.* **2014**, *289* (34), 23596–23608. https://doi.org/10.1074/jbc.M114.569061.

(51) Syed, Y. Y. Lanadelumab: A Review in Hereditary Angioedema. *Drugs* **2019**, *79*, 1777–1784. https://doi.org/10.1007/s40265-019-01206-w.

(52) Banerji, A.; Busse, P.; Shennak, M.; Lumry, W.; Davis-Lorton, M.; Wedner, H. J.; Jacobs, J.; Baker, J.; Bernstein, J. A.; Lockey, R.; Li, H. H.; Craig, T.;

Cicardi, M.; Riedl, M.; Al-Ghazawi, A.; Soo, C.; Iarrobino, R.; Sexton, D. J.; TenHoor, C.; Kenniston, J. A.; Faucette, R.; Still, J. G.; Kushner, H.; Mensah, R.; Stevens, C.; Biedenkapp, J. C.; Chyung, Y.; Adelman, B. Inhibiting Plasma Kallikrein for Hereditary Angioedema Prophylaxis. *N. Engl. J. Med.* **2017**, *376* (8), 717–728. https://doi.org/10.1056/nejmoa1605767.

(53) Riedl, M. A.; Aygören-Pürsün, E.; Baker, J.; Farkas, H.; Anderson, J.; Bernstein, J. A.; Bouillet, L.; Busse, P.; Manning, M.; Magerl, M.; Gompels, M.; Huissoon, A. P.; Longhurst, H.; Lumry, W.; Ritchie, B.; Shapiro, R.; Soteres, D.; Banerji, A.; Cancian, M.; Johnston, D. T.; Craig, T. J.; Launay, D.; Li, H. H.; Liebhaber, M.; Nickel, T.; Offenberger, J.; Rae, W.; Schrijvers, R.; Triggiani, M.; Wedner, H. J.; Dobo, S.; Cornpropst, M.; Clemons, D.; Fang, L.; Collis, P.; Sheridan, W. P.; Maurer, M. Evaluation of Avoralstat, an Oral Kallikrein Inhibitor, in a Phase 3 Hereditary Angioedema Prophylaxis Trial: The OPuS-2 Study. *Allergy Eur. J. Allergy Clin. Immunol.* **2018**, *73* (9), 1871–1880. https://doi.org/10.1111/all.13466.

(54) Kotian, P. L.; Wu, M.; Vadlakonda, S.; Chintareddy, V.; Lu, P.; Juarez, L.; Kellogg-Yelder, D.; Chen, X.; Muppa, S.; Chambers-Wilson, R.; Davis Parker, C.; Williams, J.; Polach, K. J.; Zhang, W.; Raman, K.; Babu, Y. S. Berotralstat (BCX7353): Structure-Guided Design of a Potent, Selective, and Oral Plasma Kallikrein Inhibitor to Prevent Attacks of Hereditary Angioedema (HAE). *J. Med. Chem.* **2021**, *64* (171), 12453–12468. https://doi.org/10.1021/acs.jmedchem.1c00511.

(55) Manning, M. E.; Kashkin, J. M. Berotralstat (BCX7353) Is a Novel Oral Prophylactic Treatment for Hereditary Angioedema: Review of Phase II and III Studies. *Allergy Asthma Proc.* **2021**, *42* (4), 274–282. https://doi.org/10.2500/aap.2021.42.210034.

(56) Aygören-Pürsün, E.; Bygum, A.; Grivcheva-Panovska, V.; Magerl, M.; Graff, J.; Steiner, U. C.; Fain, O.; Huissoon, A.; Kinaciyan, T.; Farkas, H.; Lleonart, R.; Longhurst, H. J.; Rae, W.; Triggiani, M.; Aberer, W.; Cancian, M.; Zanichelli, A.; Smith, W. B.; Baeza, M. L.; Du-Thanh, A.; Gompels, M.; Gonzalez-Quevedo, T.; Greve, J.; Guilarte, M.; Katelaris, C.; Dobo, S.; Cornpropst, M.; Clemons, D.; Fang, L.; Collis, P.; Sheridan, W.; Maurer, M.; Cicardi, M. Oral Plasma Kallikrein Inhibitor for Prophylaxis in Hereditary Angioedema. *N. Engl. J. Med.* **2018**, *379* (4), 352–362. https://doi.org/10.1056/nejmoa1716995.

(57) Davie, R. L.; Edwards, H. J.; Evans, D. M.; Hodgson, S. T.; Stocks, M. J.; Smith, A. J.; Rushbrooke, L. J.; Pethen, S. J.; Roe, M. B.; Clark, D. E.; McEwan, P. A.; Hampton, S. L. Sebetralstat (KVD900): A Potent and Selective Small Molecule Plasma Kallikrein Inhibitor Featuring a Novel P1 Group as a Potential Oral On-Demand Treatment for Hereditary Angioedema. *J. Med. Chem.* **2022**, *65* (20), 13629–13644. https://doi.org/10.1021/acs.jmedchem.2c00921.

(58) Maetzel, A.; Smith, M. D.; Duckworth, E. J.; Hampton, S. L.; De Donatis, G. M.; Murugesan, N.; Rushbrooke, L. J.; Li, L.; Francombe, D.; Feener, E. P.;

Yea, C. M. KVD900, an Oral on-Demand Treatment for Hereditary Angioedema: Phase 1 Study Results. *J. Allergy Clin. Immunol.* **2022**, *149* (6), 2034–2042. https://doi.org/10.1016/j.jaci.2021.10.038.

(59) Busse, P.; Kaplan, A. Specific Targeting of Plasma Kallikrein for Treatment of Hereditary Angioedema: A Revolutionary Decade. *J. Allergy Clin. Immunol. Pract.* **2022**, *10* (3), 716–722. https://doi.org/10.1016/j.jaip.2021.11.011.

(60) Perego, F.; Wu, M. A.; Valerieva, A.; Caccia, S.; Suffritti, C.; Zanichelli, A.; Bergamaschini, L.; Cicardi, M. Current and Emerging Biologics for the Treatment of Hereditary Angioedema. *Expert Opin. Biol. Ther.* **2019**, *19* (6), 517–526. https://doi.org/10.1080/14712598.2019.1595581.

(61) Craig, T. J.; Reshef, A.; Li, H. H.; Jacobs, J. S.; Bernstein, J. A.; Farkas, H.; Yang, W. H.; Stroes, E. S. G.; Ohsawa, I.; Tachdjian, R.; Manning, M. E.; Lumry, W. R.; Saguer, I. M.; Aygören-Pürsün, E.; Ritchie, B.; Sussman, G. L.; Anderson, J.; Kawahata, K.; Suzuki, Y.; Staubach, P.; Treudler, R.; Feuersenger, H.; Glassman, F.; Jacobs, I.; Magerl, M. Efficacy and Safety of Garadacimab, a Factor XIIa Inhibitor for Hereditary Angioedema Prevention (VANGUARD): A Global, Multicentre, Randomised, Double-Blind, Placebo-Controlled, Phase 3 Trial. *Lancet* **2023**, *401* (10382), 1079–1090. https://doi.org/10.1016/S0140-6736(23)00350-1.

(62) Kalfus, I.; McDonald, A.; Qian, S. Potency, Selectivity, and Exposure Evaluation of ATN-249, a New Oral Kallikrein Inhibitor for Hereditary Angioedema. *J. Allergy Clin. Immunol.* **2017**, *139* (2), 378. https://doi.org/10.1016/j.jaci.2016.12.905.

(63) Sabnis, R. W. Novel Plasma Kallikrein Inhibitors for Treating Hereditary Angioedema, Diabetic Macular Edema, and Diabetic Retinopathy. *ACS Med. Chem. Lett.* **2022**, *14* (11), 1491–1492. https://doi.org/10.1021/acsmedchemlett.2c00085.

(64) Partridge, J. R.; Choy, R. M.; Silva-Garcia, A.; Yu, C.; Li, Z.; Sham, H.; Metcalf, B. Structures of Full-Length Plasma Kallikrein Bound to Highly Specific Inhibitors Describe a New Mode of Targeted Inhibition. *J. Struct. Biol.* **2019**, *206* (2), 170–182. https://doi.org/10.1016/j.jsb.2019.03.001.

(65) Brandl, T.; Flohr, S.; Kopec, S. N-((6-Amino-Pyridin-3-Yl) Methyl)-Heteroaryl-Carboxamides As Inhibitors of Plasma Kallikrein. *WO Pat. …CA2814911A1* **2012**, 26–27.

(66) Caballero, T. Treatment of Hereditary Angioedema. *J. Investig. Allergol. Clin. Immunol.* **2021**, *31* (1), 1–16. https://doi.org/10.18176/jiaci.0653.

(67) Jose, J.; Lehman, E. B.; Craig, T. Evaluating Satisfaction of Patients with Hereditary Angioedema with Their Past and Present Treatments: Implications for Future Therapies. *Allergy Asthma Proc.* **2018**, *39* (1), 74–80. https://doi.org/10.2500/aap.2018.39.4095.

(68) Betschel, S. D.; Banerji, A.; Busse, P. J.; Cohn, D. M.; Magerl, M. Hereditary

Angioedema: A Review of the Current and Evolving Treatment Landscape. *J. Allergy Clin. Immunol. Pract.* **2023**, *11* (8), 2135–2145. https://doi.org/10.1016/j.jaip.2023.04.017.

(69) Duckworth, E. J.; Murugesan, N.; Li, L.; Rushbrooke, L. J.; Lee, D. K.; De Donatis, G. M.; Maetzel, A.; Yea, C. M.; Hampton, S. L.; Feener, E. P. Pharmacological Suppression of the Kallikrein Kinin System with KVD900: An Orally Available Plasma Kallikrein Inhibitor for the on-Demand Treatment of Hereditary Angioedema. *Clin. Exp. Allergy* **2022**, *52* (9), 1059–1070. https://doi.org/10.1111/cea.14122.

(70) Tang, J.; Yu, C. L.; Williams, S. R.; Springman, E.; Jeffery, D.; Sprengeler, P. A.; Estevez, A.; Sampang, J.; Shrader, W.; Spencer, J.; Young, W.; McGrath, M.; Katz, B. A. Expression, Crystallization, and Three-Dimensional Structure of the Catalytic Domain of Human Plasma Kallikrein. *J. Biol. Chem.* **2005**, *280* (49), 41077–41089. https://doi.org/10.1074/jbc.M506766200.

(71) Rawlings, N. D.; Salvesen, G. Handbook of Proteolytic Enzymes. *Handb. Proteolytic Enzym.* **2013**, 318–319. https://doi.org/10.1016/C2009-1-60990-4.

(72) Schechter, I.; Berger, A. On the Size of the Active Site in Proteases. I. Papain. *Biochem. Biophys. Res. Commun.* **1967**, *27* (2), 157–162. https://doi.org/10.1016/S0006-291X(67)80055-X.

(73) Botos, I.; Wlodawer, A. The Expanding Diversity of Serine Hydrolases. *Curr. Opin. Struct. Biol.* **2007**, *17* (6), 683–690. https://doi.org/10.1016/j.sbi.2007.08.003.

(74) McRae, B. J.; Powers, J. C.; Kurachi, K.; Heimark, R. L.; Fujikawa, K.; Davie, E. W. Mapping the Active Sites of Bovine Thrombin, Factor IXa, Factor Xa, Factor XIa, Factor XIIa, Plasma Kallikrein, and Trypsin with Amino Acid and Peptide Thioesters: Development of New Sensitive Substrates. *Biochemistry* **1981**, *20* (25), 7196–7206. https://doi.org/10.1021/bi00528a022.

(75) Candour, R. D.; Nabulsi, N. A. R.; Fronczek, F. R. Structural Model of a Short Carboxyl-Imidazole Hydrogen Bond with a Nearly Centrally Located Proton: Implications for the Asp-His Dyad in Serine Proteases. *J. Am. Chem. Soc.* **1990**, *112* (21), 7816–7817. https://doi.org/10.1021/ja00177a064.

(76) Rajagopalan, S.; Wang, C.; Yu, K.; Kuzin, A. P.; Richter, F.; Lew, S.; Miklos, A. E.; Matthews, M. L.; Seetharaman, J.; Su, M.; Hunt, J. F.; Cravatt, B. F.; Baker, D. Design of Activated Serine-Containing Catalytic Triads with Atomic-Level Accuracy. *Nat. Chem. Biol.* **2014**, *10*, 386–391. https://doi.org/10.1038/nchembio.1498.

(77) Rawlings, N. D.; Barrett, A. J. Evolutionary Families of Peptidases. *Biochem. J.* **1993**, *290* (1), 205–218. https://doi.org/10.1042/bj2900205.

(78) Pathak, M.; Wong, S. S.; Dreveny, I.; Emsley, J. Structure of Plasma and Tissue Kallikreins. *Thromb. Haemost.* **2013**, *110* (3), 423–433. https://doi.org/10.1160/TH12-11-0840.

(79) Popelier, P. L. A.; Harding, A. P.; Wedge, D. C. PKa Prediction from "Quantum Chemical Topology" Descriptors. *J. Chem. Inf. Model.* **2009**, *49* (8), 1914–1924. https://doi.org/10.1021/ci900172h.

(80) Evans, D. M.; Davie, R. L.; Edwards, H. J.; Teanby Hodgson, S. N-((Het) Arylmethyl)-Heteroaryl-Carboxamides Compounds as Plasma Kallikrein Inhibitors. *US10781181B2* **2020**, 56–59.

(81) Klebe, G. Applying Thermodynamic Profiling in Lead Finding and Optimization. *Nature Reviews Drug Discovery*. 2015, pp 95–110. https://doi.org/10.1038/nrd4486.

(82) Abdel-Magid, A. F. Inhibitors of Factor XIa and Plasma Kallikrein May Treat Thromboembolic Disorders and Many Diabetes Complications. *ACS Med. Chem. Lett.* **2014**, *5* (4), 286–287. https://doi.org/10.1021/ml500084u.

(83) Sutanto, F.; Konstantinidou, M.; Dömling, A. Covalent Inhibitors: A Rational Approach to Drug Discovery. *RSC Med. Chem.* **2020**, *11* (8), 876–884. https://doi.org/10.1039/d0md00154f.

(84) Potashman, M. H.; Duggan, M. E. Covalent Modifiers: An Orthogonal Approach to Drug Design. *J. Med. Chem.* **2009**, *52* (5), 1231–1246. https://doi.org/10.1021/jm8008597.

(85) Shimokawa, T.; Smith, W. L. Prostaglandin Endoperoxide Synthase. The Aspirin Acetylation Region. *J. Biol. Chem.* **1992**, *267* (17), 12387–12392. https://doi.org/10.1016/s0021-9258(19)49852-9.

(86) Kola, I.; Landis, J. Can the Pharmaceutical Industry Reduce Attrition Rates? *Nat. Rev. Drug Discov.* **2004**, *3* (8), 711–715. https://doi.org/10.1038/nrd1470.

(87) Gehringer, M.; Laufer, S. A. Emerging and Re-Emerging Warheads for Targeted Covalent Inhibitors: Applications in Medicinal Chemistry and Chemical Biology. *J. Med. Chem.* **2019**, *62* (12), 5673–5724. https://doi.org/10.1021/acs.jmedchem.8b01153.

(88) Shindo, N.; Ojida, A. Recent Progress in Covalent Warheads for in Vivo Targeting of Endogenous Proteins. *Bioorganic Med. Chem.* **2021**, *47*, 116386. https://doi.org/10.1016/j.bmc.2021.116386.

(89) Singh, J.; Petter, R. C.; Baillie, T. A.; Whitty, A. The Resurgence of Covalent Drugs. *Nat. Rev. Drug Discov.* **2011**, *10*, 307–317. https://doi.org/10.1038/nrd3410.

(90) Yu, M.; Chen, J.; Xu, Z.; Yang, B.; He, Q.; Luo, P.; Yan, H.; Yang, X. Development and Safety of PI3K Inhibitors in Cancer. *Arch. Toxicol.* **2023**, *97* (3), 635–650. https://doi.org/10.1007/s00204-023-03440-4.

(91) Adibekian, A.; Martin, B. R.; Wang, C.; Hsu, K. L.; Bachovchin, D. A.; Niessen, S.; Hoover, H.; Cravatt, B. F. Click-Generated Triazole Ureas as Ultrapotent in Vivo-Active Serine Hydrolase Inhibitors. *Nat. Chem. Biol.* **2011**, *7* (7), 469–478. https://doi.org/10.1038/nchembio.579.

(92) Otrubova, K.; Chatterjee, S.; Ghimire, S.; Cravatt, B. F.; Boger, D. L. N-Acyl Pyrazoles: Effective and Tunable Inhibitors of Serine Hydrolases. *Bioorganic Med. Chem.* **2019**, *27* (8), 1693–1703. https://doi.org/10.1016/j.bmc.2019.03.020.

(93) Korff, M.; Imberg, L.; Will, J. M.; Bückreiß, N.; Kalinina, S. A.; Wenzel, B. M.; Kastner, G. A.; Daniliuc, C. G.; Barth, M.; Ovsepyan, R. A.; Butov, K. R.; Humpf, H. U.; Lehr, M.; Panteleev, M. A.; Poso, A.; Karst, U.; Steinmetzer, T.; Bendas, G.; Kalinin, D. V. Acylated 1 H-1,2,4-Triazol-5-Amines Targeting Human Coagulation Factor XIIa and Thrombin: Conventional and Microscale Synthesis, Anticoagulant Properties, and Mechanism of Action. *J. Med. Chem.* **2020**, *63* (21), 13159–13186. https://doi.org/10.1021/acs.jmedchem.0c01635.

(94) Boike, L.; Henning, N. J.; Nomura, D. K. Advances in Covalent Drug Discovery. *Nat. Rev. Drug Discov.* **2022**, *21* (12), 881–898. https://doi.org/10.1038/s41573-022-00542-z.

(95) Kwong, A. D.; Kauffman, R. S.; Hurter, P.; Mueller, P. Discovery and Development of Telaprevir: An NS3-4A Protease Inhibitor for Treating Genotype 1 Chronic Hepatitis C Virus. *Nat. Biotechnol.* **2011**, *29* (11), 993–1003. https://doi.org/10.1038/nbt.2020.

(96) Raney, K. D.; Sharma, S. D.; Moustafa, I. M.; Cameron, C. E. Hepatitis C Virus Non-Structural Protein 3 (HCV NS3): A Multifunctional Antiviral Target. *J. Biol. Chem.* **2010**, *285* (30), 22725–22731. https://doi.org/10.1074/jbc.R110.125294.

(97) Augeri, D. J.; Robl, J. A.; Betebenner, D. A.; Magnin, D. R.; Khanna, A.; Robertson, J. G.; Wang, A.; Simpkins, L. M.; Taunk, P.; Huang, Q.; Han, S. P.; Abboa-Offei, B.; Cap, M.; Xin, L.; Tao, L.; Tozzo, E.; Welzel, G. E.; Egan, D. M.; Marcinkeviciene, J.; Chang, S. Y.; Biller, S. A.; Kirby, M. S.; Parker, R. A.; Hamann, L. G. Discovery and Preclinical Profile of Saxagliptin (BMS-477118): A Highly Potent, Long-Acting, Orally Active Dipeptidyl Peptidase IV Inhibitor for the Treatment of Type 2 Diabetes. *J. Med. Chem.* **2005**, *48* (15), 5025–5037. https://doi.org/10.1021/jm050261p.

(98) Brouwer, A. J.; Ceylan, T.; Jonker, A. M.; Linden, T. Van Der; Liskamp, R. M. J. Synthesis and Biological Evaluation of Novel Irreversible Serine Protease Inhibitors Using Amino Acid Based Sulfonyl Fluorides as an Electrophilic Trap. *Bioorganic Med. Chem.* **2011**, *19* (7), 2397–2406. https://doi.org/10.1016/j.bmc.2011.02.014.

(99) Rauber, P.; Angliker, H.; Walker, B.; Shaw, E. The Synthesis of Peptidylfluoromethanes and Their Properties as Inhibitors of Serine Proteinases and Cysteine Proteinases. *Biochem. J.* **1986**, *239* (3), 633–640.

https://doi.org/10.1042/bj2390633.

(100) Ueda, T.; Kam, C. M.; Powers, J. C. The Synthesis of Arginylfluoroalkanes, Their Inhibition of Trypsin and Blood-Coagulation Serine Proteinases and Their Anticoagulant Activity. *Biochem. J.* **1990**, *265* (2), 539–545. https://doi.org/10.1042/bj2650539.

(101) Powers, J. C.; Asgian, J. L.; Ekici, Ö. D.; James, K. E. Irreversible Inhibitors of Serine, Cysteine, and Threonine Proteases. *Chem. Rev.* **2002**, *102* (12), 4639–4750. https://doi.org/10.1021/cr010182v.

(102) Dewerchin, M.; Lijnen, H. R.; Van Hoef, B.; De Cock, F.; Collen, D. Characterisation of Conjugates of Thrombin-Treated Single Chain Urokinase-Type Plasminogen Activator with a Monoclonal Antibody Specific for Crosslinked Fibrin. *Fibrinolysis and Proteolysis* **1990**, *4* (1), 19–26. https://doi.org/10.1016/S0268-9499(05)80036-0.

(103) Gandossi, E.; Lunven, C.; Berry, C. N. Role of Clot-Associated (-Derived) Thrombin in Cell Proliferation Induced by Fibrin Clots in Vitro. *Br. J. Pharmacol.* **2000**, *129* (5), 1021–1027. https://doi.org/10.1038/sj.bjp.0703137.

(104) Powers, J. C. [16] Reaction of Serine Proteases with Halomethyl Ketones. *Methods Enzymol.* **1977**, *46* (C), 197–208. https://doi.org/10.1016/S0076-6879(77)46020-8.

(105) Diaz, D. B.; Yudin, A. K. The Versatility of Boron in Biological Target Engagement. *Nat. Chem.* **2017**, *9*, 731–747. https://doi.org/10.1038/NCHEM.2814.

(106) Zervosen, A.; Herman, R.; Kerff, F.; Herman, A.; Bouillez, A.; Prati, F.; Pratt, R. F.; Frère, J. M.; Joris, B.; Luxen, A.; Charlier, P.; Sauvage, E. Unexpected Tricovalent Binding Mode of Boronic Acids within the Active Site of a Penicillin-Binding Protein. *J. Am. Chem. Soc.* **2011**, *133* (28), 10839–10848. https://doi.org/10.1021/ja200696y.

(107) Kouroukis, T. C.; Baldassarre, F. G.; Haynes, A. E.; Imrie, K.; Reece, D. E.; Cheung, M. C. Bortezomib in Multiple Myeloma: Systematic Review and Clinical Considerations. *Curr. Oncol.* **2014**, *21* (4), 346–364. https://doi.org/10.3747/co.21.1798.

(108) Groll, M.; Berkers, C. R.; Ploegh, H. L.; Ovaa, H. Crystal Structure of the Boronic Acid-Based Proteasome Inhibitor Bortezomib in Complex with the Yeast 20S Proteasome. *Structure* **2006**, *14* (3), 451–456. https://doi.org/10.1016/j.str.2005.11.019.

(109) Arkwright, R.; Pham, T. M.; Zonder, J. A.; Dou, Q. P. The Preclinical Discovery and Development of Bortezomib for the Treatment of Mantle Cell Lymphoma. *Expert Opin. Drug Discov.* **2017**, *12* (2), 225–235. https://doi.org/10.1080/17460441.2017.1268596.

(110) Periyasamy-Thandavan, S.; Jackson, W. H.; Samaddar, J. S.; Erickson, B.;

Barrett, J. R.; Raney, L.; Gopal, E.; Ganapathy, V.; Hill, W. D.; Bhalla, K. N.; Schoenlein, P. V. Bortezomib Blocks the Catabolic Process of Autophagy via a Cathepsin-Dependent Mechanism, Affects Endoplasmic Reticulum Stress and Induces Caspase-Dependent Cell Death in Antiestrogen-Sensitive and Resistant ER + Breast Cancer Cells. *Autophagy* **2010**, *6* (1), 19–35. https://doi.org/10.4161/auto.6.1.10323.

(111) Liu, B.; Trout, R. E. L.; Chu, G. H.; Mcgarry, D.; Jackson, R. W.; Hamrick, J. C.; Daigle, D. M.; Cusick, S. M.; Pozzi, C.; De Luca, F.; Benvenuti, M.; Mangani, S.; Docquier, J. D.; Weiss, W. J.; Pevear, D. C.; Xerri, L.; Burns, C. J. Discovery of Taniborbactam (VNRX-5133): A Broad-Spectrum Serine- And Metallo-β-Lactamase Inhibitor for Carbapenem-Resistant Bacterial Infections. *J. Med. Chem.* **2020**, *63* (6), 2789–2801. https://doi.org/10.1021/acs.jmedchem.9b01518.

(112) Lence, E.; González-Bello, C. Bicyclic Boronate β-Lactamase Inhibitors: The Present Hope against Deadly Bacterial Pathogens. *Adv. Ther.* **2021**, *4* (5), 200–246. https://doi.org/10.1002/adtp.202000246.

(113) Hamrick, J. C.; Docquier, J. D.; Uehara, T.; Myers, C. L.; Six, D. A.; Chatwin, C. L.; John, K. J.; Vernacchio, S. F.; Cusick, S. M.; Trout, R. E. L.; Pozzi, C.; De Luca, F.; Benvenuti, M.; Mangani, S.; Liu, B.; Jackson, R. W.; Moeck, G.; Xerri, L.; Burns, C. J.; Pevear, D. C.; Daigle, D. M. VNRX-5133 (Taniborbactam), a Broad-Spectrum Inhibitor of Serine- And Metallo-β-Lactamases, Restores Activity of Cefepime in Enterobacterales and Pseudomonas Aeruginosa. *Antimicrob. Agents Chemother.* **2020**, *64* (3), 568–579. https://doi.org/10.1128/AAC.01963-19.

(114) Baker, S. J.; Zhang, Y. K.; Akama, T.; Lau, A.; Zhou, H.; Hernandez, V.; Mao, W.; Alley, M. R. K.; Sanders, V.; Plattner, J. J. Discovery of a New Boron-Containing Antifungal Agent, 5-Fluoro-1,3-Dihydro- 1-Hydroxy-2,1-Benzoxaborole (AN2690), for the Potential Treatment of Onychomycosis. *J. Med. Chem.* **2006**, *49* (15), 4447–4450. https://doi.org/10.1021/jm0603724.

(115) Elewski, B. E.; Charif, M. A. Prevalence of Onychomycosis in Patients Attending a Dermatology Clinic in Northeastern Ohio for Other Conditions [3]. *Arch. Dermatol.* **1997**, *133* (9), 1172–1173. https://doi.org/10.1001/archderm.133.9.1172.

(116) Rock, F. L.; Mao, W.; Yaremchuk, A.; Tukalo, M.; Crépin, T.; Zhou, H.; Zhang, Y. K.; Hernandez, V.; Akama, T.; Baker, S. J.; Plattner, J. J.; Shapiro, L.; Martinis, S. A.; Benkovic, S. J.; Cusack, S.; Alley, M. R. K. An Antifungal Agent Inhibits an Aminoacyl-TRNA Synthetase by Trapping TRNA in the Editing Site. *Science (80-.).* **2007**, *316* (5832), 1759–1761. https://doi.org/10.1126/science.1142189.

(117) Akama, T.; Baker, S. J.; Zhang, Y. K.; Hernandez, V.; Zhou, H.; Sanders, V.; Freund, Y.; Kimura, R.; Maples, K. R.; Plattner, J. J. Discovery and Structure-Activity Study of a Novel Benzoxaborole Anti-Inflammatory

Agent (AN2728) for the Potential Topical Treatment of Psoriasis and Atopic Dermatitis. *Bioorganic Med. Chem. Lett.* **2009**, *19* (8), 2129–2132. https://doi.org/10.1016/j.bmcl.2009.03.007.

(118) Dementiev, A.; Silva, A.; Yee, C.; Li, Z.; Flavin, M. T.; Sham, H.; Partridge, J. R. Structures of Human Plasma β–Factor XIIa Cocrystallized with Potent Inhibitors. *Blood Adv.* **2018**, *2* (5), 549–558. https://doi.org/10.1182/bloodadvances.2018016337.

(119) Martin, J. S.; MacKenzie, C. J.; Fletcher, D.; Gilbert, I. H. Characterising Covalent Warhead Reactivity. *Bioorganic Med. Chem.* **2019**, *27* (10), 2066–2074. https://doi.org/10.1016/j.bmc.2019.04.002.

(120) Mucsi, Z.; Chass, G. A.; Ábrányi-Balogh, P.; Jójárt, B.; Fang, D. C.; Ramirez-Cuesta, A. J.; Viskolcz, B.; Csizmadia, I. G. Penicillin's Catalytic Mechanism Revealed by Inelastic Neutrons and Quantum Chemical Theory. *Phys. Chem. Chem. Phys.* **2013**, *15* (47), 20447–20455. https://doi.org/10.1039/c3cp50868d.

(121) McGann, M. FRED and HYBRID Docking Performance on Standardized Datasets. *J. Comput. Aided. Mol. Des.* **2012**, *26* (8), 897–906. https://doi.org/10.1007/s10822-012-9584-8.

(122) Hall, D. G. Boronic Acids: Preparation, Applications in Organic Synthesis and Medicine. *Boronic Acids Prep. Appl. Org. Synth. Med.* **2006**, 1–549. https://doi.org/10.1002/3527606548.

(123) Matteson, D. S.; Man, H.-W. Hydrolysis of Substituted 1,3,2-Dioxaborolanes and an Asymmetric Synthesis of a Differentially Protected Syn , Syn -3-Methyl-2,4-Hexanediol. *J. Org. Chem.* **1996**, *61* (17), 6047–6051. https://doi.org/10.1021/jo960684m.

(124) Hong, K.; Liu, X.; Morken, J. P. Simple Access to Elusive α-Boryl Carbanions and Their Alkylation: An Umpolung Construction for Organic Synthesis. *J. Am. Chem. Soc.* **2014**, *136* (30), 10581–10584. https://doi.org/10.1021/ja505455z.

(125) Matteson, D. S.; Majumdar, D. α-Chloro Boronic Esters from Homologation of Boronic Esters. *J. Am. Chem. Soc.* **1980**, *102* (25), 7588–7590. https://doi.org/10.1021/ja00545a045.

(126) Matteson, D. S.; Beedle, E. C. A Directed Chiral Synthesis of Amino Acids from Boronic Esters. *Tetrahedron Lett.* **1987**, *28* (39), 4499–4502. https://doi.org/10.1016/S0040-4039(00)96547-X.

(127) Kinsinger, T.; Kazmaier, U. Matteson Homologation of Arylboronic Esters. *European J. Org. Chem.* **2022**, *2022* (31), 597–603. https://doi.org/10.1002/ejoc.202200625.

(128) Matteson, D. S.; Majumdar, D. Homologation of Boronic Esters to α-Chloro Boronic Esters. *Organometallics* **1983**, *2* (11), 1529–1535. https://doi.org/10.1021/om50005a008.

(129) Zhu, Y.; Wu, G.; Zhu, X.; Ma, Y.; Zhao, X.; Li, Y.; Yuan, Y.; Yang, J.; Yu, S.; Shao, F.; Lei, M. Synthesis, in Vitro and in Vivo Biological Evaluation, and Comprehensive Understanding of Structure-Activity Relationships of Dipeptidyl Boronic Acid Proteasome Inhibitors Constructed from β-Amino Acids. *J. Med. Chem.* **2010**, *53* (24), 8619–8626. https://doi.org/10.1021/jm1009742.

(130) Yang, F.; Zhu, M.; Zhang, J.; Zhou, H. Synthesis of Biologically Active Boron-Containing Compounds. *MedChemComm*. 2018, pp 201–211. https://doi.org/10.1039/c7md00552k.

(131) Wu, X.; Sun, P.; Chen, X.; Hua, L.; Cai, H.; Liu, Z.; Zhang, C.; Liang, S.; Chen, Y.; Wu, D.; Ou, Y.; Hu, W.; Yang, Z. Discovery of a Novel Oral Proteasome Inhibitor to Block NLRP3 Inflammasome Activation with Anti-Inflammation Activity. *J. Med. Chem.* **2022**, *65* (18), 11985–12001. https://doi.org/10.1021/acs.jmedchem.2c00523.

(132) Hinkes, S. P. A.; Klein, C. D. P. Virtues of Volatility: A Facile Transesterification Approach to Boronic Acids. *Org. Lett.* **2019**, *21* (9), 3048–3052. https://doi.org/10.1021/acs.orglett.9b00584.

(133) Gorovoy, A. S.; Gozhina, O.; Svendsen, J. S.; Tetz, G. V.; Domorad, A.; Tetz, V. V.; Lejon, T. Syntheses and Anti-Tubercular Activity of β-Substituted and α,β-Disubstituted Peptidyl β-Aminoboronates and Boronic Acids. *J. Pept. Sci.* **2013**, *19* (10), 613–618. https://doi.org/10.1002/psc.2537.

(134) Gorovoy, A. S.; Gozhina, O. V.; Svendsen, J. S.; Domorad, A. A.; Tetz, G. V.; Tetz, V. V.; Lejon, T. Boron-Containing Peptidomimetics - A Novel Class of Selective Anti-Tubercular Drugs. *Chem. Biol. Drug De(1) Gorovoy, A. S.; Gozhina, O. V.; Svendsen, J. S.; Domorad, A. A.; Tetz, G. V.; Tetz, V. V.; Lejon, T. Boron-Containing Pept. - A Nov. Cl. Sel. Anti-Tubercular Drugs. Chem. Biol. Drug Des. 2013, 81 (3), 4* **2013**, *81* (3), 408–413. https://doi.org/10.1111/cbdd.12091.

(135) Ohmura, T.; Awano, T.; Suginome, M. α-Amidobenzylation of Aryl and Alkenyl Halides via Palladium-Catalyzed Suzuki-Miyaura Coupling with α-(Acylamino) Benzylboronic Esters. *Chem. Lett.* **2009**, *38* (7), 664–665. https://doi.org/10.1246/cl.2009.664.

(136) Ohmura, T.; Awano, T.; Suginome, M. Stereospecific Suzuki-Miyaura Coupling of Chiral α-(Acylamino) Benzylboronic Esters with Inversion of Configuration. *J. Am. Chem. Soc.* **2010**, *132* (38), 13191–13193. https://doi.org/10.1021/ja106632j.

(137) Awano, T.; Ohmura, T.; Suginome, M. Inversion or Retention? Effects of Acidic Additives on the Stereochemical Course in Enantiospecific Suzuki-Miyaura Coupling of α-(Acetylamino) Benzylboronic Esters. *J. Am. Chem. Soc.* **2011**, *133* (51), 20738–20741. https://doi.org/10.1021/ja210025q.

(138) Ohmura, T.; Miwa, K.; Awano, T.; Suginome, M. Enantiospecific Suzuki–Miyaura Coupling of Nonbenzylic α-(Acylamino)Alkylboronic Acid

Derivatives. *Chem. - An Asian J.* **2018**, *13* (17), 2414–2417. https://doi.org/10.1002/asia.201800536.

(139) Priestley, E. S.; De Lucca, I.; Ghavimi, B.; Erickson-Viitanen, S.; Decicco, C. P. P1 Phenethyl Peptide Boronic Acid Inhibitors of HCV NS3 Protease. *Bioorganic Med. Chem. Lett.* **2002**, *12* (21), 3199–3202. https://doi.org/10.1016/S0960-894X(02)00682-0.

(140) Morandi, F.; Caselli, E.; Morandi, S.; Focia, P. J.; Blázquez, J.; Shoichet, B. K.; Prati, F. Nanomolar Inhibitors of AmpC β-Lactamase. *J. Am. Chem. Soc.* **2003**, *125* (3), 685–695. https://doi.org/10.1021/ja0288338.

(141) Inglis, S. R.; Woon, E. C. Y.; Thompson, A. L.; Schofield, C. J. Observations on the Deprotection of Pinanediol and Pinacol Boronate Esters via Fluorinated Intermediates. *J. Org. Chem.* **2010**, *75* (2), 468–471. https://doi.org/10.1021/jo901930v.

(142) Kuivila, H. G.; Nahabedian, K. V. Electrophilic Displacement Reactions, X. General Acid Catalysis in the Protodeboronation of Areneboronic Acids. *J. Am. Chem. Soc.* **1961**, *83* (9), 2159–2163. https://doi.org/10.1021/ja01470a028.

(143) Strelow, J. M. A Perspective on the Kinetics of Covalent and Irreversible Inhibition. *Journal of Biomolecular Screening*. 2017, pp 3–20. https://doi.org/10.1177/1087057116671509.

(144) McWhirter, C. Kinetic Mechanisms of Covalent Inhibition. In *Annual Reports in Medicinal Chemistry*; 2021; Vol. 56, pp 1–31. https://doi.org/10.1016/bs.armc.2020.11.001.

(145) Mons, E.; Roet, S.; Kim, R. Q.; Mulder, M. P. C. A Comprehensive Guide for Assessing Covalent Inhibition in Enzymatic Assays Illustrated with Kinetic Simulations. *Curr. Protoc.* **2022**, *2* (6). https://doi.org/10.1002/cpz1.419.

(146) Ponczek, M. B.; Shamanaev, A.; LaPlace, A.; Dickeson, S. K.; Srivastava, P.; Sun, M. F.; Gruber, A.; Kastrup, C.; Emsley, J.; Gailani, D. The Evolution of Factor XI and the Kallikrein-Kinin System. *Blood Adv.* **2020**, *4* (24), 6135–6147. https://doi.org/10.1182/bloodadvances.2020002456.

(147) Mohammed, B. M.; Matafonov, A.; Ivanov, I.; Sun, M. fu; Cheng, Q.; Dickeson, S. K.; Li, C.; Sun, D.; Verhamme, I. M.; Emsley, J.; Gailani, D. An Update on Factor XI Structure and Function. *Thromb. Res.* **2018**, *161*, 94–105. https://doi.org/10.1016/j.thromres.2017.10.008.

(148) Copeland, R. A.; Basavapathruni, A.; Moyer, M.; Scott, M. P. Impact of Enzyme Concentration and Residence Time on Apparent Activity Recovery in Jump Dilution Analysis. *Anal. Biochem.* **2011**, *416* (2), 206–210. https://doi.org/10.1016/j.ab.2011.05.029.

(149) Kumar, M.; Lowery, R. G. A High-Throughput Method for Measuring Drug Residence Time Using the Transcreener ADP Assay. *SLAS Discov.* **2017**, *22* (7), 915–922. https://doi.org/10.1177/2472555217695080.

(150) Bhatwadekar, A. D.; Kansara, V. S.; Ciulla, T. A. Investigational Plasma Kallikrein Inhibitors for the Treatment of Diabetic Macular Edema: An Expert Assessment. *Expert Opinion on Investigational Drugs*. 2020, pp 237–244. https://doi.org/10.1080/13543784.2020.1723078.

(151) Tankersley, D. L.; Alving, B. M.; Finlayson, J. S. Activation of Factor XII by Dextran Sulfate: The Basis for an Assay of Factor XII. *Blood* **1983**, *62* (2), 448–456. https://doi.org/10.1182/blood.v62.2.448.448.

(152) Morrissey, J. H. Polyphosphate: A Link between Platelets, Coagulation and Inflammation. *Int. J. Hematol.* **2012**, *95* (4), 346–352. https://doi.org/10.1007/s12185-012-1054-5.

(153) Cao, B.; Li, S.; Kong, W.; Guo, J.; Tian, Z.; Zhang, G. Green and Efficient Synthesis of Pinacol over Photoactive Acetonyl-Platinum Complexes on Pt Nanoparticle Surfaces Photocatalyst. *Inorg. Chem. Commun.* **2020**, *121*. https://doi.org/10.1016/j.inoche.2020.108227.

(154) Liu, C.; Li, R.; Zhou, W.; Liang, Y.; Shi, Y.; Li, R. L.; Ling, Y.; Yu, Y.; Li, J.; Zhang, B. Selectivity Origin of Organic Electrosynthesis Controlled by Electrode Materials: A Case Study on Pinacols. *ACS Catal.* **2021**, *11* (14), 8958–8967. https://doi.org/10.1021/acscatal.1c01382.

(155) Wang, Y. L.; Liu, S.; Yu, Z. J.; Lei, Y.; Huang, M. Y.; Yan, Y. H.; Ma, Q.; Zheng, Y.; Deng, H.; Sun, Y.; Wu, C.; Yu, Y.; Chen, Q.; Wang, Z.; Wu, Y.; Li, G. B. Structure-Based Development of (1-(3'-Mercaptopropanamido)Methyl)Boronic Acid Derived Broad-Spectrum, Dual-Action Inhibitors of Metallo- And Serine-β-Lactamases. *J. Med. Chem.* **2019**, *62* (15), 7160–7184. https://doi.org/10.1021/acs.jmedchem.9b00735.

(156) Zhang, L.; Jiao, L. Pyridine-Catalyzed Radical Borylation of Aryl Halides. *J. Am. Chem. Soc.* **2017**, *139* (2), 607–610. https://doi.org/10.1021/jacs.6b11813.

(157) Kuleshova, O.; Asako, S.; Ilies, L. Ligand-Enabled, Iridium-Catalyzed Ortho-Borylation of Fluoroarenes. *ACS Catal.* **2021**, *11* (10), 5968–5973. https://doi.org/10.1021/acscatal.1c01206.

(158) Jin, S.; Dang, H. T.; Haug, G. C.; He, R.; Nguyen, V. D.; Nguyen, V. T.; Arman, H. D.; Schanze, K. S.; Larionov, O. V. Visible Light-Induced Borylation of C-O, C-N, and C-X Bonds. *J. Am. Chem. Soc.* **2020**, *142* (3), 1603–1613. https://doi.org/10.1021/jacs.9b12519.

(159) Leermann, T.; Leroux, F. R.; Colobert, F. Highly Efficient One-Pot Access to Functionalized Arylboronic Acids via Noncryogenic Bromine/Magnesium Exchanges. *Org. Lett.* **2011**, *13* (17), 4479–4481. https://doi.org/10.1021/ol2016252.

(160) Ang, N. W. J.; Buettner, C. S.; Docherty, S.; Bismuto, A.; Carney, J. R.; Docherty, J. H.; Cowley, M. J.; Thomas, S. P. Borane-Catalysed Hydroboration of Alkynes and Alkenes. *Synth.* **2018**, *50* (4), 803–808.

https://doi.org/10.1055/s-0036-1591719.

(161) Miyaura, N.; Yamada, K.; Suzuki, A. A New Stereospecific Cross-Coupling by the Palladium-Catalyzed Reaction of 1-Alkenylboranes with 1-Alkenyl or 1-Alkynyl Halides. *Tetrahedron Lett.* **1979**, *20* (36), 3437–3440. https://doi.org/10.1016/S0040-4039(01)95429-2.

(162) Suzuki, A. Synthetic Studies via the Cross-Coupling Reaction of Organoboron Derivatives with Organic Halides. *Pure Appl. Chem.* **1991**, *63* (3), 419–422. https://doi.org/10.1351/pac199163030419.

(163) Miyaura, N.; Suzuki, A. Palladium-Catalyzed Cross-Coupling Reactions of Organoboron Compounds. *Chem. Rev.* **1995**, *95* (7), 2457–2483. https://doi.org/10.1021/cr00039a007.

(164) Ishiyama, T.; Murata, M.; Miyaura, N. Palladium(0)-Catalyzed Cross-Coupling Reaction of Alkoxydiboron with Haloarenes: A Direct Procedure for Arylboronic Esters. *J. Org. Chem.* **1995**, *60* (23), 7508–7510. https://doi.org/10.1021/jo00128a024.

(165) Takagi, J.; Takahashi, K.; Ishiyama, T.; Miyaura, N. Palladium-Catalyzed Cross-Coupling Reaction of Bis(Pinacolato)Diboron with 1-Alkenyl Halides or Triflates: Convenient Synthesis of Unsymmetrical 1,3-Dienes via the Borylation-Coupling Sequence. *J. Am. Chem. Soc.* **2002**, *124* (27), 8001–8006. https://doi.org/10.1021/ja0202255.

(166) Hemming, D.; Fritzemeier, R.; Westcott, S. A.; Santos, W. L.; Steel, P. G. Copper-Boryl Mediated Organic Synthesis. *Chem. Soc. Rev.* **2018**, *47* (19), 7477–7494. https://doi.org/10.1039/c7cs00816c.

(167) Takahashi, K.; Ishiyama, T.; Miyaura, N. Addition and Coupling Reactions of Bis(Pinacolato)Diboron Mediated by CuCl in the Presence of Potassium Acetate. *Chem. Lett.* **2000**, No. 9, 982–983. https://doi.org/10.1246/cl.2000.982.

(168) Itoa, H.; Yamanakab, H.; Tateiwab, J. I.; Hosomi, A. Boration of an α,β-Enone Using a Diboron Promoted by a Copper(I) - Phosphine Mixture Catalyst. *Tetrahedron Lett.* **2000**, *41* (35), 6821–6825. https://doi.org/10.1016/s0040-4039(00)01161-8.

(169) Gao, M.; Thorpe, S. B.; Santos, W. L. Sp2 - Sp3 Hybridized Mixed Diboron: Synthesis, Characterization, and Copper-Catalyzed β-Boration of α,β-Unsaturated Conjugated Compounds. *Org. Lett.* **2009**, *11* (15), 3478–3481. https://doi.org/10.1021/ol901359n.

(170) Mun, S.; Lee, J. E.; Yun, J. Copper-Catalyzed β-Boration of α,β-Unsaturated Carbonyl Compounds: Rate Acceleration by Alcohol Additives. *Org. Lett.* **2006**, *8* (21), 4887–4889. https://doi.org/10.1021/ol061955a.

(171) Yang, J.; Chen, F. Highly Efficient Syntheses of β-Cyanoketones via Conjugate Addition of Me3SiCN to Aromatic Enones. *Chinese J. Chem.* **2010**, *28* (6), 981–987. https://doi.org/10.1002/cjoc.201090182.

(172) Moccia, M.; Fini, F.; Scagnetti, M.; Adamo, M. F. A. Catalytic Enantioselective Addition of Sodium Bisulfite to Chalcones. *Angew. Chemie - Int. Ed.* **2011**, *50* (30), 6893–6895. https://doi.org/10.1002/anie.201102162.

(173) Maekawa, H.; Nishiyama, Y. Selective Introduction of a Trifluoroacetyl Group onto 4-Vinylpyridines through Magnesium-Promoted Reduction. *Tetrahedron* **2015**, *71* (38), 6694–6700. https://doi.org/10.1016/j.tet.2015.07.046.

(174) Xu, M.; Chen, Y.; Xu, P.; Andreasen, P. A.; Jiang, L.; Li, J.; Huang, M. Crystal Structure of Plasma Kallikrein Reveals the Unusual Flexibility of the S1 Pocket Triggered by Glu217. *FEBS Lett.* **2018**, *592* (15), 2658–2667. https://doi.org/10.1002/1873-3468.13191.

(175) Cabildo, P.; Sanz, D.; Claramunt, R. M.; Bourne, S. A.; Alkorta, I.; Elguero, J. Synthesis and Structural Studies of Some [14]Paracyclo-Bis-(1,2)Pyrazolium- and (1,3)Imidazolium-Phanes. *Tetrahedron* **1999**, *55* (8), 2327–2340. https://doi.org/10.1016/S0040-4020(99)00013-7.

(176) Lomovskaya, O.; Sun, D.; Rubio-Aparicio, D.; Nelson, K.; Tsivkovski, R.; Griffith, D. C.; Dudley, M. N. Vaborbactam: Spectrum of Beta-Lactamase Inhibition and Impact of Resistance Mechanisms on Activity in Enterobacteriaceae. *Antimicrob. Agents Chemother.* **2017**, *61* (11). https://doi.org/10.1128/AAC.01443-17.

(177) Tsivkovski, R.; Lomovskayaa, O. Biochemical Activity of Vaborbactam. *Antimicrob. Agents Chemother.* **2020**, *64* (2). https://doi.org/10.1128/AAC.01935-19.

(178) Beckmann, E.; Desai, V.; Hoppe, D. Stereospecific Reaction of α-Carbamoyloxy-2-Alkenylboronates and α-Carbamoyloxy-Alkylboronates with Grignard Reagents - Synthesis of Highly Enantioenriched Secondary Alcohols. *Synlett* **2004**, No. 13, 2275–2280. https://doi.org/10.1055/s-2004-832835.

(179) Leonori, D.; Aggarwal, V. K. Lithiation-Borylation Methodology and Its Application in Synthesis. *Acc. Chem. Res.* **2014**, *47* (10), 3174–3183. https://doi.org/10.1021/ar5002473.

(180) Bold, C. P.; Yeung, K.; Pape, F.; Kaiser, D.; Aggarwal, V. K. Application of Lithiation-Borylation to the Total Synthesis of (-)-Rakicidin F. *Org. Lett.* **2022**, *24* (51), 9398–9402. https://doi.org/10.1021/acs.orglett.2c03716.

(181) Yeung, K.; Mykura, R. C.; Aggarwal, V. K. Lithiation–Borylation Methodology in the Total Synthesis of Natural Products. *Nat. Synth.* **2022**, *1* (2), 117–126. https://doi.org/10.1038/s44160-021-00012-1.